2009

Synthesis Of Novel Fluorene-based Two-photon Absorbing Molecules And Their Applications In Optical Data Storage, Microfabricatio

Ciceron Yanez
University of Central Florida

SYNTHESIS OF NOVEL FLUORENE-BASED TWO-PHOTON ABSORBING MOLECULES AND THEIR APPLICATIONS IN OPTICAL DATA STORAGE, MICROFABRICATION, AND STIMULATED EMISSION DEPLETION

by

CICERON YANEZ
B. S. Universidad Simon Bolivar, 2003

A dissertation submitted in partial fulfillment of the requirements
for the degree of Doctor of Philosophy
in the Department of Chemistry
in the College of Sciences
at the University of Central Florida
Orlando, Florida

Fall Term 2009
Major Professor: Kevin D. Belfield

ABSTRACT

Two-photon absorption (2PA) has been used for a number of scientific and technological applications, exploiting the fact that the 2PA probability is directly proportional to the square of the incident light intensity (while one-photon absorption bears a linear relation to the incident light intensity). This intrinsic property of 2PA leads to 3D spatial localization, important in fields such as optical data storage, fluorescence microscopy, and 3D microfabrication. The spatial confinement that 2PA enables has been used to induce photochemical and photophysical events in increasingly smaller volumes and allowed nonlinear, 2PA-based, technologies to reach sub-diffraction limit resolutions.

The primary focus of this dissertation is the development of novel, efficient 2PA, fluorene-based molecules to be used either as photoacid generators (PAGs) or fluorophores. A second aim is to develop more effective methods of synthesizing these compounds. As a third and final objective, the new molecules were used to develop a write-once-read many (WORM) optical data storage system, and stimulated emission depletion probes for bioimaging. In Chapter I, the microwave-assisted synthesis of triarylsulfonium salt photoacid generators (PAGs) from their diphenyliodonium counterparts is reported. The microwave-assisted synthesis of these novel sulfonium salts afforded reaction times 90 to 420 times faster than conventional thermal conditions, with photoacid quantum yields of new sulfonium PAGs ranging from 0.01 to 0.4.

These PAGs were used to develop a fluorescence readout-based, nonlinear three-dimensional (3D) optical data storage system (Chapter II). In this system, writing was achieved by acid generation upon two-photon absorption (2PA) of a PAG (at 710 or 730 nm). Readout was then performed by interrogating two-photon absorbing dyes, after protonation, at 860 nm. Two-photon recording and readout of voxels was demonstrated in five and eight consecutive, crosstalk-free layers within a polymer matrix, generating a data storage capacity of up to 1.8×10^{13} bits/cm^3.

The possibility of using these PAGs in microfabrication is described in Chapter III, where two-photon induced cationic ring-opening polymerization (CROP) crosslinking of an SU8 resin is employed to produce free-standing microstructures.

Chapter IV describes the investigation of one- and two-photon stimulated emission transitions by the fluorescence quenching of a sulfonyl-containing fluorene compound in solution at room temperate using a picosecond pump-probe technique. The nature of stimulated transitions under various fluorescence excitation and quenching conditions were analyzed theoretically, and good agreement with experimental data was demonstrated. Two-photon stimulated transitions $S_1 \rightarrow S_0$ were shown at λ_q = 1064 nm. The two-photon stimulated emission cross section of the sulfonyl fluorophore was estimated as $\delta_{2PE}(\lambda_q) \approx$ 240 - 280 GM, making this compound a good candidate for use in two-photon stimulated emission depletion (STED) microscopy.

PUBLICATIONS TO DATE FROM DISSERTATION WORK

1. Yanez, C. O.; Andrade, C. D.; Belfield, K. D. *Chemical Communications* **2009**, 827-829.
2. Yanez, C. O.; Andrade, C. D.; Yao, S.; Luchita, G.; Bondar, M. V.; Belfield, K. D. ACS *Applied Materials & Interfaces* **2009**, *1*, 2219-2229.
3. Belfield, K. D.; Bondar, M. V.; Yanez, C. O.; Hernandez, F. E.; Przhonska, O. V. *Journal of Materials Chemistry* **2009**, *19*, 7498-7502.
4. Belfield, K. D.; Bondar, M. V.; Yanez, C. O.; Hernandez, F. E.; Przhonska, O. V. *Journal of Physical Chemistry B* **2009**, *113*, 7101-7106.
5. Morales, A. R.; Yanez, C. O.; Schafer-Hales, K. J.; Marcus, A. I.; Belfield, K. D. *Bioconjugate Chemistry* **2009**, *20*, 1992-2000.
6. Morales, A. R.; Schafer-Hales, K. J.; Yanez, C. O.; Bondar, M. V.; Przhonska, O. V.; Marcus, A. I.; Belfield, K. D. *ChemPhysChem* **2009**, *10*, 2073-2081.
7. Bondar, M. V.; Przhonska, O. V.; Yanez, C. O.; Belfield, K. D. *Ukranian Journal of Physics* **2009**, *54*, 14-21.
8. Yanez, C. O.; Andrade, C. D.; Yao, S.; Luchita, G.; Bondar, M. V. Materials and Thin Films, ACS Symposium Series; Oxford University Press, in press.
9. Belfield, K. D.; Yanez, C. O.; Andrade, C. D.; Yao, S.; *Polymer Preprints* (American Chemical Society, Division of Polymer Chemistry) **2008**, *49*, 980-981.
10. Belfield, K. D.; Yanez, C. O.; Huang, Z.-L. *RadTech Report* **2007**, *21*, 42-47.

PATENTS TO DATE FROM DISSERTATION WORK

Belfield, K. D. and Ciceron O. Yanez, "Microwave-Assisted Formation of Sulfonium Photacid Generators" Filed: April 14 2008. Patent Pending US 61-044722.

CONFERENCES AND PRESENTATIONS TO DATE FROM DISSERTATION WORK

1. Kevin D. Belfield, Ciceron O. Yanez, Gheroghe Luchita."PAG-based Two-Photon 3D WORM Optical Data Storage." ICONO 11. Beijing, China, 2009.
2. Ciceron O. Yanez, Kevin D. Belfield. "New Probes for Endosomal and Lysosomal Two-Photon Bioimaging.", 2009 Multiphoton Excitation Conference User Group Meeting. Kannapolis, North Carolina, United States, 2009.
3. Kevin D. Belfield, Mykhailo V. Bondar, Ciceron O. Yanez, and Olga V. Przhonska. "Stimulated Emission Depletion of a Bis-Sulfonyl Fluorene Derivative Via One- and Two-Photon Excitation." 238th ACS National Meeting, Washington, D.C., United States, 2009.
4. Carolina D. Andrade, Maher A. Qaddoura, Ciceron O. Yanez, Mykhailo V. Bondar, and Kevin D. Belfield. "Two-Photon Absorbing Fluorescent Dye-Containing Micelles for Bioimaging." 238th ACS National Meeting, Washington, D.C., United States, 2009.
5. Kevin D. Belfield, Alma R. Morales, Ciceron O. Yanez, Mykhailo V. Bondar, and Olga V. Przhonska. "Photophysics, Excited State Intramolecular Proton Transfer, and Imaging of a Fluorenyl Two-Photon Absorbing Fluorescent Probe." 238th ACS National Meeting, Washington, D.C., United States, 2009.
6. Carolina D. Andrade, Ciceron O. Yanez, and Kevin D. Belfield. "Two-Photon Absorbing Molecules." 85th Annual FAME meeting, Orlando, FL, United States, 2009.

7. Mykhailo V. Bondar, Ciceron O. Yanez, Olga V. Przhonska, and Kevin D. Belfield. "Two-Photon Stimulated Depletion of a New Sulfonyl-Containing Fluorene Derivative." 85th Annual FAME meeting, Orlando, FL, United States, 2009.
8. Ciceron O. Yanez, Carolina D. Andrade, Sheng Yao, Gheorghe Luchita, and Kevin D. Belfield. "Photosensitive Polymeric Materials for Two-Photon 3D WORM Optical Data Storage Systems." 85th Annual FAME meeting, Orlando, FL, United States, 2009.
9. Belfield, K. D.; Yanez, C. O.; Andrade, C. D.; Yao, S., "New Photosensitive Polymeric Materials for Two-Photon 3D WORM Optical Data Storage." (American Chemical Society, Division of Polymer Chemistry) 2008, 49, (2), 980-981.
10. Belfield, K. D.; Yanez, C. O.; Andrade, C. D.; Yao, S. "In New Photosensitive Polymeric Materials for Two-Photon 3-D WORM Optical Data Storage.", 236th ACS National Meeting, Philadelphia, PA, United States, 2008 Philadelphia, PA, United States, 2008
11. Yanez, C. O.; Andrade, C. D.; Belfield, K. D.; "In Formation of New Sulfonium Photoacid Generators by Microwave Assisted Reaction of Diphenyl Sulfides with Diphenyl Iodonium Salts.", 236th ACS National Meeting, Philadelphia, PA, United States, 2008; Philadelphia, PA, United States, 2008.
12. Belfield, K. D.; Yanez, C. O.; Bondar, M. V. "Synthesis and Application of Novel Flourenyl-Based Two-Photon Absorbing PAGs in 3D Microfabrication.", ICONO 10, Santa Fe, New Mexico, 2008; Santa Fe, New Mexico, 2008.

13. Andrade, C. D.; Yanez, C. O.; Belfield, K. D. “Synthesis and Characterization of Novel Fluorene-Based Two-Photon Absorbing Molecules.”, 236th ACS National Meeting, Philadelphia, PA, United States, 2008; Philadelphia, PA, United States, 2008.
14. Yanez, C. O.; Carolina D. Andrade, Sheng Yao, Gheorghe Luchita, and Belfield, K. D. “Photosensitive Polymeric Materials for Two-Photon 3D WORM Optical Data Storage Systems”, CREOL Industrial Affiliates Day 2008, Orlando, FL, 2008.
15. Yanez, C. O.; Belfield, K. D.; Corredor, C. C. “Improved Photosensitive Polymeric Materials for 3-D Optical Data Storage Using Two-Photon Fluoresent Writing and Readout.”, 83rd Annual Florida Meeting and Exposition (FAME), 2007; 2007.
16. Belfield, K. D.; Yanez, C. O.; Yao, S.; Huang, Z.-L.; Corredor, C. C.; “Improved Photosensitive Polymeric Materials for 3-D WORM Optical Data Storage Using Two-Photon Fluorescent Writing and Readout.”, 233rd ACS National Meeting, Chicago, IL, United States, 2007; Chicago, IL, United States, 2007.
17. Yanez, C. O.; Belfield, K. D. “Synthesis and Application of Novel Fluorenyl-Based Two-Photon Absorbing PAGs in 3D Microfabrication”, CREOL Industrial Affiliates Day 2007, Orlando, FL, 2007.

To my family. Especially to Caro, my wife, who has accompanied me in all my academic and research amusements and made them her own. This is also for you Steph.

ACKNOWLEDGMENTS

I would like to thank my advisor Dr. Kevin Belfield from whom I've never received a word of discouragement. His constant support, guidance, and optimism have led me to consolidate this dissertation. Dr. Belfield's guidance has been defined by an exceptional work ethic, contagious curiosity and commitment.

I would also like to thank my colleagues, the members of Dr. Belfield's research group for their friendship and comments throughout my Ph.D. studies. This work is the result of teamwork efforts put in by many of the members of Dr. Belfield's group. I would like to especially thank Dr. Sheng Yao for trusting me with his precious compounds. Also, I would like to thank Carolina Andrade for the compounds she so generously shared with me. I would like to acknowledge Dr. Mykhailo Bondar for his constant kind words of advice and his guidance in the photophysical characterization of many of the compounds and his help with the STED experiments. Thanks to Gheorghe Luchita for developing and aiding me in the use of the motorized stage-computer interface. The original setup of the home-built two-photon laser scanning microscope used for data storage and bioimaging was originally set up by Dr. Katherine Schafer-Hales to whom I'm also thankful for aiding us in the use of this instrument.

TABLE OF CONTENTS

LIST OF FIGURES

LIST OF TABLES

LIST OF SCHEMES

LIST OF ACRONYMS AND ABREVIATIONS

^{13}C	Carbon 13 isotope
2PA	Two-photon absorption
A-D-A	Acceptor-donor-acceptor
A-π-A	Acceptor-π-acceptor
ACN	Acetonitrile
AcOH	Acetic acid
Anal.	Analysis
Ar	Argon or aromatic system
bp	Boiling point
Calcd.	Calculated
CDCl3	Deuterated chloroform
cm^{-1}	Wavenumber
d	Doublet
D-A-D	Donor-acceptor-donor
D-π-A	Donor-π-acceptor
ESA	Excited state absorption
EtOH	Ethanol

fs	Femtosecond (10^{-15} s)
g	Gram
GM	Goppert-Mayer unit for the 2PA cross-section (1 x10^{-50} cm^4 s $photon^{-1}$ $molecule^{-1}$)
h	Hour
IR	Infrared
L	Liter
lit.	Literature value
m	Multiplet
MEMs	Microelectromechanical systems or devices
min	Minute
mL	Milliliter (10^{-3} L)
mmol	Millimoles (10^{-3} moles)
mp	Melting point
MS	Mass spectrum
ms	Millisecond
MW	Microwave
mW	Milliwatts
n-BuLi	*n*-Butyllithium
N. A.	Numerical aperture

nm	Nanometer (10^{-9} m)
NMR	Nuclear magnetic resonance
ODS	Optical data storage
$P(OEt)_3$	Triethylphosphite
PAG	Photoacid generator
ppm	Parts per million
psi	Pounds per square inch
r. t.	Room temperature
s	Seconds or singlet
S_1	First excited state, singlet
S_o	Ground state, singlet
t	Triplet
THF	Tetrahydrofurane
TLC	Thin layer chromatography
TMS	Tetramethylsilane
UV	Ultraviolet
W	Watts
wt%	Weight percent
δ	ppm or 2PA cross section
Δ	Conventional heating
ε_o	Molar absorptivity coefficient
λmax	Wavelength of maximum absorption

λ_q	Quenching wavelength
τ_d	Time delay
τ_F	Fluorescence lifetime
Φ	Fluorescence quantum yield
Φ_{H+}	Photoacid quantum yield
^1H	Hydrogen 1 isotope

CHAPTER I: MICROWAVE-ASSISTED FORMATION OF NOVEL SULFONIUM PHOTOACID GENERATORS FROM DIPHENYLSULFIDES

Reproduced with permission of the Royal Chemistry Society from: Yanez, C. O.; Andrade, C. D.; Belfield, K. D. *Chemical Communications* **2009**, 827-829.

I.1 Abstract

Microwave-assisted synthesis of triarylsulfonium salt photoacid generators (PAGs) afforded reaction times 90 to 420 times faster than conventional thermal conditions, with photoacid quantum yields of new sulfonium PAGs ranging from 0.01 to 0.4.

I.2 Introduction

Since their discovery, the use of photoacid-generators, PAGs, have been widely adopted by the polymer industry in coatings, paints, anticorrosives, photoresists, and microelectronics,[1] and 2D and 3D lithographic patterning.[2,3]

Two-photon absorption (2PA) has been reported for a number of scientific and technological applications, exploiting the fact that the 2PA probability is directly proportional to the square of the incident light intensity (while one- photon absorption bears a linear relation to the incident light intensity).[4] This intrinsic property of 2PA leads to 3D spatial localization, important in fields such as optical data storage,[5-7] fluorescence microscopy,[8,9] and 3D microfabrication.[10,11] There have been demonstrations of successful two-photon microfabrication using commercial PAGs,[11,12] even though the 2PA cross section of these initiators is reportedly low.[13] Two-photon 3D microfabrication with a novel PAG was reported to fabricate MEMs structures.[14] To

further advance a number of emerging technologies, there is a great need for PAGs with high 2PA cross sections in the near-IR spectral range.

Microwave-facilitated synthesis has been the subject of substantial interest over the last decade.[15,16] Seipel *et al.* recently reported microwave-assisted reaction times 80 times faster than conventional heating reaction times,[17] and are potentially more energy-efficient than conventional heating. To our knowledge, there are no reports of the microwave-assisted synthesis of sulfonium salts.

I.3 Results and Discussion

The synthesis of triarylsulfonium salts by photolysis of their diphenyliodonium counterpart, in the presence of a diphenylsulfide, was originally reported by Crivello *et al.*[18,19] Herein, we report the microwave-assisted synthesis of triarylsulfonium salt PAGs. Several of the PAGs are novel and have potential for use as 2PA photoinitiators in negative resists for 3D microfabrication or in optical data storage. Furthermore, the efficiency of forming these sulfonium salts by the microwave-assisted process was evaluated relative to the conventional thermal reaction of diphenylsulfides in the presence diphenyliodonium salts. Finally, photoacid quantum yields were determined for several of the novel PAGs.

The new PAGs were designed to exhibit high 2PA cross sections. Because of its high thermal and photochemical stability, fluorene was chosen as the core structure of the PAGs.[20] Quite advantageously, fluorene lends itself to ready substitution in its 2-, 7-, and 9- positions. Stilbene or thiophene motifs were introduced (2- and 7- positions) in order

to extend the π-conjugation. Ultimately, two acceptor groups (triarylsulfonium and nitro) were introduced.

In order to enhance the photoacid quantum yield per molecule, the first approach was to incorporate two sulfonium salt motifs onto the fluorenyl scaffold, such as **7** in Scheme I-1. However, this molecule exhibited high fluorescence quantum yield (0.80), limiting the photoacid quantum yield to (0.1) when excited at 400 nm. The direct photolysis of triarylsulfonium salts has been reported to occur primarily from the first excited singlet state. However, sensitization studies have shown that triplet triarylsulfonium salts are also labile.[21] Consequently, we proceeded to incorporate a nitro group in the structures to induce intersystem crossing.

Table I-1. Fluorescence Quantum Yields and Photoacid Quantum Yields of Sulfide Precursors and PAGs.

Compound	Φ_F	Φ_{H+}
5	1.0	--
7	0.8	0.03[a]
10	0.0	--
11	0.0	0.16[a]; 0.30[b]
12	0.0	--
13	0.1	0.01[b]; 0.04[d]
20	--	0.53[c]

[a]400 nm irradiation; [b]350 nm irradiation.[c]lit.[22]; [d]270 nm irradiation

As a result of this strategy, the fluorescence quantum yield of precursors **10** and **12**, and sulfonium salts **11** and **13**, were significantly decreased (Table I-1), thereby reducing the radiative decay pathway. Nitro-containing sulfonium salt **11** exhibited an increased photoacid quantum yield (Table I-1). The photoacid quantum yields were determined by a steady state method in which solutions of the PAGs in acetonitrile were selectively irradiated at the desired wavelength with an excitation source and monochromator of a spectrofluorometer. Rhodamine B was used as a sensor for photoacid generation, as reported by Scaiano *et al*.[23] Special care was taken to record the photodecomposition conversion no greater than 5% in order keep secondary photoproduct generation to a minimum.

Precursor **5** was prepared by a convergent synthesis (Scheme I-1) of benzyl bromide **2** and bisformylfluorene **4**. The phosphonate was obtained from 4-(phenylthio)benzaldehyde which was first reduced with $NaBH_4$ (10% in silica) aided by conventional, multimode microwave radiation.[24] Since hydrogen is extruded during the reaction, when carried out in scales larger than 0.500 g safety concerns lead us to run reaction at room temperature for 24 h.

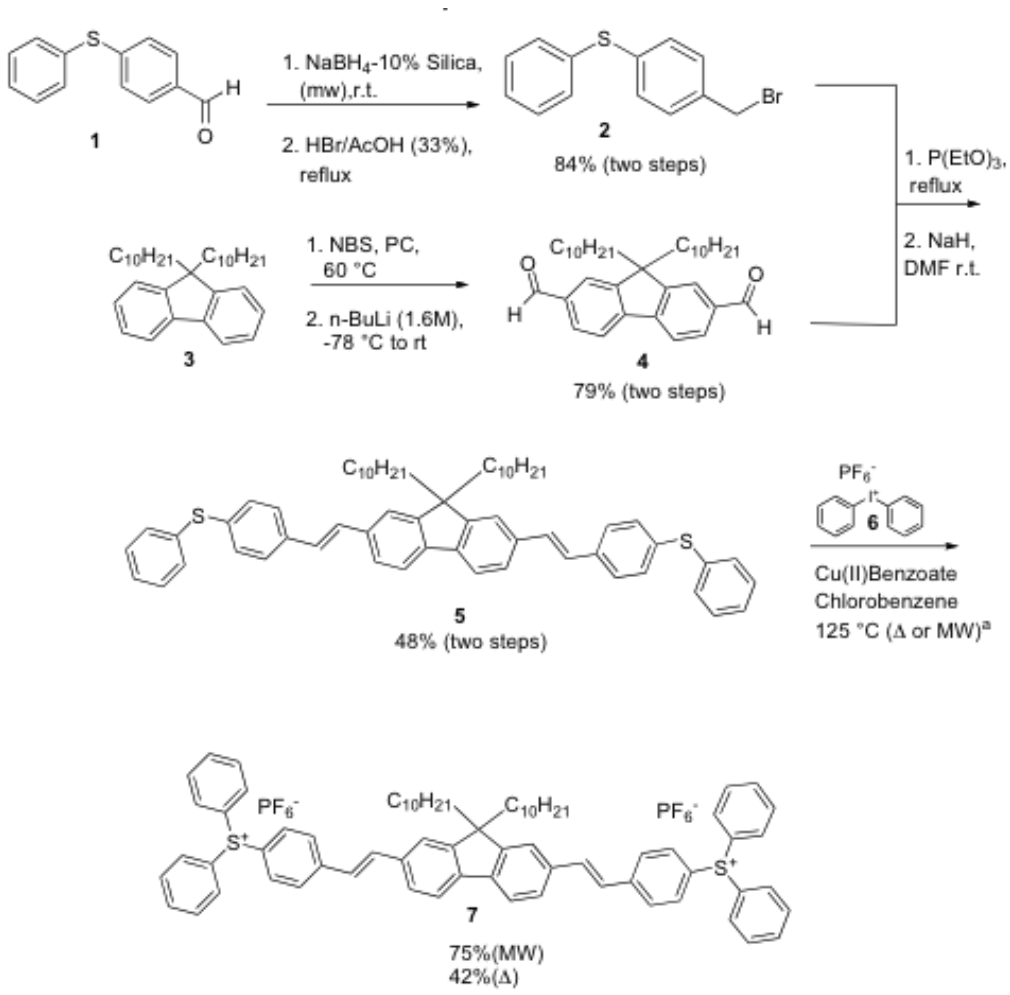

Scheme I-1. Synthesis of PAG **7.**

[a] Reactions were carried out both by conventional, Δ, and microwave heating methods, MW.

The resulting alcohol was refluxed in HBr (33% in AcOH) to obtain the benzylic bromide intermediate, subsequently used to obtain the bisphosphonate. The second branch of the synthesis started from fluorene, alkylation of the 9- position with bromodecane imparted the desired solubility to the molecule **3**.[25] Bromination with NBS of the 2- and 7- positions of the alkylated fluorene was followed by introduction of the

formyl group. Bisformyl fluorene **4** and the bisphosphonate were coupled via a Wadsworth-Horner-Emmons reaction, yielding exclusively the trans-isomer **5**. Bissulfide **5** was the precursor for bissulfonium salt **7** under both conventional and microwave-assisted procedures.

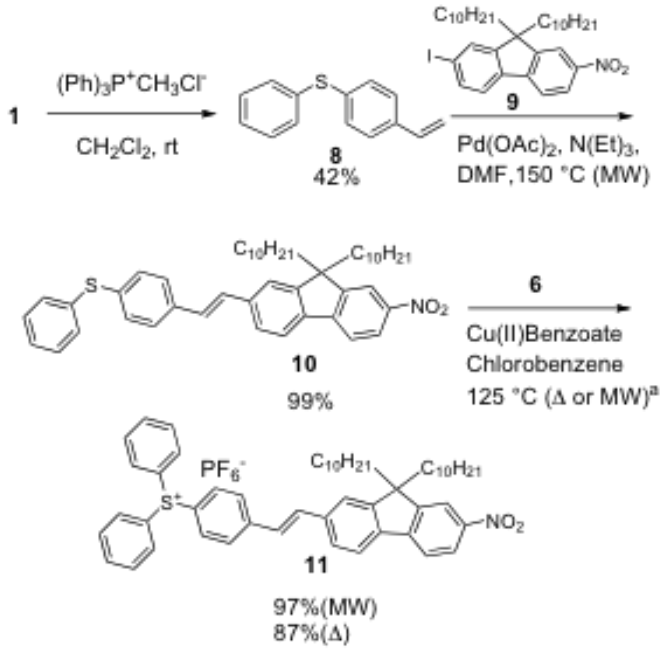

Scheme I-2. Synthesis of PAG **11.**

[a]Δ: 125 °C; MW: 100 W, closed vessel, standard mode; 40 psi; 125 °C.

Versatile 2-iodo-7-nitro-9,9-didecylfluorene **9** was used as a precursor in the synthesis sulfonium salts **11** and **13** (Schemes I-2 and I-3). It was prepared as reported by Belfield *et al.*[25] Interestingly, stilbenyl sulfide **10** was obtained quantitatively via a microwave-assisted palladium acetate-catalyzed Heck reaction, coupling vinyl sulfide **8** and precursor **9**. The yields for both conventional and microwave-assisted methods were the

highest for PAG **11** of the entire series. Fluorenylphenylsulfide **12** was prepared from Cu-catalyzed S-arylation of **9** and thiophenol.

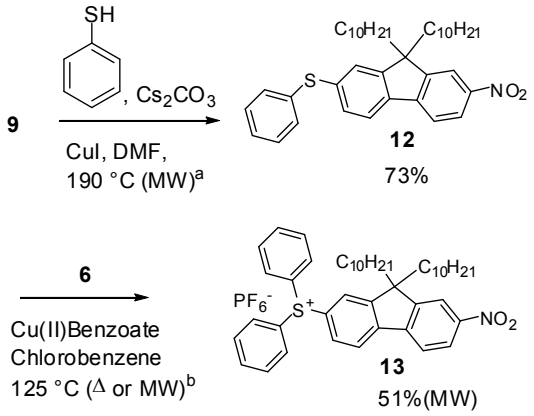

Scheme I-3. Synthesis of PAG **13.**

[a]150 W, closed vessel, standard mode; 100 psi; 190 °C. [b]Δ: 125 °C; MW: 100 W, closed vessel, standard mode, 40 psi, 125 °C.

Diphenyl sulfide **15** was prepared to evaluate how the thiophene and chalcone functionalities would withstand the rapid heating conditions of the microwave-assisted (MW) method, further demonstrating the versatility of the MW-method. Precursor **15** resulted from a straightforward Claisen condensation of acetylthiophene **14** and formyl phenyl phenyl sulfide **1** (Scheme I-4). Both functionalities were intact after the microwave assisted reaction was carried out.

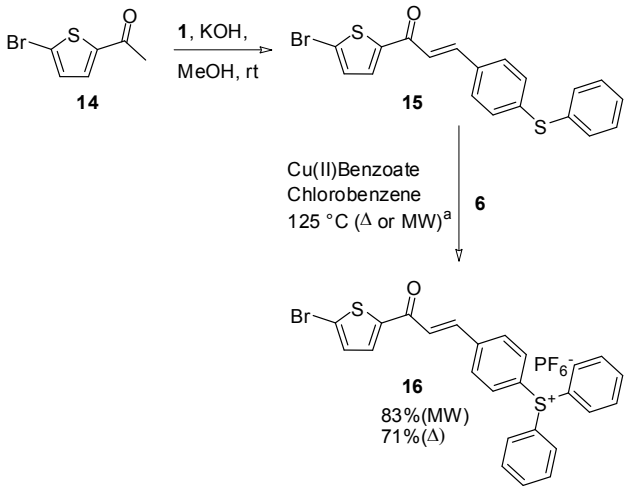

Scheme I-4. Synthesis of PAG **16.**

Δ: 125 °C; MW: 100 W, closed vessel, standard mode, 40 psi, 125 °C.

Furthermore, we sought to compare the effectiveness of this method when performed on less conjugated sulfides that may be more relevant in UV or deep UV lithographic applications (Scheme I-5). The yields of **18** and **20** were comparable to those reported in the literature. As in the previous precursors, microwave heating significantly reduced reactions times for the formation of these sulfonium salts when compared to conventional heating times performed by us, **21,** or reported in the literature, **20** and **22** (Table I-2).

The reactions that were carried out under conventional conditions were performed in an oil bath heated to 125 ºC at atmospheric pressure; whereas the microwave-assisted reactions were run at the same temperature in closed vessel mode, reaching pressures no higher that 30 psi.

In every case, the reactions that were heated conventionally took significantly longer than the analogous microwave reactions. Furthermore, in nearly every case the yields

were higher for the microwave-assisted preparation of the sulfonium salts than those formed by conventional heating.

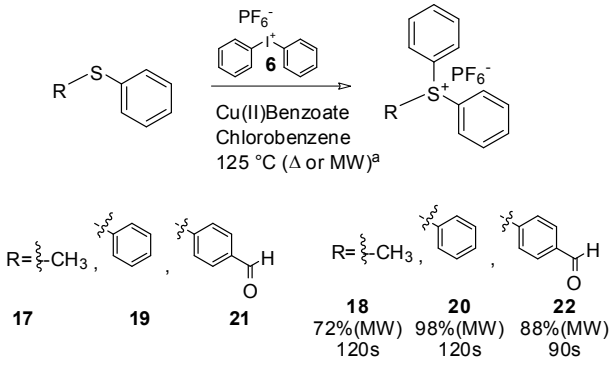

Scheme I-5. Synthesis of PAGs **18, 20** and **22.**

[a]Δ: 125 [o]C; MW: 100 W, closed vessel, standard mode, 40 psi, 125 [o]C.

Table I-2. Microwave-assisted vs. Conventional Heating Reaction Times for Sulfonium Salt PAG Formation.

Reagent	Product	MW Time (Yield)	Δ Time (Yield)
5	**7**	6 min (75%)	29 h (42%)
10	**11**	8 min (97%)	8 h (87%)
12	**13**	10 min (51%)	70 h (10%)
15	**16**	14 min (83%)	24 h (71%)
17	**18**	120 s (72%)	3 h (100%)[a]
19	**20**	120 s (98%)	3 h (97%)[b]
21	**22**	90 s (88%)	3 h (83%)

[a]literature[26]; [b]literature[18]

In conclusion, we have developed a new, more favorable methodology for the formation of sulfonium salts via microwave-assisted decomposition of diphenyliodonium salts in the presence of diphenylsulfides. Microwave-assisted reaction times were 90 to 420 times faster, resulting in generally higher yields. We have also shown that the

introduction of groups that favor intersystem crossing is a viable means for increasing the photoacid quantum yield of novel triarylsulfonium salt PAGs.

I.4 Experimental

I.4.1 Materials

Compounds **1**,[27] **4**,[28] and **9**,[11] were synthesized according to methods reported in the literature. Thioanisole and phenyl sulfide were used as provided by suppliers. All glassware was flamed dried and cooled in a desiccator over calcium chloride. All reactions were carried out under N_2 atmosphere. All sulfonium salt synthesis and purification were carried out under yellow light, red light, or in the dark. The sulfonium salt preparation, when carried out by conventional heating methods, was done according literature procedures using chlorobenzene as a solvent.[18]

I.4.2 Instrumentation

Absorption spectra were recorded with an Agilent 8453 UV–visible spectrophotometer. Steady-state fluorescence spectra were measured with a PTI Quantamaster spectrofluorometer in the photon counting regime of the PMT using an L-format configuration. The fluorescence spectra were corrected for the spectral dependence of the PMT. All measurements were performed at room temperature in 1 cm quartz cuvettes, with dye concentrations in the order of 10^{-6} M. Spectroscopic grade solvents, hexanes, THF, acetonitrile were obtained from Aldrich and used without any further purification. Fluorescence quantum yields of were determined relative to 9, 10-diphenylanthracene in cyclohexane as a standard.[29] In steady-state photoacid quantum yield determinations, the

excitation monochromator of the PTI spectrofluorometer was used to selectively excite the sample at the desired wavelength, and the intensity of the incident radiation was measured with an Ophir Power Star power meter equipped with a UV 1.44 cm^2 detector head. Rhodamine B was used as a sensor of photoacid generation, observing the change in optical density of the sulfonium salt did not exceed 5% as suggested in the literature.[23] All microwave-assisted reactions were run in a CEM Discover unit in closed vessel mode.

I.4.3 Synthetic Procedures and Characterization

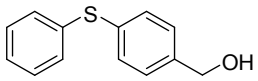

Preparation of (4-(phenylthio)phenyl)methanol. 4-(Phenylthio)benzadehyde **1** (2.00 g, 9.36 mmol), 0.36 g (9.42 mmol) $NaBH_4$, and 3.589 g of neutral alumina were placed in a 250 mL round bottom flask and stirred under. The reaction was followed by TLC (ethyl acetate:hexane 1:1) and stopped after 25.5 h, once the starting material was consumed entirely. The product was extracted with ethyl acetate and concentrated *in vacuo*. The crude product was purified by column chromatography (ethyl acetate:hexane 1:1) to obtain 1.77 g (88%) colorless needles. Mp 48.1-48.9 ºC; ^{1}H NMR (300 MHz, $CDCl_3$) 7.27 (m, 9H), 4.65 (d, 5.7 Hz, 2H), 1.77 (t, 5.4 Hz, 1H); ^{13}C NMR (75 MHz, $CDCl_3$) 141.2 (C), 136 (C), 135.2 (C), 132.8 (CH), 131.5 (CH), 129.8 (CH), 128.2 (CH), 127.3 (CH), 65.2 (CH_2), ^{13}C NMR DEPT 135 (75 MHz, $CDCl_3$) 132.8 (CH), 131.5 (CH), 129.8 (CH), 128.2 (CH), 127.3 (CH), 65.2 (CH_2). Elemental Analysis Calcd. for ($C_{13}H_{12}OS$): C, 72.19; H, 5.59; S, 14.82, Found C, 72.25; H, 5.58; S, 14.83.

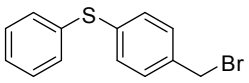

Preparation of (4-(bromomethyl)phenyl)(phenyl)sulfide, 2. The synthesis of (4-(bromomethyl)phenyl)(phenyl)sulfide was performed based on a modified procedure from Boekelheide *et al*.[30] (4-(Phenylthio)phenyl)methanol (0.532 g, 2.46 mmol) was refluxed in 10 mL of an HBr (33% in AcOH) for 2 h and later taken to room temperature. The reaction progress was followed by TLC every 15 min. Upon completion (12 h), the solution was extracted with chloroform (2x). The fractions were combined and washed with a sodium bicarbonate solution, rinsed with water (2x), and dried with anhydrous magnesium sulfate. After concentration, in vacuo, the crude was purified by column chromatography (ethyl acetate:hexane 1:1) to obtain 0.65 g (95%) of a colorless oil. ^{1}H NMR (300 MHz, $CDCl_3$) 7.088 (m, 9H), 4.23 (s, 2H); ^{13}C NMR (75 MHz, $CDCl_3$) 137.3 (C), 136.3 (C), 134.8 (C), 132.2 (CH), 130.5 (CH), 130.0 (CH), 129.6 (CH), 127.9 (CH), 33.5 (CH_2), ^{13}C NMR DEPT 135 (75 MHz, $CDCl_3$) 132.3 (CH), 130.5 (CH), 130.2 (CH), 129.8 (CH), 128.0 (CH), 33.7 (CH_2). Elemental Analysis Calcd. for ($C_{13}H_{11}BrS$): C, 55.92; H, 3.97; S, 11.48, Found: C, 56.00; H, 4.06; S, 11.37.

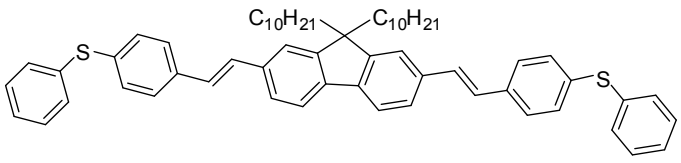

Preparation of (4,4'-(1E,1'E)-2,2'-(9,9-didecyl-9H-fluorene-2,7-diyl)bis(ethene-2,1-diyl)bis(4,1-phenylene))bis(phenylsulfane), 5. In a two-neck, 250 mL round bottom

flask, 0.651 g (2.33 mmol of (4-(bromomethyl)phenyl)(phenyl)sulfide, **2**, were dissolved in 6 mL of dry, freshly distilled triethylphosphite. The mixture, was taken to reflux and monitored by TLC until complete conversion of the starting material was observed (6 h). The unreacted triethylphosphite was evaporated by vacuum distillation, affording a viscous, pale yellow oil, which was used for the Horner-Emmons-Wadsworth reaction without further purification. The phosphonate, was dissolved in 10 mL of dry DMF and 1.11 g of NaH was added portion-wise to the solution. The mixture was stirred at room temperature for 1 h. A solution of 2,7-bisformylfluorene, **4**, (0.60 g, 1.2 mmol, in 5 mL of dry DMF) was added drop wise to the solution, which was then monitored by TLC until no 2,7-bisformylfluorene was observed (21 h). Once the reaction was complete, the solution was added drop wise to 150 mL of 0 ºC water. The resulting yellow oil was extracted with methylene chloride (2x) and washed (3x) with water, and dried with magnesium sulfate. The crude was purified by column chromatography on silica gel using an ethyl acetate:hexane mixture of 1:1 and run under N_2. The yellow oil obtained 0.96 g (48% in two steps) crystallized after several days. Mp 59.6-61.1ºC; ^{1}H NMR (300 MHz, $CDCl_3$) 7.66 (d, 4.8 Hz, 2H), 7.33 (m, 26H), 2.02 (m, 4H), 1.10 (m, 28H), .093(m, 42 H); ^{13}C NMR (75 MHz, $CDCl_3$) 151.8 (C), 140.9 (C), 136.7 (C), 136.3 (C), 136.0 (C), 134.9 (C), 131.5 (CH), 131.2 (CH), 129.9 (C), 129.4 (CH), 127.3 (CH), 127.3 (C), 126.0 (C), 121.0 (C), 120.2 (C). 109.1 (C), 55.3 (C), 40.8 (C), 32.2 (C), 30.4 (C), 30.0 (C), 29.9 (C), 29.7 (C), 24.1 (C), 23.0 (C), 14.5 (C). Elemental Analysis Calcd. for ($C_{61}H_{70}S_2$): C, 84.47; H, 8.13; S, 7.39, Found: C, 84.28; H, 8.24; S, 7.21.

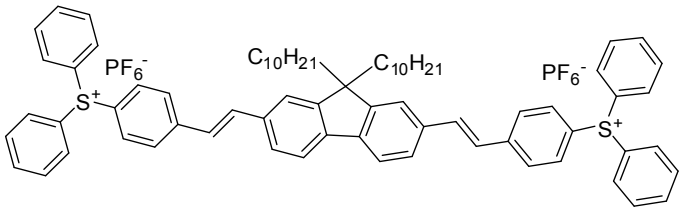

General procedure for the microwave-assisted preparation of sulfonium salts. Preparation of (4,4'-(1E,1'E)-2,2'-(9,9-didecyl-9H-fluorene-2,7-diyl)bis(ethene-2,1-diyl)bis(4,1-phenylene))bis(diphenylsulfonium) hexafluorophosphate(V), 7. In a 2 mL glass reaction vessel, 0.21 g (0.24 mmol) of **5**, 0.21 g (0.48 mmol) of diphenyliodonium hexafluoro phosphate (V), **6**, and 0.006 g (5% molar) copper(II) benzoate were mixed in the dark in 2 mL of chlorobenzene while being purged with N_2. The microwave was set to closed vessel standard mode; maximum pressure 40 psi; maximum temperature 125 ºC, maximum power 100 W, high speed stirring. The run time (time at which the reaction reaches max temperature or pressure) was set for 30 s and the hold time for 1 min. The reaction was monitored by TLC until most of the starting material had disappeared. Upon completion, 12 min hold time, the solvent was vacuum distilled affording a dark yellow crude. ^{1}H NMR revealed the presence of what appeared to mono-(45%) and bissulfonium (55%). The derivatives that were separated by column chromatography using hexane:ethyl acetate 6:4 as eluent, the faster eluting fraction (likely the mono-sulfonium) quickly decomposed and wasn't characterized. The second fraction was a dark yellow solid (0.239 g, 77%): Mp 63.5-65.8 ºC; ^{1}H NMR (500 MHz, acetone-d_6) 8.08 (d, 10 Hz, 4H), 7.93 (m, 28H), 7.70 (m, 4H), 7.53(d, 20 Hz, 2H), 2.15 (m, 4H), 1.14 (m, 28H), 0.78 (t, 5Hz, 6H), 0.65 (m, 4H). ^{13}C NMR (125 MHz, acetone-d_6) 151.8 (C), 144.4 (C), 141.7 (C), 136.0 (C), 134.7 (CH), 134.5 (C), 131.9

(CH), 131.6 (CH), 131.2 (CH), 129.0 (CH), 126.9 (C), 125.5 (C), 125.3 (CH), 121.8 (C), 120.5 (C), 120.4 (C), 55.1 (C), 40.0 (C), 31.7 (C), 23.6 (C), 22.3 (C), 13.5 (C). Elemental Analysis Calcd. for ($C_{73}H_{80}F_{12}P_2S_2$): C, 66.85; H, 6.15; S, 4.89, Found: C, 66.94; H, 6.28; S, 4.69.

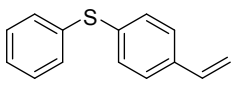

Preparation of phenyl(4-vinylphenyl)sulfane, 8. Methyl triphenyl phosphonium bromide (1.10 g, 3.1 mmol), was dissolved in methylene chloride while the vessel was purged with nitrogen. Sodium methoxide (1.46 g, 27 mmol) was quickly added and the vessel was nitrogen purged for another 15 min and subsequently stirred for 2 h. A solution of **1** (0.50 g, 2.35 mmol in 2.0 mL of methylene chloride) was added dropwise in the mixture. The reaction was kept at room temperature and followed to completion by TLC (18 h). Upon completion, the solvent was evaporated *in vacu*o and the resulting oil was redisolved in ethyl ether to precipitate triphenylphosphine oxide. The filtrate was concentrated and purified by column chromatography on silica gel using hexane as an eluent, affording pale yellow oil, 0.21 g (42%).

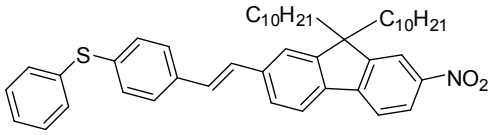

Preparation of (E)-(4-(2-(9,9-didecyl-7-nitro-9H-fluoren-2-yl)vinyl)phenyl)(phenyl)sulfane, 10. In a 2 mL glass reaction vessel 9,9-didecyl-2-iodo-7-nitro-9H-fluorene, **9** (0.49 g, 0.73 mmol) and phenyl(4-vinylphenyl)sulfane, **8** (0.12 g, 0.60 mmol) were dissolved in 2 mL of dry DMF with 0.01 g (0.06 mmol, 10% molar) of palladium acetate, and 0.80 g (7.9 mmol) of triethylamine. The mixture was purged with N_2 for 15 min while it was stirred. The microwave was set to closed vessel standard mode; maximum pressure 250 psi; maximum temperature 150 ºC, maximum power 60 W, high speed stirring. The run time (time at which the reaction reaches max temperature or pressure) was set for 30 s and the hold time for 30 min. The reaction was monitored by TLC every 30 s, and after 7.5 min the starting material was not observed. The mixture was cooled to room temperature and filtered through a Celite plug. The filtrate was dissolved with methylene chloride, washed with water (4x), dried over anhydrous magnesium sulfate, and concentrated. The resulting dark brown oil was purified by column chromatography (hexane:ethyl acetate 9:1). A yellow oil 0.38 g (99%) was obtained, that crystallized on standing after several days. Mp 71.6-72.3 ºC; ^{1}H NMR (300 MHz, $CDCl_3$) 8.25 (dd,3 Hz, 9Hz 1 H), 8.16 (d, 1.5Hz, 1H), 7.72 (dd, 3 Hz, 9Hz, 2 H), 7.52(d, 17 Hz, 1H), 7.46 (m, 3H), 7.30 (m, 7H), 7.17 (s, 2H), 2.04 (t, 6 Hz, 4H), 1.14 (m, 28H), 0.78 (t, 5Hz, 6H), 0.65 (m, 4H). ^{13}C NMR (75 MHz, $CDCl_3$) 153.1 (C), 152.3 (C), 147.4 (C), 147.2 (C), 138.6 (C), 138.5 (C), 136.1 (C), 135.8 (C),

135.6 (C), 131.5 (CH), 131.2 (CH), 129.5 (CH), 129.1 (C), 128.8 (C), 127.5 (CH), 126.2 (C), 123.6 (C), 121.7 (C), 121.2 (CH), 119.9 (C), 118.4 (C), 56.0 (C), 40.5 (C), 33.9(C), 32.2 (C), 30.2 (C), 29.9 (C), 29.6 (C), 29.6 (C), 24.1 (C), 23.0 (C), 14.5 (C). Elemental analysis calcd. $C_{47}H_{59}NO_2S$: C, 80.41; H, 8.47; S, 4.57; Found: C, 80.20; H, 8.32; S, 4.45.

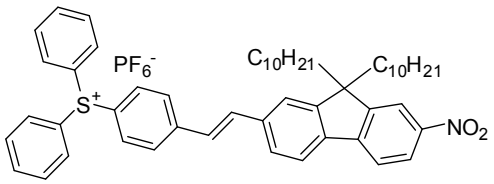

Preparation of (E)-(4-(2-(9,9-didecyl-7-nitro-9H-fluoren-2-yl)vinyl)phenyl)diphenylsulfonium hexaflourophosphate (V), 11. The preparation of sulfonium salt **11** was carried out according to the general procedure reported above. After purification, a yellow solid was obtained (0.23 g, 97%). Mp 62.4-64.5 ºC; ^{1}H NMR (300 MHz, DMSO-d_6) 8.26 (d, 2Hz 1 H), 8.18 (dd, 2 Hz, 8 Hz, 1H), 7.96 (m, 4 H), 7.74 (m, 14H), 7.58 (d, 16.2 Hz, 1H), 7.46 (d, 16.2 Hz, 1H), 7.17 (s, 2H), 2.04 (t, 6 Hz, 4H), 1.01 (m, 28H), 0.69 (t, 5Hz, 6H), 0.41 (m, 4H). ^{13}C NMR (75 MHz, $CDCl_3$): 153.1 (C), 152.3 (C), 147.4 (C), 147.1 (C), 138.6 (C), 138.5 (C), 136.0, (C), 135.8 (C), 135.6 (C), 131.5 (CH), 131.1 (CH), 129.5 (CH), 129.1 (C), 128.8 (C), 127.5 (CH), 126.3 (C), 123.6 (C), 121.7 (C), 121.2 (CH), 119.9 (C), 118.4 (C), 56.0 (C), 40.5 (C), 33.9(C), 32.2 (C), 30.2 (C), 29.9 (C), 29.6 (C), 29.6 (C), 24.1 (C), 23.0 (C), 14.5 (C) Elemental analysis calcd. $C_{53}H_{64}F_6NO_2PS$: C, 68.88; H, 6.98; S, 3.47; Found: C, 68.60; H, 7.03; S, 3.47.

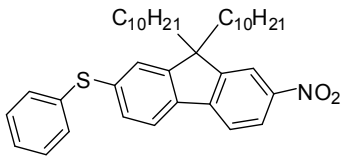

Preparation of 9,9-didecyl-7-nitro-9H-fluoren-2-yl)(phenyl)sulfane, 12.

In a 2 mL glass reaction vessel 9,9-didecyl-2-iodo-7-nitro-9H-fluorene, **9** (0.52 g, 0.84 mmol) and thiophenol (0.11 g, 1.03 mmol) were dissolved in 2 mL of dry DMF with copper iodide (0.01 g, 0.07 mmol, 8% molar), and cesium carbonate (0.62 g, 1.92 mmol). The mixture was purged with N_2 for 15 min while it was stirred. The microwave was set to closed vessel standard mode; maximum pressure 100 psi; maximum temperature 190 ºC, maximum power 150 W, and high speed stirring. The run time (time at which the reaction reaches max temperature or pressure) was set for 30 s and the hold time for 2 min. The reaction was monitored by TLC every 2 min, after 8 min the starting material had disappeared. The mixture was cooled to room temperature and was dissolved with methylene chloride, washed with water (4x), dried over anhydrous magnesium sulfate, and concentrated. The resulting light brown oil was purified by column chromatography (hexane:ethyl acetate 99:1). A light yellow oil 0.37 g (73%) was obtained. ^{1}H NMR (300 MHz, $CDCl_3$) 8.23 (d, 9Hz 1 H), 8.16 (s, 1H), 7.73 (d, 8 Hz, m, 1H), 7.66 (d, 8 Hz, m, 1H), 7.30 (m, 7H), 1.95 (m 4H), 1.10 (m, 28H), 0.85 (t, 6Hz, 6H), 0.57 (m, 4H); ^{13}C NMR (75 MHz, $CDCl_3$) 153.5 (C), 152.0 (C), 147.3 (C), 147.0 (C), 137.9 (C), 137.8(C), 131.3 (CH), 130.1 (C), 129.5 (CH), 127.6 (C), 125.7 (C), 123.6 (C), 122.0 (C), 120.0 (C), 118.5 (C), 56.1 (C), 40.3 (C), 32.3 (C), 30.2 (C), 29.9 (C), 29.7 (C), 24.2 (C), 23.1 (C),

14.5 (C). Elemental analysis calcd. $C_{39}H_{53}NO_2S$: C, 78.08; H, 8.90; S, 5.34: Found: C, 77.84; H, 8.65; S, 5.13.

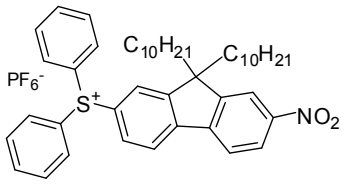

Preparation of (9,9-didecyl-7-nitro-9H-fluoren-2-yl)diphenylsulfonium hexafluorophosphate(V), 13. The preparation of sulfonium salt **11** was performed according to the general procedure reported above. After purification, a light yellow solid was obtained (0.08 g, 51%). Mp 42.7-44.6 ºC; ^{1}H NMR (300 MHz, $CDCl_3$) 8.33 (dd, 3Hz, 6Hz, 1 H), 8.25 (d, 3 Hz, 1H), 8.14 (d, 6Hz, 1 H), 7.97 (d, 6Hz, 1 H), 7.72 (m, 12H), 2.04 (t, 3 Hz, 4H), 1.10 (m, 28H), 0.85 (t, 5Hz, 6H), 0.51 (m, 4H). ^{13}C NMR (75 MHz, $CDCl_3$) Elemental analysis calcd. $C_{45}H_{58}F_6NO_2PS$: C, 65.75; H, 7.11; S, 3.90 ; Found: C, 65.90; H, 7.11; S, 4.11.

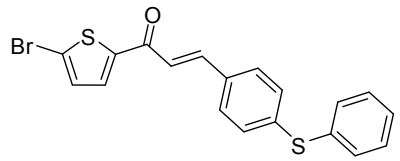

Preparation of (E)-1-(5-bromothiophen-2-yl)-3-(4-(phenylthio)phenyl)prop-2-en-1-one, 15. To a solution of acetylthiophene **16** (0.40 g, 2.00 mmol) in methanol at room temperature was added 0.11 g of powdered KOH. The mixture was stirred for 30 min then formyl phenyl phenyl sulfide **1** (0.43g, 2.0 mmol) was added. The reaction was let stir 10 h, resulting in a solid that was crystallized from an acetone water solution,

yielding 0.6507 g (81%) of a colorless solid. Mp 149.8-150.2 ºC; ^{1}H NMR (500 MHz, $CDCl_3$) 7.78 (d, 15Hz, 1 H), 7.57 (d, 5 Hz, 1H), 7.52 (d, 9Hz, 2 H), 7.47 (m, 2 H), 7.39 (m, 2H), 7.26 (m, 4H), 7.15 (d, 5 Hz, 1H). ^{13}C NMR (125 MHz, $CDCl_3$) 180.7 (CHO), 152.0 (C), 147.3 (C), 147.0 (C), 143.8 (CH), 141.0 (C), 133.1 (CH), 133.3 (C), 131.7 (CH), 131.3 (CH), 129.6(CH), 129.1 (CH). 129.0 (CH), 128.3 (CH), 123.1 (C), 120.0 (CH). Elemental analysis calcd. $C_{19}H_{13}BrOS_2$ C, 56.86; H, 3.26; S, 15.98: Found: C, 57.01; H, 3.28; 16.04.

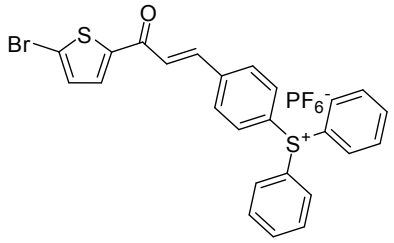

Preparation of (E)-(4-(3-(5-bromothiophen-2-yl)-3-oxoprop-1-enyl)phenyl)diphenylsulfonium hexafluorophosphate(V), 16. The preparation of sulfonium salt **11** was accomplished according to the general procedure reported above. After purification, a light yellow solid was obtained (0.225 g, 83%). Mp 72.1-73.9ºC; ^{1}H NMR (500 MHz, $CDCl_3$) 8.25 (d, 9Hz, 2 H), 8.06 (d, 5 Hz, 1H), 7.89 (m, 14H), 7.35 (d, 5Hz, 1H). ^{13}C NMR (125 MHz, $CDCl_3$) 180.2 (CHO), 147.2 (C), 140.8 (C), 140.6 (C), 134.9 (CH), 134.2 (C), 132.5 (C), 131.8 (CH), 131.7 (CH), 131.4 (CH), 131.2 (CH), 126.0 (C), 125.1(C). 124.8 (C), 123.0 (C). $C_{25}H_{18}BrF_6OPS_2$: C, 48.17; H, 2.91; S, 10.29, Found: C, 48.25; H, 3.03; S, 10.17.

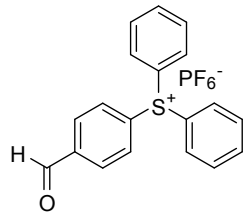

Preparation of (4-formylphenyl)diphenylsulfonium hexafluorophosphate(V), 22. The preparation of sulfonium salt **22** was carried out according to the general procedure reported above from the commercially available sulfide **21**. After purification, a colorless solid was obtained (0.378 g, 88%). ^{1}H NMR (500 MHz, acetone-d_6) 10.24 (s, 1 H), 8.34 (d, 9 Hz, 2H), 8.15 (d, 9 Hz, 2H), 8.08 (m, 6H), 7.91 (t, 9Hz, 4H) ^{13}C NMR (125 MHz, acetone-d_6) 191.2 (CHO), 140.3 (C), 135.0 (CH), 131.9 (CH), 131.7 (CH), 131.6 (CH), 131.5 (CH), 130.8 (C), 124.4 (CH). $C_{19}H_{15}F_6OPS$: C, 52.30; H, 3.46; S, 7.35, Found: C, 52.47; H, 3.43; S, 7.25.

CHAPTER II: PHOTOSENSITIVE POLYMERIC MATERILAS FOR TWO-PHOTON 3D WORM OPTICAL DATA STORAGE SYSTEMS

Reproduced with permission from: Yanez, C. O.; Andrade, C. D.; Yao, S.; Luchita, G.; Bondar, M. V.; Belfield, K. D. *ACS Applied Materials & Interfaces* **2009**. DOI: 10.1021/am900587.

II.1 Abstract

We report the photochemistry and development of a fluorescence readout-based, nonlinear absorption three-dimensional (3D) optical data storage system. In this system, writing was achieved by acid generation upon two-photon absorption (2PA) of a photoacid generator (PAG) (at 710 or 730 nm). Readout was then performed by interrogating two-photon absorbing dyes, after protonation, at 860 nm. Linear and nonlinear photophsyical characterization of 2PA PAGs and acid-sensitive fluorescent dyes demonstrate good spectral resolution between the PAG and protonated 2PA dye and relatively high two-photon absorptivity. Solution spectroscopic studies confirm photoacid generation and dye protonation. Two-photon recording and readout of voxels was demonstrated in five and eight consecutive, crosstalk-free layers within a polymer matrix, generating a data storage capacity of up to 1.8×10^{13} bits/cm^3.

II.2 Introduction

Data is being generated at a remarkably explosive rate. For example in 2006 alone, 161 exabytes (161 billion gigabytes) of new data was generated worldwide and is projected to grow to 1800 exabytes by 2011. The key driving force of future development is expected to be the rapid expansion of the internet and multimedia, such as high definition television (HDTV) with their requirements for higher bandwidth and storage capacity. The storage capacities of current optical data storage (ODS) technologies like the compact disc (CD), digital video disc (DVD), and Blu-ray depend on bit density that can be achieved on the two-dimensional, 2D, recording surface. In all of these technologies this bit density is limited by the Raleigh criterion, that when applied to ODS can be expressed as: $D \alpha k (S . NA^2/ \lambda^2)$ where D is the storage capacity (usually expressed in bytes), S is the effective recording surface, NA is the numerical aperture of the scanning objective used for the writing process, and λ is the wavelength used for recording the information.[31] Currently, the capacity of ODS systems has increased by increasing the NA of the scanning objective, decreasing the wavelength of the source, or both. Further changes in these two parameters, beyond what is currently employed by the Blu-ray™ system (N.A. = 0.85, λ = 405 nm), is not feasible or too expensive to be implemented in commercial ODS systems.

To overcome the limitations imposed by the diffraction limit of the wavelength used for writing and readout, new ODS systems have relied on nonlinear optical properties of their components. The storage capacity advantage that nonlinear absorption-based ODS systems have over their linear counterparts is based on the quadratic dependence of two-

photon absorption (2PA) with respect to the intensity of incident light. This quadratic dependence of 2PA enables the photochemical or photophysical processes that depend on this absorption to be confined to very small volumes. Hence, this nonlinear dependence leads to immense data storage capacity.[32] Several efforts have been made to further develop both erasable (rewritable)[7] and non-erasable (permanent or write-once read-many, WORM)[6,32,33] systems. The increased spatial resolution of nonlinear absorption processes enables true three-dimensional, 3D, ODS, and many recent efforts have proven that sub diffraction limit features can be recorded when the 2PA properties of the ODS systems are exploited. A key step in this direction in the ODS field was reported by Rentzepis *et. al.* in 1989.[5] In this work two-photon writing, erasing, and reading were achieved by the photochromic interconversion of spyrobenzopyranes.

We previously reported a 2D fluorescence readout WORM system where the protonation of a 2PA dye **23** was achieved by using a commercially available PAG, developed originally for UV-curing.[6] Because of limited p-conjugation, the 2PA cross sections of commercially available PAGs are low,[13] significantly hindering development of this type of ODS system. To increase the efficiency of this system, 2PA PAGs with higher cross sections were needed. Herein, we report the use of new photosensitive polymeric systems, comprised of novel, acid sensitive 2PA absorbing dyes **24**-**26** and significantly improved sulfonium PAGs **4**-**6** (Figure II-1) in different polymer matrices. One of these new systems, containing novel PAG **11** and a new 2PA absorbing dye **24** enabled true 3D (multilayer) WORM optical data storage where the two-photon advantage is fully exploited. This improved ODS system allowed the two-photon

recording and readout of voxels in eight consecutive layers within the polymer matrix, resulting in a crosstalk-free system in which the 3D character of this 2PA ODS was demonstrated.

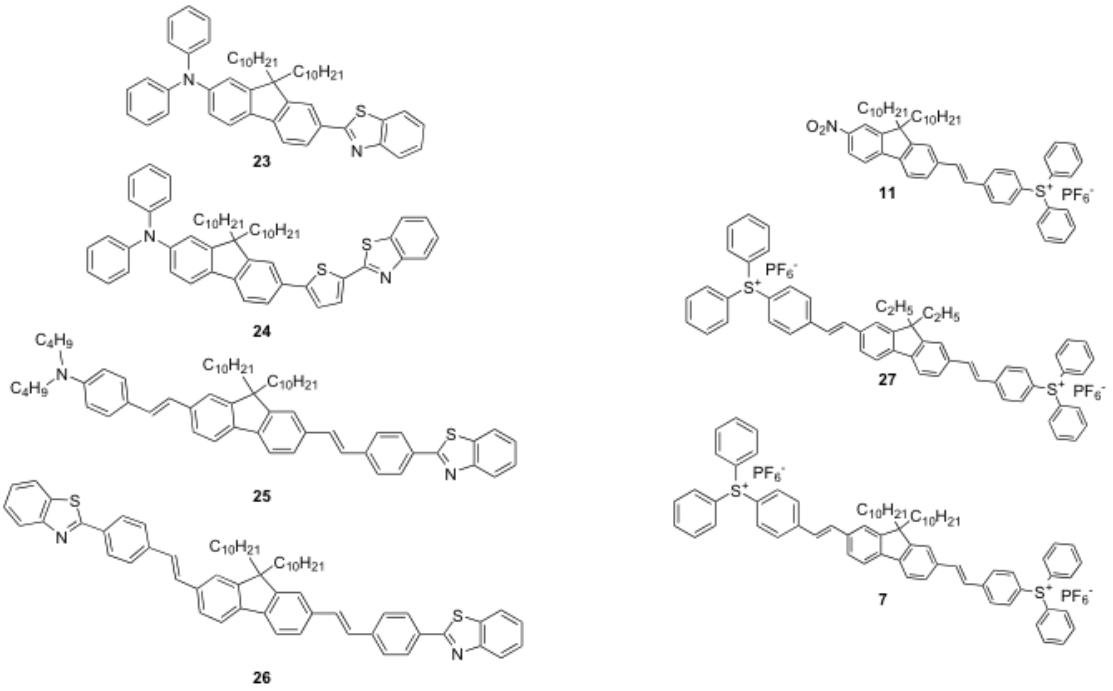

Figure II-1. 2PA acid-sensitive dyes **1-4** and 2PA sulfonium PAGs **5-7.**

II.3 Results and Discussion

II.3.1 The System

The ODS system is composed of an acid-sensitive fluorescent dye, a PAG, and a polymer substrate. Information recording or writing in the ODS system was achieved by the monoprotonation of the 2PA fluorescent dye upon photogeneration of H^+. For example, when dye **23** was used, the benzothiazole nitrogen was protonated when the

corresponding PAG was exposed by one or two-photon irradiation. Irradiation of localized volumes within the polymer matrix, where the sulfonium salt is found in 5% (w/w), induced the generation of hexafluorophosphoric acid. In the particular case of dye **23**, because the pK_b of the benzothiazole nitrogen ($pK_b \approx 13$)[34] is lower than that of the diphenylamino nitrogen functionality ($pK_b \approx 19$),[35] the benzothiazole nitrogen was the first to be protonated upon production of superacid. The monoprotonated species of the 2PA dye exhibited a large bathochromic shift in the absorption spectrum (Figure II-2, **23a**), due to the increase of electron withdrawing character of the protonated benzothiazole. Hence, emission of the monoprotonated form is at longer wavelengths than that of the unexposed, neutral form of the dye.[6] Nonprotonated **23** and protonated **23a** can be interrogated for readout, enabling positive and negative images when addressing the exposed polymer at shorter or longer wavelengths, respectively (i.e., at short wavelength readout, one excites the nonprotonated dye, resulting in short wavelength emission while one can irradiate the protonated dye at longer wavelength, resulting in long wavelength emission for two channel readout). Longer wavelength readout had the advantage that the photoacid was unaffected at these wavelengths, resulting in nondestructive readout. All three components of the ODS system were evaluated: 2PA dye, polymer matrix, and 2PA PAG.

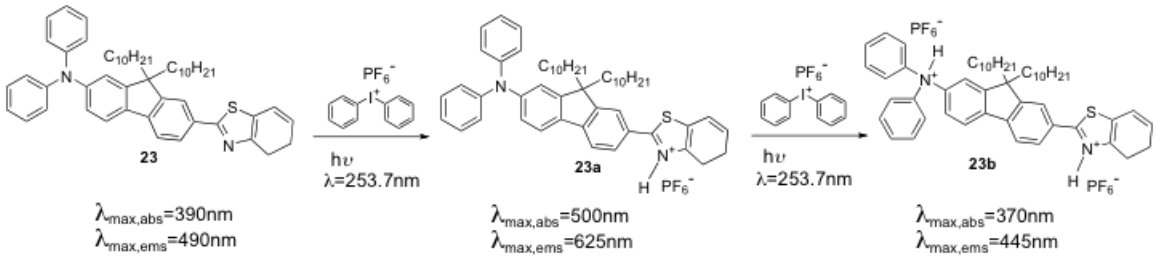

Figure II-2. Protonation of 2PA fluorescent dye 23 in ACN solution with excess of diphenyliodonium hexafluorophospahte. Exposure to 254 nm radiation produces and increase in photoacid concentration, including dye protonation.

II.3.2 2PA Fluorescent Dyes

II.3.2.1 Spectroscopic Studies in Solution

The dyes that were tested had nitrogen atoms of varying basicity that can undergo protonation upon the generation of photoacid and, as a consequence, change their absorption and emission properties. Besides amines, the only other scaffold that has been used for nonlinear WORM ODS systems with a PAG has been lactones (rhodamine B base) that have been interrogated upon ring opening.[33] To assess advantages and disadvantages of using systems with more basic N,N-dibutyl anilines (instead of triaryl anilines) for writing and readout, dye **25** was characterized and evaluated. Spectrophotometric absorption studies of **25** in solution with dipheyliodonium hexaflourophosphate show an initial, rapid blue shift of the absorption λ_{max} of this dye after 3 s irradiation (Figure II-3, **25a**), due to the protonation of the N,N-dibutyl aniline, as demonstrated by ^{1}H NMR and COSY studies (not shown). This blue shift was followed by a progressive red shift, due to the formation of species **25b**, which facilitated

recording and image readout from both channels (shorter and longer wavelength). As can be seen in Figure II-4, the highest concentration in solution of the protonated species **25b** was reached after 15 s irradiation. Overexposure leads to a hypsochromic shift, resulting in a species with an absorption λ_{max} of approximately 330 nm. Interrogating this blue shifted species would result in destructive readout because either the absorption or fluorescence spectra would overlap with the spectrum of the PAG, likely inducing the photoacid generation. Furthermore, the 2PA wavelength would be below the output window (700-1000 nm) of commercial Ti:sapphire femtosecond laser systems. Despite these limitations, the versatility of the system allowed recording and read out, via one-photon absorption (1PA), in both channels (Figure II-6).

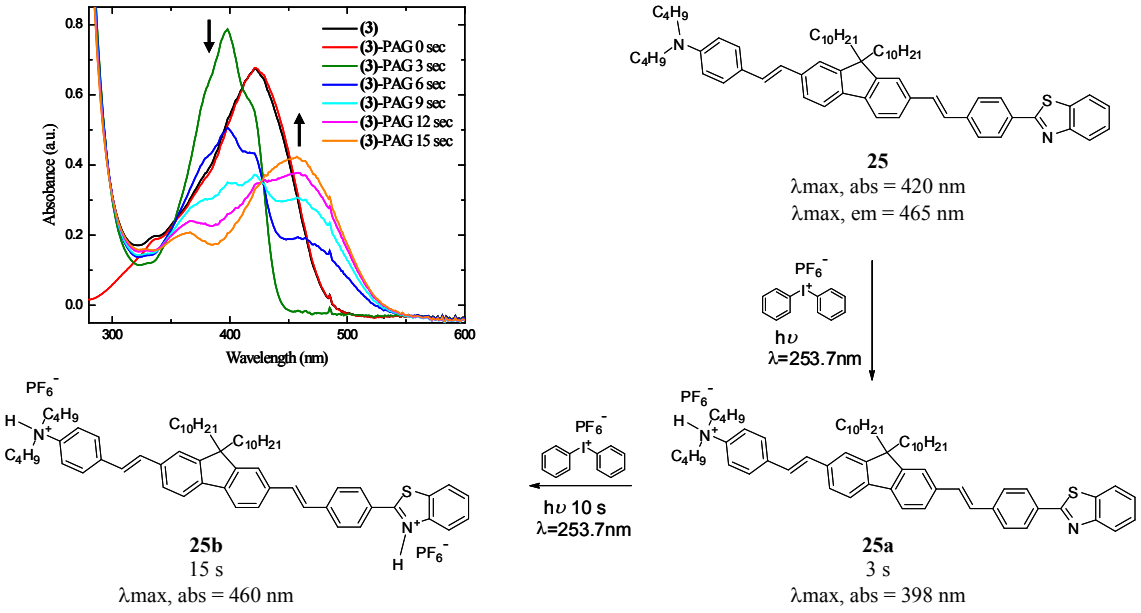

Figure II-3. Spectral changes of **25** in ACN solution with diphenyliodonium hexafluorophosphate upon irradiation at 254 nm. Equilibrium of species **25** and **25a** after 0-3 s of irradiation. Equilibrium of species **25** and **25b** after 3-15 s of irradiation.

The behavior of dyes containing aromatic amines as a donor and benzothiazole as an electron acceptor moiety (D-π-A), such as **23** and **24,** is more predictable since the benzothaizole nitrogen is slightly more basic and will be the first to protonate once the acid is generated upon irradiation, yielding, e.g., species **24a**. Solution studies of dye **24** (Figure II-4) indicated that overexposure resulted in less of a blue shift upon generation of diprotonated species **24b**. This effect gave the system greater tolerance to excessive irradiation time and power as species **24a** and **24b** can both be interrogated at wavelengths at which the PAGs will not absorb. Furthermore, the absorption band profile of species **24a** extended beyond 600 nm, this ultimately enabled effective 2PA readout at longer wavelengths (860 nm), see below, where 2PA of the PAG was negligible.

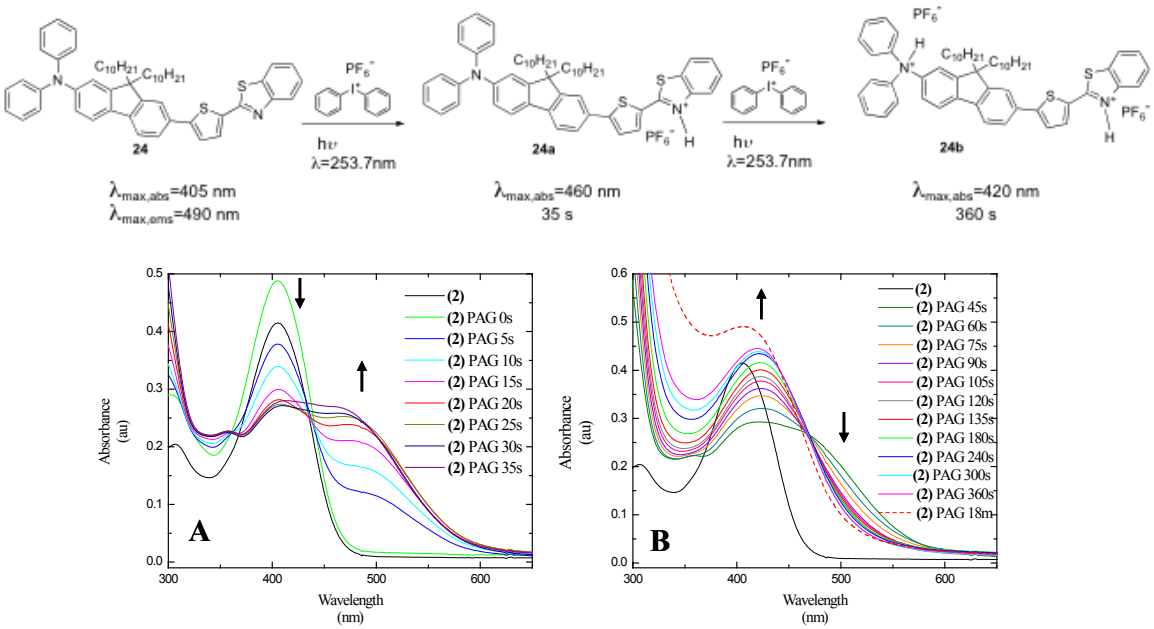

Figure II-4. Spectral changes of **24** in ACN solution with diphenyliodonium hexafluorophosphate (PAG) upon irradiation at 254 nm. A) Equilibrium of species **24** and **24a** at 0-35 s of irradiation. B) Equilibrium of species **24a** and **24b** at 45 s-18 min of irradiation.

The symmetrical A-π-A system of dye **26** was quickly converted to a D-π-A structure upon photoacid generation, as shown by Figure II-5, generating species **26a**. The clear transitions observed in solution studies reveal the protonation of one benzothiazole group, generating a bathochromic shift due to the increased electron withdrawing properties of the protonated benzothiazole, followed by the protonation of the second benzothaizole and subsequent hypsochromic shift, generating species **26b**. This dye, however, presented solubility problems within the polymer matrix. At concentrations higher than

1.5% (W/W) the dye molecules crystallized, generating scattering domains that significantly affected the optical quality of the polymer film.

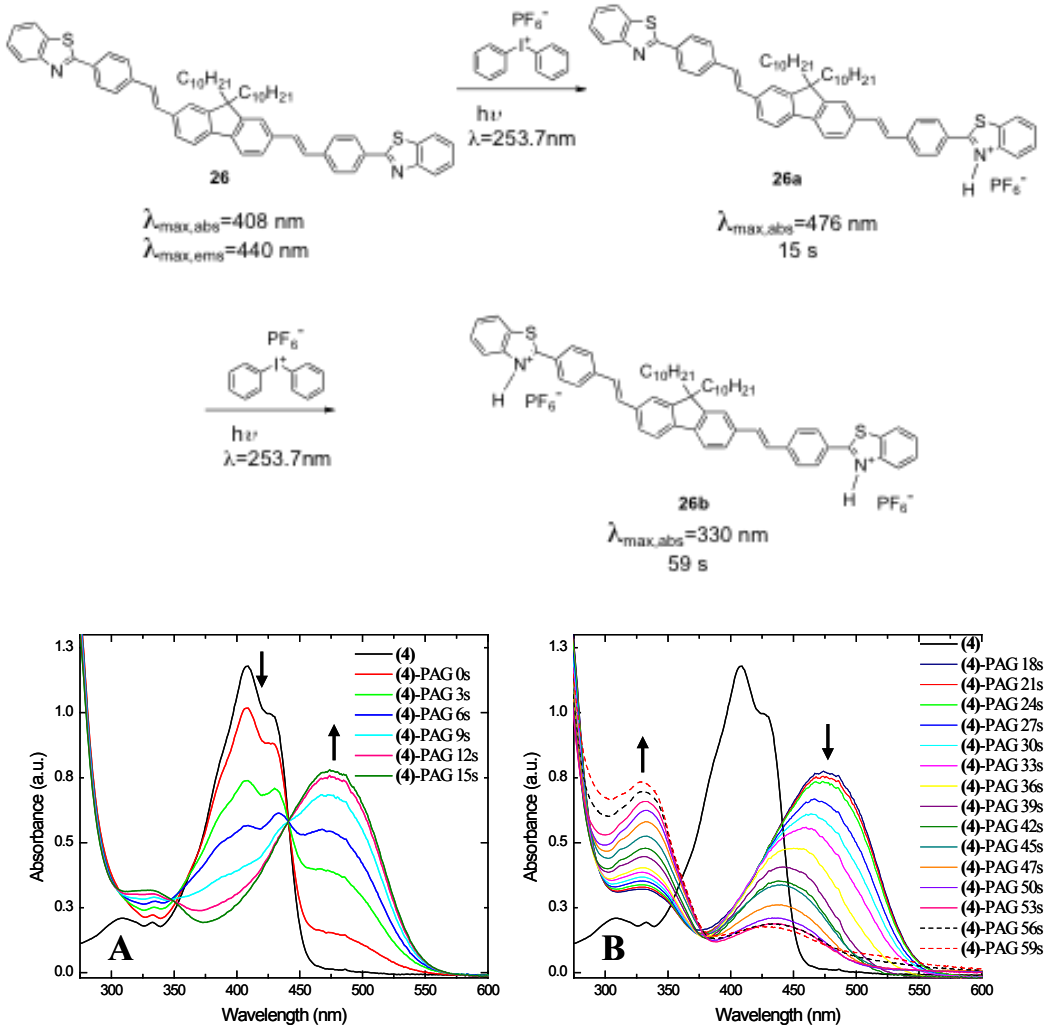

Figure II-5. Spectral changes of **26** in ACN solution with diphenyliodonium hexafluorophosphate (PAG) upon irradiation at 254 nm. A) Equilibrium of species **26** and **26a** at 0-15 s of irradiation. B) Equilibrium of species **26a** and **26b** at 18-59 s of irradiation.

II.3.2.2 Photophysical Properties

The two-photon absorption cross sections of the fluorescent unprotonated dyes ranged between 28-1550 GM at 730 nm and between 0-550 GM at 860 nm (Table I-1). As discussed for the PAGs, the 2PA cross section values and the fluorescence quantum yields are key parameters for the 2PA fluorescent dyes in these optical data storage systems. However, the other properties discussed above such as: 1) immediate red shift upon protonation and 2) resilience of the dye to blue shift when excess acid is generated due to overexposure are also important. Consideration of all photophysical properties (high two-photon cross sections, high fluorescence quantum yields, immediate red shift upon protonation, and no blue shifting of the dye upon overexposure) were considered as a whole and led us to prefer dye **24** over dyes **23**, **25**, and **26** when developing the final system.

Table II-1. Fluorescence Quantum Yields (Φ_F) and 2PA cross sections (δ) of 2PA dyes **23-26** (measured in hexane except for **25** which was measured in cyclohexane).

Compound	Φ_F*	δ_{730nm} (GM)	δ_{760nm} (GM)	δ_{860nm} (GM)
1	0.61 ± 0.05	28 ± 5†	54 ± 6†	<20†
2	0.86 ± 0.05	248 ± 25	193 ± 19	132 ± 13
3	1.00 ± 0.05	464 ± 46	238 ± 71	316 ± 32
4	1.00 ± 0.05	1550 ± 155†	1450±145†	550 ± 55†

†lit.[36], ‡ lit.[20]

II.3.3 The Polymer Matrix

Three different polymer matrices were used as supports. Phosphorylated poly(VBC-*co*-MMA) (**31** in Figure II-6) is a highly transparent, robust matrix in which all of the dyes (except **26**) and the PAGs were very soluble. However, this matrix required the use of solvents to help dissolve all of the system components for casting the polymers onto glass slide supports. The solvents must be low vapor pressure solvents to ensure that a bubble free film will be produced after solvent drying. Ultimately, this translates into

film drying procedures that can be fairly lengthy, thus alternative processing and polymers were explored.

To expedite the film drying process, creation of a polymer matrix from liquid monomers that can dissolve both the 2PA dye and PAG was investigated. Two thiolene polymer substrates were prepared from the photocrosslinking of enes **28** and **29** with different proportions of thiol **30** (Figure II-6), in the presence of a free radical photoinitiator (Irgacure 184), and doped with the PAG-dye mixture. Even though thiolene crosslinked polymer matrices are formed by a free radical initiated mechanism, these reactions are typically not sensitive to oxygen. Furthermore, many different mechanical and visco-elastic properties of the resulting polymer can be obtained by tailoring the structure and proportions of the momomers.[37] Special care was taken in choosing the free radical photoinitiator to have one with an appropriate λ_{max} so as to not generate photoacid during the formation of the polymer film. The films were made in 3 to 10 min, and images were successfully recorded and read out on both channels (Figure II-6). The FITC filter cube of the confocal microscope was equipped with an excitation bandpass filter (452-502 nm), a dichroic mirror (507 nm) and an emission bandpass filter (496-556 nm) that allowed fluorescence readout of the nonprotonated dye where the resist (polymer composite) remained unexposed. A modified TRITC filter cube, equipped with an excitation bandpass filter (505-545 nm), a dichroic mirror (555 nm), and an emission bandpass filter (604-644 nm), was used to capture the fluorescence of the exposed protonated form of 25.

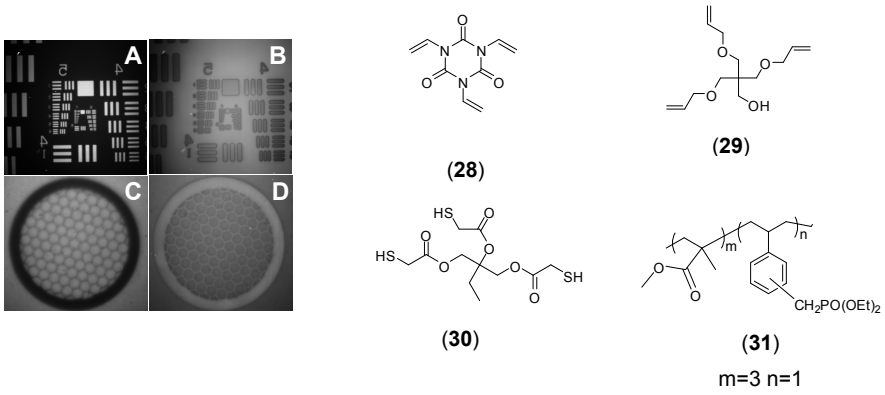

Figure II-6. One-photon writing and readout images with contact (A and B) and projection (C and D) photomasks. Composition (W/W): **27** 12%; **25** 1.3%; **28** 25%; **29** 25%; **30** 50%. Exposed at 254 nm (3 min) to form film. Later exposed at 300-400 nm (40 s) for image recording.

II.3.4 2PA Photoacid Generators

Since commercially available PAGs are not conjugated enough to generate photoacid by 2PA in the tuning window of Ti:sapphire lasers (700-1000 nm) and because their 2PA cross sections are low, the PAGs used in this system were designed to have to have high 2PA cross sections at wavelengths accessible to a Ti:sapphire laser system. The PAGs used were prepared as we previously reported.[10] It has been observed that symmetrical and unsymmetrical conjugated systems with two electron-donating groups (D) or electron-accepting substituents (A) tend to have significant two-photon absorptivity.[8,38,39] Based on the high thermal and photochemical stabilities of the fluorenyl π-system,[20] fluorene was chosen as the core structure when designing the PAGs. Since fluorene can be readily substituted in its 2-, 7-, and 9- positions, a stilbene or thiophene motif was introduced (2-,7- positions) to provide additional p-conjugation.

In an attempt to increase the photoacid generation efficiency per molecule, two sulfonium salt motifs were introduced in the original model compounds which exhibited

an A-π-A architecture, **7** and 27. However, the high fluorescence efficiencies of these molecules, as demonstrated by their high fluorescence quantum yield values, hindered the efficiency of photoacid generation (Table II-2). The direct photolysis of triarylsulfonium salts has been reported to occur mainly from the singlet state. However, sensitization studies have shown that the triplet triarylsulfonium salts are also labile.[21] Consequently, we incorporated a nitro group in the architecture of PAG **11** to quench the fluorescence of the PAG by inducing intersystem crossing and increase the photoacid quantum yields.

The elimination of the radiative decay pathway was demonstrated by a dramatic decrease in the florescence quantum yield of **11** relative to **7**. The photoacid quantum yield of PAG **5** (Table II-2) showed a significant improvement in photoacid generation efficiency when compared to PAG **7**, indicating that introduction of groups that favor intersystem crossing, such as functionalities that permit spin orbital coupling (e.g. the nitro group), is a viable mechanism for increasing the photoacid quantum yield of highly fluorescent triarylsulfonium salt PAGs. The photoacid quantum yields were determined by a steady state method. The solutions of the PAGs in acetonitrile were selectively irradiated at the desired wavelength with an excitation source of a spectrofluorometer. Rhodamine B was used as a sensor for photoacid generation as reported by Scaiano *et al*.[23] Special care was taken in observing a photodecomposition conversion no greater than 5% in order restrict secondary photoproduct acid generation.

The two-photon absorption (2PA) cross sections, however, were found to be up to 5 times higher for PAG **7** than for PAG **11** (Table II-2). This disparity in cross section values vs. photoacid quantum yield values make it difficult to rank these PAGs by their

overall efficiencies. Using only one of these two photophysical properties would be incomplete and could lead to erroneous interpretations. A more accurate value to compare these PAGs is the 2PA action cross section of photoacid generation given by the product of photoacid generation quantum yield and the 2PA cross section at a specific wavelength. Based on the two-photon action cross section, the overall efficiency of PAG **11** was higher than that of PAG **7**. Hence, the former was chosen as the preferred PAG in the development of the 2PA ODS system.

Table II-2. Photophysical Characterization of PAGs **5** and **7.**

Compound	Φ_F*	Φ_{H+}†	ε_o‡ ($M^{-1}cm^{-1}$)	δ_{710nm} (GM)	δ_{730nm} (GM)	δ_{760nm} (GM)	$\Phi_{H+}*\delta_{710nm}$ (GM)
11	0.10±0.01	0.40±0.04	51000±5000[1]	240±24	80±8	60±6	96±10
7	0.80±0.06	0.03±0.0005	73000±5000[2]	1275±130	350±35	115±12	38±4

*Fluorescence Quantum Yields, Φ_F, DPA in cyclohexane as standard; †Φ_{H+} photoacid quantum yields at 350 nm RhB^+ as indicator; ‡ε_o molar absorptivity coefficients in acetonitrile at [1]380 nm and [2]400 nm; δ two photon absorption cross sections measured at the three different wavelengths used for writing; $\Phi_{H+}*\delta_{710nm}$ two-photon action cross section of photoacid generation at 710 nm.

II.3.5 One-Photon vs Two-Photon Writing and Readout

The advantage of using two-photon absorbing dyes is clearly evidenced in the initial two-photon readout experiments, Figure II-**7**, in which the images were recorded by projecting the image of a 600 mesh TEM hexagonal grid onto the photoreactive polymer surface using a 200 W mercury lamp as an irradiation source. After recording the image by 1PA, the fluorescent image was collected by both 1PA and 2PA. The two-photon, upconverted fluorescence image (readout) proved to be much more forgiving to film defects when compared to the one photon readout, perhaps due to less scattering when longer excitation wavelengths are employed. Furthermore, the inherent nonlinearity of the 2PA system allowed better contrast and sharper images than the one-photon readout Figure II-7a. Scanning across the line indicated on the one-photon readout images, afforded the fluorescence intensity scan in Figure II-7c. A threshold can be established over which any fluorescence signal can be translated into a binary digital signal. The full width at half maximum (FWHM) of the fluorescence intensity scan peaks was used to estimate the minimum size feature (ca. 3 μm) for one-photon recording with two-photon readout.

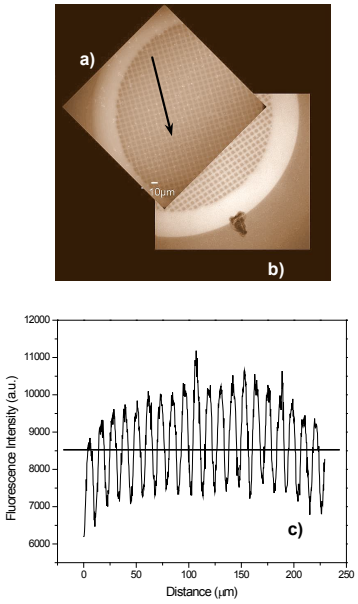

Figure II-7. Readout images using a TEM 600 mesh projection mask of a mixture of dye 1 and PAG 5 in phosphorylated poly(VBC-*co*-MMA). (a) One-photon (FITC 40X readout 20 ms, writing 180 s). (b) Two-photon readout (40x-800 nm-2mW-510IF-550RIF). (c) Fluorescence intensity plot for one photon readout when traced along the arrow indicated in (a).

The advantage of using 2PA for writing and readout in all three dimensions of the polymer matrix was demonstrated by an experiment in which voxels were recorded by 2PA in five layers using 730 nm to induce the photoacid generation by 2PA of PAG **11**. An electronic shutter was programmed to open for 50 ms at 10 μm intervals in the x and y axes. After recording (60x, 1.4 N.A., oil immersion objective) an x-y layer of voxels, the microscope objective was moved ca. 4 μm to focus deeper into the polymer matrix, generating another layer of voxels. To ensure that the entire depth of the polymer matrix was used for recording, this process was repeated until the objective focal point had well cleared the polymer matrix. After recording, the voxels were readout by both one- and

two-photon excitation. One-photon readout was performed by taking a series of confocal fluorescence pictures of the recorded volume at consecutive focal planes of the objective separated by a distance of 0.4 μm. Similarly, the two-photon upconverted fluorescence readout was performed by scanning consecutive 0.4 μm layers of the polymer film at 860 nm in order to excite protonated 2PA dye **24**.

The one-photon confocal fluorescence images were taken using a FITC filter cube (Ex:477/50; DM: 507; Em:536/40) and a modified TRITC filter cube (Ex:525/40; DM: 555; Em:624/40). One and two-photon fluorescence intensity vs. distance (μm) graphs were then recorded for each voxel layer in order to compare the readout quality obtained by each of the readout methods (Figure II-8, one-photon readout and Figure II-9, two-photon readout). Clearly, the signal-to-noise ratio in the one-photon readout fluorescence intensity plot (Figure II-8) is significantly attenuated as one focuses deeper into the polymer film (Figure II-8). In the case of two-photon readout (Figure II-9), the fluorescence signal readout shows well defined voxels and comparable, consistently good signal-to-noise ratio for all five layers throughout the entire polymer matrix, a testament of the two-photon advantage. Furthermore, the nonlinearity of the system ensured a crosstalk-free system (Figure II-10).

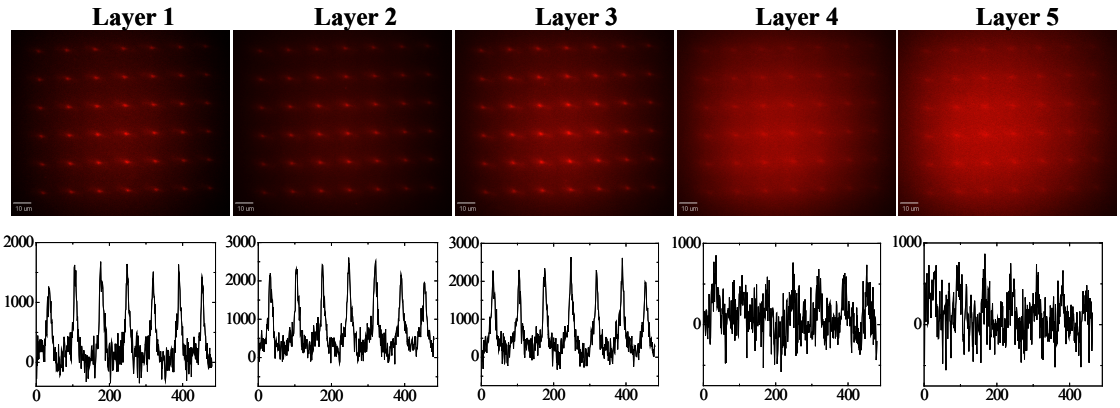

Figure II-8. Photosensitive polymeric system used for 3D, two-photon optical data storage and one-photon readout. Composition (W/W): **24** (1%), **11** (5%), **31** (94%). Two-photon writing was performed at 730 nm (2.4 mW), 200 fs, 60 ms exposure/voxel with a 60x, 1.4 NA oil immersion objective. One-photon readout (upper) was performed, layer-by-layer (~0.4 μm/layer), with a modified TRITC filter cube (Ex:525/40; DM: 555; Em:624/40), with the same objective used for writing. Layers 1-5 show significant reduction of the signal-to-noise ratio (lower) in the fluorescence intensity scan for all the layers. Scale bar: 10 μm.

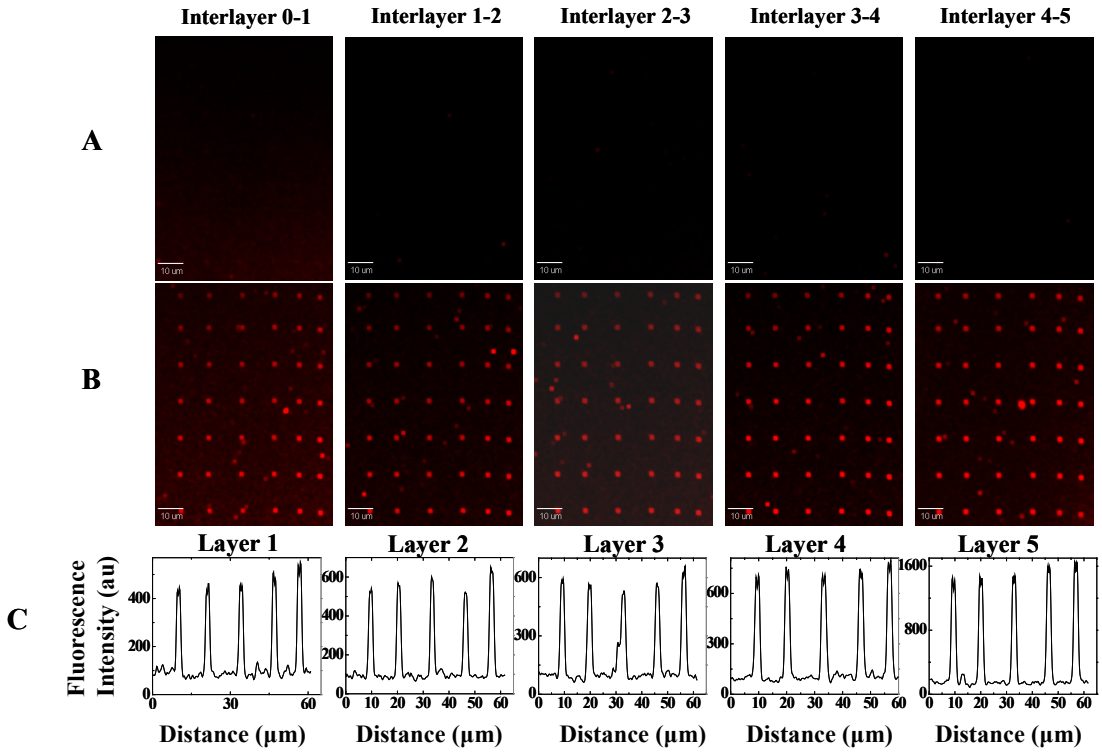

Figure II-9. Photosensitive polymeric system used for 3D, two-photon optical data storage and two-photon readout. Composition (W/W): **24** (1%), **11** (5%), **31** (94%). Two-photon writing was performed at 730 nm (2.4 mW), 200 fs, 60 ms exposure/voxel with a 60x, 1.4 NA oil immersion objective. Two-photon readout was performed, layer-by-layer (~0.4 μm/layer), at 860 nm (7 mW), 200 fs, with the same objective used for writing. (A) Blank interlayers (unrecorded volume between voxel layers). (B) Two-photon readout of five layers of recorded voxels. (C) Fluorescence intensity scans of each layer showing consistently good signal-to-noise ratio throughout all five recorded layers of data. Note that because there is virtually no fluorescence signal in between the layers (A), the system is crosstalk-free. Scale bar: 10 μm.

A reconstruction of the 3D image of these voxels was obtained by overlaying all five layers of the upconverted fluorescence images using SlideBook 4.1 (Figure II-10A). This reconstruction reveals the absence of crosstalk between voxels within a layer and, importantly, between the layers, illustrating the potential of this system for 3D data

storage. The fluorescence intensities scans (from Figure II-9C) were normalized and shown in Figure II-10B to illustrate how consistent the signal-to-noise ratio is from layer to layer. The size of the voxels is not yet optimized and can be further reduced to increase the storage density of the system.

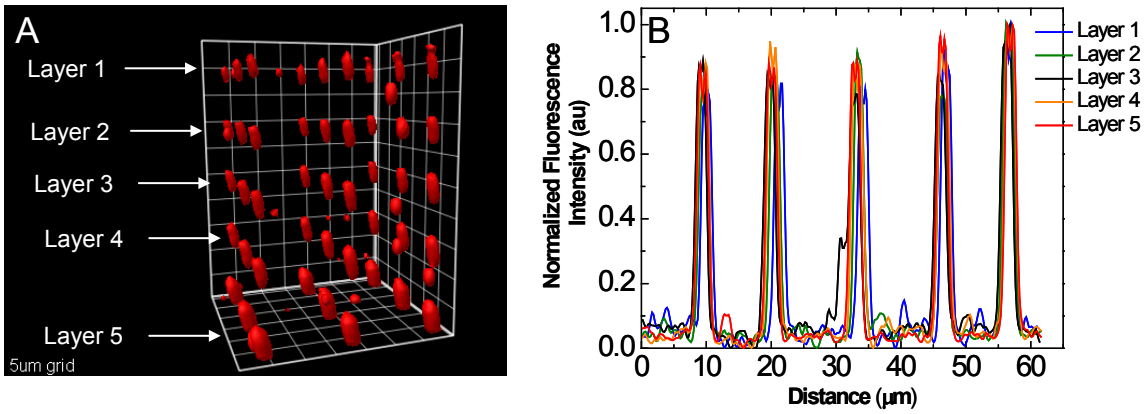

Figure II-10. Photosensitive polymeric system used for 3D, two-photon optical data storage. Composition (W/W): **11** 5%; **24** 1%; **31** 94%. Two-photon writing was performed at 730 nm (2.4 mW), 200 fs, 60 ms exposure/voxel with a 60x, 1.4 N.A. oil immersion objective. Two-photon readout was performed, layer-by-layer (~0.4 μm/scaning), at 860 nm (7 mW), 200 fs, with same objective used for writing. (A) 3D image reconstruction was done by overlaying all readout layers using SlideBook 4.1 (surface mode). (B) Normalized fluorescence intensity scan of all layers shows excellent signal-to-noise ratio throughout the entire polymer matrix. Note that because there is virtually no fluorescence signal in between the layers, the system is crosstalk-free. Scale: 5 μm grid.

Once the conditions were optimized for writing and readout, in terms of exposure times and laser beam profile, even smaller voxels were obtained. The reduction of the size features facilitated recording and readout of eight crosstalk-free layers of voxels (Figures II-11, and II-12 and Figure C1 in Appendix C). Though the voxels are difficult to visualize in the figure (Figure II-11B), one can easily observe the fluorescence signals in the fluorescence intensity plots in Figure II-11C. The average voxel size in these

layers was estimated to be 250 nm in radial diameter and 650 nm in axial diameter (Figure II-12), as determined by surveying the average size of the voxels in layers 3 and 4 of the eight layer series. Based on this feature size, we estimated the maximum storage capacity to be approximately 1.8×10^{13} bits/cm^3.

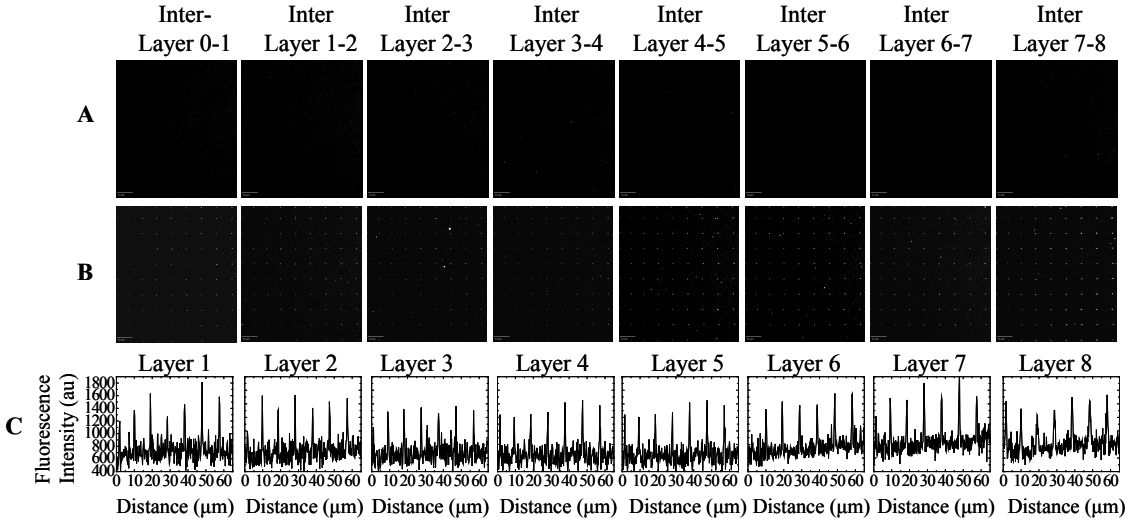

Figure II-11. Photosensitive polymeric system used for 3D, two-photon optical data storage showing eight crosstalk-free layers. Composition (W/W): **11** 5%; **24** 1%; **31** 94%. Two-photon writing was performed at 710 nm (1.6 mW), 200 fs, 60 ms exposure/voxel with a 60x, 1.4 N.A. oil immersion objective. Two-photon readout was performed, layer-by-layer (~0.4μm/scaning), at 860 nm (9 mW), 200 fs, with the same objective used for writing. (A) Blank interlayers (unrecorded volume between voxel layers). (B) Two-photon readout of the eight layers. (C) Fluorescence intensity scans of each layer showing good signal-to-noise ratio throughout all eight recorded layers of data. Note that because there is virtually no fluorescence signal in between the layers (A), the system is crosstalk-free. Scale bar: 10 μm.

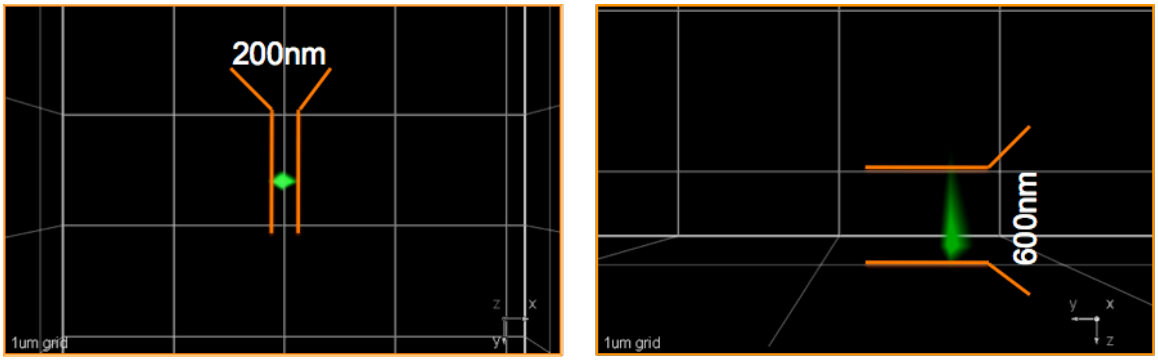

Figure II-12. Voxel size from eight layer writing experiment in Photosensitive polymeric system used for 3D, two-photon optical data storage. Composition **11** 5%; **24** 1%; **31** 94%. Two-photon writing was performed at 710 nm (1.6 mW), 200 fs, 60 ms exposure/voxel with a 60x, 1.4 N.A. oil immersion objective. Two-photon readout was performed, layer-by-layer (~0.4μm/scaning), at 860 nm (9 mW), 200 fs, with same objective used for writing. This voxel represents an average voxel as determined by surveying the average size of the voxels in layers 3 and 4 of the eight layer series. Based on these size features we estimated the maximum storage capacity to be approximately 1.8×10^{13} bits/cm^3.

II.4 Experimental

II.4.1 *Materials*

The syntheses of fluorescent dyes **23** and **26** and all PAGs are reported elsewhere.[25,40,41] The synthesis of all PAGs are reported in Chapter I and in the literature.[41] The phosphorylated poly(vinylbenzilchloride-co-methylmethacrylate), poly(VBC-co-MMA) **19** (see Figure II-6 for structure), used as polymer matrix was synthesized according to the literature.[38] 9,9-Didecyl-9*H*-fluorene-2,7-dicarbaldehyde **3**,[9] (4-(dibutylamino)benzyl) triphenylphosphonium iodide **32**,[42] diethyl 4-(benzo[*d*]thiazol-2-yl)benzylphosphonate **33**,[43] 2-(5-bromothiophen-2-yl)benzothiazole **34**,[25,44] and 9,9-didecyl-2-iodo-7-nitro-9H-fluorene **36**,[25,44] were prepared according to the literature methods. All solvents and monomers were used as received. Masks used during

photoexposure of photosensitive polymer films included TEM grids (600-mesh and 400-mesh hexagonal grids from Polysciences) and glass resolution targets (negative slide with the 1951 USAF test pattern from Edmund Scientific).

II.4.2 Synthetic Procedures and Characterization

[4-(2-[7-[2-(4-Benzothiazol-2-yl-phenyl)-vinyl]-9,9-didecyl-9*H*-fluoren-2-yl]-vinyl)-phenyl]-dibutyl-amine 25 (Scheme II-1). 9,9-Didecyl-9*H*-fluorene-2,7-dicarbaldehyde **8** (0.25 g, 0.5 mmol), 4-(*N*,*N*-dibutylaminobenzyl) triphenylphosphonium iodide **32** (0.30 g, 0.5 mmol) and diethyl 4-(benzo[*d*]thiazol-2-yl) benzylphosphonate **33** (0.18 g, 0.5 mmol) in 10 mL of dry DMF was degassed by Ar for 30 min. NaH (0.24 g, 10.0 mmol) was then added and the mixture stirred at room temperature under Ar for 20 h. The crude product precipitated by slowly addition of water was collected by filtration and purified by column chromatography using hexane/CH_2Cl_2 = 1/3 as eluent to afford 0.20 g of compound **5** (43% yield), m.p. 95–96°C. ^{1}H NMR (300 MHz, $CDCl_3$) δ 8.07 (m, 3H, Ph-H), 7.89 (d, J = 7.8 Hz, 1H, Ph-H), 7.63 (m, 4H, Ph-H), 7.51–7.38 (m, 8H, Ph-H), 7.31 (d, J = 16.8 Hz, 2H, CH=), 7.17 (d, J=16.2 Hz, 2H, CH=), 7.08 (d, J=16.2 Hz, 2H, CH=), 6.95 (d, J=16.2 Hz, 2H, CH=), 6.62 (d, J=8.1 Hz, 2H, Ph-H), 3.29 (m, 4H, NCH_2), 2.02 (m, 4H, CH_2), 1.58 (m, 4H, CH_2), 1.37 (m, 4H, CH_2), 1.15–1.06 (m, 28H, CH_2), 0.97 (t, J = 7.1 Hz, 6H, CH_3), 0.82 (t, J = 5.9 Hz, 6H, CH_3), 0.68 (m, 4H, CH_2). ^{13}C NMR (75MHz, $CDCl_3$) δ 154.29, 151.60, 147.85, 141.59, 140.47, 139.51, 137.70, 135.54, 135.13, 132.43, 131.33, 128.54, 128.05, 127.89, 127.02, 126.70, 126.49, 126.08, 125.26, 124.79, 124.35, 123.28, 121.77, 121.08, 120.31, 120.09, 119.93, 111.81, 55.31, 51.18, 40.98, 32.32, 32.05, 30.54, 30.08, 30.01, 29.95, 29.74, 24.25, 23.13, 20.86, 14.62,

14.53. Anal. Calcd. for $C_{64}H_{82}N_2S$ (911.42): C, 84.34; H, 9.07; N, 3.07. Found: C, 84.34; H, 9.28; N, 3.08.

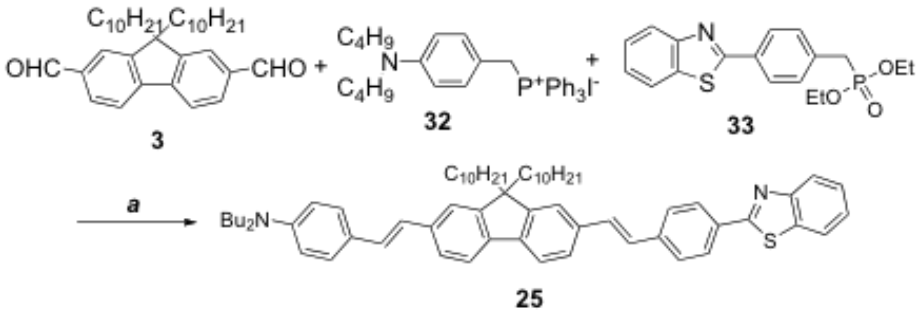

Scheme II-1. Synthesis of 2PA dye **25.**

a) DMF, NaH, r.t., 20 h, 43%.

Synthesis of 7-(5-(benzothiazol-2-yl)thiophen-2-yl)-9,9-didecyl-N,N-diphenyl-9H-fluoren-2-amine 24. Transformation of benzothiazole derivative **34** into tin derivative **35**, and subsequent Pd-catalyzed Stille coupling with the key fluorene intermediate **36** was accomplished, as shown in Scheme II-2, by using methodology previously reported by our group, affording compound **37** in excellent yield. Reduction of nitrofluorene derivative **37** and posterior reaction of amine **38** with iodobenzene under Ullmann conditions generated the D-π-A type fluorescent dye **24.**

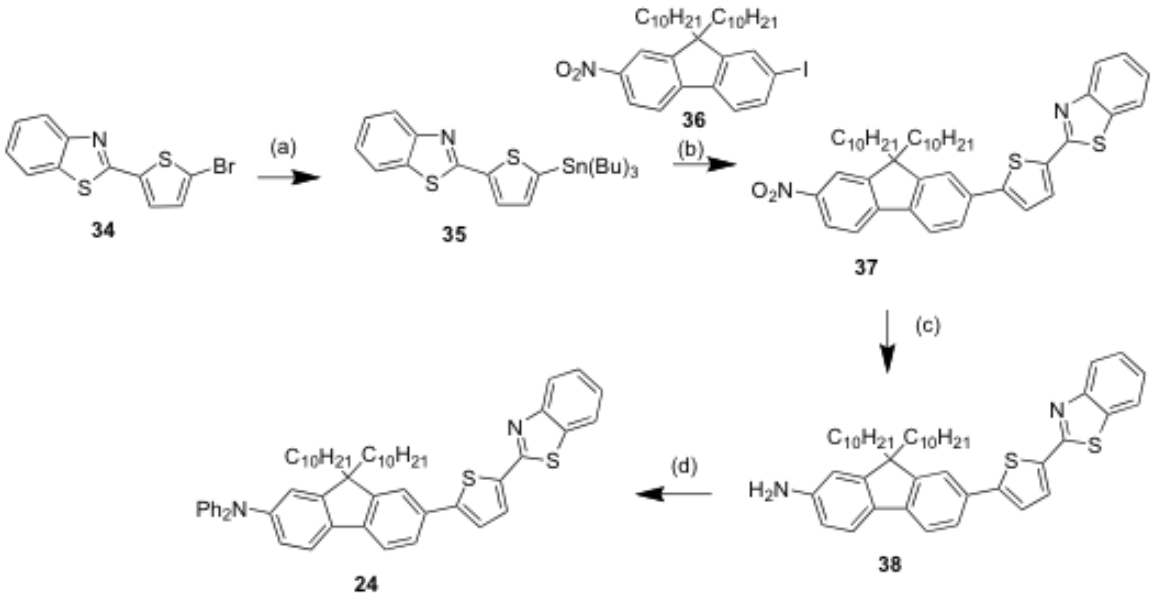

Scheme II-2. Synthesis of 2PA dye **24.**

a) i) THF, -78 °C, $Sn(Bu)_3Cl$, 1 h; (ii) rt, overnight, 70%; b) toluene, $Pd(PPh3)_2Cl_2$ reflux, 5 h, 98%; c) THF:EtOH 1:1, $NH_2NH_2.2H_2O$, 10% Pd/C, 70 °C, 20 h, 84%; d) 1,2-dichlorobenzene, iodobenzene, Cu-bronze, 18-crown-6, K_2CO_3, 180 °C, 48 h, 94%.

Synthesis of 2-(5-(tributylstannyl)thiophen-2-yl)benzothiazole 35. At -78 ^oC, 2-(5-bromothiophen-2-yl)benzothiazole **34** (200 mg, 0.67 mmol) was dissolved in dry THF (5 mL). A solution of *n*-BuLi in hexanes (0.27 mL, 2.5 M, 0.68 mmol) was added drop wise into the reaction mixture. After stirring for 1 h, $Sn(Bu)_3Cl$ (360 mg, 1.10 mmol) was added and the mixture was allowed to reach room temperature, and stirred overnight. The mixture was added to water, extracted with Et_2O twice, dried over Mg_2SO_4, and purified by column chromatography, using a mixture of hexane:ethyl acetate (9:1) as eluent, to yield 240 mg (70%) of viscous oil. ^1H NMR (500 MHz, $CDCl_3$) δ 8.02 (d, J=8.2 Hz, 1H, Ph-H), 7.82 (d, J = 8.0 Hz, 1H, Ph-H), 7.74 (d, J = 3.5 Hz, 1H, Ar-H), 7.45 (m, 1H, Ph-H), 7.33 (m, 1H, Ph-H), 7.18 (d, J=3.5 Hz, 1H, Ar-H), 1.59 (m, 6H, CH_2), 1.35 (m, 6H,

CH_2), 1.16 (m, 6H, CH_2), 0.90 (t, *J*=7.34 Hz, 9H, CH_3). ^{13}C NMR (125 MHz, $CDCl_3$) δ 161.40, 153.85, 143.46, 142.35, 136.18, 134.70, 129.60, 126.23, 125.06, 122.85, 121.44, 28.94, 27.28, 13.72, 10.98. Anal. Calcd for $C_{23}H_{33}NS_2Sn$: C, 54.56; H, 6.57; N, 2.77. Found: C, 54.85; H, 6.67; N, 2.86.

Synthesis of 2-(5-(9,9-didecyl-7-nitro-9H-fluoren-2-yl)thiophen-2-yl)benzothiazole 37. 9,9-Didecyl-2-Iodo-7-nitro-9H-fluorene **36** (200 mg, 0.32 mmol), 2-(5-(tributylstannyl)thiophen-2-yl)benzothiazole **35** (191 mg, 0.38 mmol) and $Pd(PPh_3)_2Cl_2$ (6 mg, 0.008 mmol) were dissolved in toluene (4 mL). The mixture was heated under reflux for 5 h. The solvent was removed under reduced pressure and the crude was purified by column chromatography, using a mixture of hexane:ethyl acetate (9.5:0.5) as eluent, to yield 222 mg (98%) of yellow oil that solidified upon standing. m.p.: 73.2-74.9 °C. ^{1}H NMR (500 MHz, $CDCl_3$) δ 8.28 (dd, *J* = 8.3 Hz, *J* = 2.0 Hz, 1H, Ph-H), 8.22 (d, *J* = 2.0 Hz, 1H, Ph-H), 8.05 (d, *J* = 8.0 Hz,1H, Ph-H), 7.88 (d, *J* = 7.8 Hz, 1H, Ph-H), 7.82 (m, 2H, Ph-H), 7.74 (m, 1H, Ph-H), 7.69 (d, *J*=1.4 Hz, 1H, Ph-H), 7.66 (d, *J*=3.7 Hz, 1H, Ar-H), 7.50 (m, 1H, Ph-H), 7.46 (d, *J*=3.7 Hz, 1H, Ar-H), 7.39 (m, 1H, Ph-H), 2.06 (m, 4H, CH_2), 1.09 (m, 28H, CH_2), 0.82 (t, *J*=7.0 Hz, 6H, CH_3), 0.62 (m, 4H, CH_2). ^{13}C NMR (125 MHz, $CDCl_3$) δ 160.97, 153.69, 153.38, 152.20, 147.89, 147.24, 146.80, 139.03, 136.59, 134.68, 134.37, 129.48, 126.59, 125.29, 124.40, 124.36, 123.45, 122.95, 121.84, 121.51, 120.43, 119.97, 118.28, 55.87, 40.07, 31.84, 29.83, 29.49, 29.47, 29.24, 29.19, 23.78, 22.63, 14.08. Anal. Calcd for $C_{44}H_{54}N_2O_2S_2$: C, 74.74; H, 7.70; N, 3.96. Found: C, 74.97; H, 7.85; N, 3.97.

Synthesis of 7-(5-(benzothiazol-2-yl)thiophen-2-yl)-9,9-didecyl-9H-fluoren-2-amine 38. 2-(5-(9,9-Didecyl-7-nitro-9H-fluoren-2-yl)thiophen-2-yl)benzothiazole **37** (160 mg, 0.23 mmol) and 10% Pd/C (16 mg) were dissolved in a mixture 1:1 of THF:EtOH,.(8 mL). $NH_2NH_2.2H_2O$ (136 mg, 2.7 mmol) was added to the mixture slowly at room temperature then heated to 70 ^oC for 20 h. The mixture was filtered though a silica plug with CH_2Cl_2, and, after removing the solvent under reduced pressure, the crude product was purified by column chromatography, using a mixture of hexane:ethyl acetate (9:1) as eluent, to yield 130 mg (84%) of dark yellow oil. Due to the sensitivity of the amine, **15** was used directly in the next step. ^1H NMR (500 MHz, $CDCl_3$) δ 8.04 (d, J = 8.0 Hz, 1H, Ph-H), 7.85 (d, J = 8.0 Hz, 1H, Ph-H), 7.61 (m, 2H, Ph-H), 7.56 (m, 2H, Ph-H), 7.48 (m, 2H, Ph-H), 7.36 (m, 2H, Ar-H), 6.67 (m, 2H, Ph-H), 3.79 (s, 2H, NH_2), 1.91 (m, 4H, CH_2), 1.11 (m, 28H, CH_2), 0.83 (t, J=7.0 Hz, 6H, CH_3), 0.67 (m, 4H, CH_2). ^{13}C NMR (125 MHz, $CDCl_3$) δ 161.38, 153.75, 153.11, 150.74, 149.56, 146.40, 142.35, 135.01, 134.60, 131.62, 130.45, 129.54, 126.42, 125.05, 124.69, 123.02, 122.78, 121.42, 120.81, 120.06, 118.76, 114.05, 109.65, 54.93, 40.62, 31.87, 30.09, 29.63, 29.53, 29.29, 29.28, 23.75, 22.65, 14.10.

Synthesis of 7-(5-(benzothiazol-2-yl)thiophen-2-yl)-9,9-didecyl-N,N-diphenyl-9H-fluoren-2-amine 24. 7-(5-(Benzothiazol-2-yl)thiophen-2-yl)-9,9-didecyl-9H-fluoren-2-amine **38** (130 mg, 0.19 mmol), iodobenzene (157 mg, 0.77 mmol), Cu-bronze (61 mg, 0.96 mmol), 18-crown-6 (15 mg, 0.058 mmol), and K_2CO_3 (212 mg, 1.54 mmol) were combined with 1,2-dichlorobenzene (3 mL). The mixture was heated to 180 ^oC for 48 h. The product was passed through a silica plug with CH_2Cl_2 The solvent was removed

under reduced pressure, and the crude product was purified by column chromatography on silica gel, using a mixture of hexane:ethyl acetate (9:1) as eluent, to yield 150 mg (94%) of a yellow solid, m.p.: 107.5-109.5 °C. ^{1}H NMR (500 MHz, $CDCl_3$) δ 8.04 (d, J = 8.0 Hz, 1H, Ph-H), 7.84 (d, J = 8.0 Hz, 1H, Ph-H), 7.62 (m, 4H, Ph-H), 7.56 (d, J = 8.0 Hz, 1H, Ph-H), 7.47 (m, 1H, Ph-H), 7.35 (m, 2H, Ar-H), 7.26 (m, 5H, Ph-H), 7.14 (m, 5H, Ph-H), 7.02 (m, 2H, Ph-H), 1.91 (m, 4H, CH_2), 1.12 (m, 28H, CH_2), 0.85 (t, J=7.0 Hz, 6H, CH_3), 0.70 (m, 4H, CH_2). ^{13}C NMR (125 MHz, $CDCl_3$) δ 161.31, 153.75, 152.48, 151.63, 149.22, 147.88, 147.53, 141.61, 135.37, 134.63, 131.38, 129.57, 129.49, 129.24, 129.16, 125.16, 125.02, 123.97, 123.91, 123.37, 123.29, 122.84, 122.64, 121.47, 121.43, 120.10, 104.99, 55.18, 40.24, 31.91, 30.00, 29.61, 29.57, 29.32, 23.87, 22.67, 14.12. Anal. Calcd for $C_{56}H_{64}N_2S_2$: C, 81.11; H, 7.78; N, 3.38. Found: C, 80.81; H, 7.74; N, 3.30.

II.4.3 One-Photon Recording and Readout

One-photon recording was carried out by irradiating the photoreactive polymer with a Loctite 97034 light source equipped with a 200 W mercury lamp and an internal shutter to control the exposure times. The photomask was either projected or placed (as a contact mask) on the dry polymeric film. Output from the waveguide of the light source was focused into the condenser of an Olympus IX-81 confocal microscope. One-photon fluorescence images were recorded on this microscope that was equipped with a Hamamatsu EM-CCD C9100 digital camera. One-photon confocal fluorescence images for readout were taken using a FITC filter cube (Ex:477/50; DM: 507; Em:536/40) and a

modified TRITC filter cube (Ex:525/40; DM: 555; Em:624/40) for the neutral and protonated forms of the dyes, respectively.

Photosensitive polymer films were solution cast onto 2.5 x 2.5 cm microscope glass cover slips. The film thickness of the polymer films was approximated by focusing on the glass surface and then on upper surface of the polymer and determining the distance the z stage traveled from one surface to the other.

II.4.4 Two-Photon Recording and Readout

Two-photon recording and readout were performed on a modified Olympus Fluoview FV300 laser scanning confocal microscopy system equipped with a broadband, tunable Coherent Mira Ti:sapphire laser (recording at 730 or 760 nm; readout at 860 nm, 115 fs pulse width, 76 MHz repetition rate), pumped by a 10 W Coherent Verdi frequency doubled Nd:YAG laser. In two-photon writing, the exposure time and position was controlled by means of an electronic shutter and electronic stage, respectively, both from Thor Labs.

II.4.5 Spectra

Absorption spectra were recorded with an Agilent 8453UV–vis spectrophotometer. Steady-state fluorescence spectra were measured with a PTI Quantamaster spectrofluorometer.

II.4.6 Fluorescence Quantum Yield Measurements

Fluorescence quantum yields were determined relative to 9,10 diphenylanthracene in cyclohexane as a standard.[29] Measurements were made in the photon counting regime of a PMT using an L-format configuration using a PTI Quantamaster spectrofluorometer.

The fluorescence spectra were corrected for the spectral dependence of the PMT. All measurements were performed at room temperature in 1 cm quartz cuvettes with dye concentrations on the order of 10^{-6} M.

II.4.7 Photoacid Quantum Yield Measurements

Steady-state photoacid quantum yields were measured by selectively exciting PAG solutions at the desired wavelength using the monochromator of the PTI spectrofluorometer. Irradiance of the incident radiation was measured with an Ophir Power Star power meter equipped with a UV 1.44 cm^2 detector head. Rhodamine B was used as a sensor of photoacid generation, observing that the change in optical density of the sulfonium salt didn't exceed 5%.[23] Photoacid quantum yields were calculated by means of the following expression:

$$\Phi_{\lambda}^{H+} = \frac{\frac{\Delta OD^{555nm}}{\varepsilon_{555nm}^{RhB} * d * V_{sol}} N}{\Delta S * I_0 * \Delta t * (1 - 10^{-OD_0})} \qquad (1)$$

Where ΔOD^{555nm} is the change in optical density upon generation of rhodamine B measured at 555 nm, ε^{RhB}_{555} is the extinction coefficient of rhodamine B at 555 nm in acetonitrile, d is the irradiation path length (typically 1 cm) of cuvette, ΔS is the area of the irradiated solution (photon flux area), Δt is the irradiation time, and OD_0 is the average absorption intensity (which did not change by more than 0.5% at any given time). The quantum yield of photoacid generation of triphenylsulfonium tetrafluoroborate was determined by this method ($\Phi^+ = 0.57$), and was comparable to the literature value (0.54).[11] PAG solutions were on the order of 10^{-5} M in acetonitrile.

II.4.8 Two-photon Cross Section Measurements

Two-photon absorption (2PA) cross sections of the PAGs and fluorescent dyes were determined by the two-photon induced fluorescence method.[45] A tunable *Mira 900-F* femtosecond Ti:sapphire laser pumped by a Verdi V-10 frequency-doubled Nd:YAG laser (Coherent) was used as the excitation source and a PTI Quantamaster spectrofluorometer with PMT detectors was used for measurement. The linear polarization and the power of the laser light was adjusted by an optical attenuator (OA) consisting of two Glan-Thompson polarizers and a half-waveplate. The laser beam was divided with a beam splitter (BS) from where the transmitted beam was expanded with a beam expander (BE) and passed through the sample (S) after being focused with an objective lens. The reflected beam was sent to the power meter (PM) to monitor the variation of the incident power on the sample (S). The upconverted fluorescence was collected by the PMT of the PTI Quantamaster spectrofluorometer at a direction perpendicular to the pump beam. The numerical estimation of the 2PA cross sections δ was performed by comparison with a known reference using equation (2):

$$\delta = \delta_R \frac{\langle I \rangle}{\langle I_R \rangle} \frac{C_R}{C} \frac{n^2}{n_R{}^2} \frac{Q_R}{Q} \frac{P_R{}^2}{P^2} \qquad (2)$$

where the subscript R refers to the reference, $<I>$ is the integrated intensity from two-photon excitation, C is the concentration, n is the refractive index, Q is the quantum yield, and P is the incident power on the sample. All spectra were corrected for the spectral responsivity of PTI detection system. Follow-up fluorescence spectra after each measurement ensured that the exposure during the experiment did not induce photodecomposition greater than 0.5% for any of the 2PA molecules.

II.5 Conclusions

The ODS system proved to be versatile enough to tolerate a wide range of pK_b's of the 2PA absorbing dyes. A wide variety of architectures can be used as the dye, as long as these dyes exhibit an appreciable bathochromic shift upon acid generation, along with possessing high 2PA cross sections and high fluorescence quantum yields. The structures of the 2PA PAGs proved to be very useful in this type of system and should also be of considerable value in systems in which photoacid generation by 2PA is of the essence (i.e. 2PA microfabrication). These PAGs represent an important contribution to the very few sulfonium salt structures reported to generate photoacid upon 2PA.[46,47] Of the different polymer matrices that were used as supports, the phosphorylated poly(VBC-*co*-MMA) **31** gave the best results because of its transparency, and because it was a robust matrix in which the dyes and PAGs were generally very soluble. The photo-induced formation of a thiolene polymer matrix is, however, a feasible alternative in which one can easily obtain recording media of different mechanical and optical properties.

The 2PA WORM ODS system, consisting of 5 wt% of PAG **11**; 1 wt% of 2PA dye **24**, and 94 wt% of host polymer **31**, proved to be resilient to overexposure, and the inherent nonlinearity and sensitivity of this system enabled multilayer recording and readout of crosstalk-free 3D optical data with sub diffraction-limited voxel sizes. The advantages of two-photon writing and readout were clearly demonstrated, providing a storage density capacity of 1.8×10^{13} bits/cm^3.

CHAPTER III: APPLICATION OF NOVEL PAGS IN TWO-PHOTON INDUCED CATIONIC RING OPENING POLYMERIZATION MICROFABRICATION.

III.1 Abstract

PAGs that have proven to be useful in ODS (Chapter II) are herein used as a photoinitiator, in a negative resist, for 3D microfabrication. The PAGs were designed to have a high 2PA cross sections and to trigger the crosslinking of epoxy monomers or resins by 2PA-induced, acid catalyzed, ring opening polymerization (also referred to in the literature as CROP, for cationic ring opening polymerization). These versatile PAGs were used to create free standing structures from a PAG-Epon SU8 mixture.

III.2 Introduction

In 1972, the polymer industry had the pressing need to replace the thermally cured, solvent based UV curing procedures that had traditionally been employed. This spawned the development aryl sulfonium and aryl iodonium salts as photoacid generators (PAGs), molecules that form Brønsted acids upon photo-excitation, to induce the photo-polymerization of epoxides, vinyl ethers, and the crosslinking of epoxy polymer resins,[18,48] Since their discovery, the use of PAGs has been widely adopted by the polymer industry in coatings, paints, anticorrosives, and electronics.[1] The use PAGs in epoxide photoresists has been extensively studied for 2D and 3D lithographic patterning induced by one-photon absorption (1PA) and two-photon absorption (2PA).[2,3]

Recently, very versatile two-photon, 2D patterning techniques have been reported, in which projection of any given object is used as a photomask to obtain lateral features sizes as small as 120 nm.[49] There have been studies of successful two photon microfabrication using commercial PAGs,[11,12] however the two-photon absorption cross section of these initiators has been reported to be low.[13] In 2003, the synthesis of a PAG for two-photon 3D microfabrication was developed and its potential for its use in the fabrication of MEMs was evaluted.[14,50]

III.3 Results and Discussion

III.3.1 1PA Lithographic Studies.

The resist was deposited onto a glass cover slip by means of spin coating as indicated above, and left to dry overnight (see details in the experimental section below). In the one-photon fabrication experiments, the resist system, consisting of Epon SU-8 and Sartomer K-126 (in an 8:2 ratio) as epoxy monomers and **27** as the photoacid generator, was exposed to UV-visible radiation of a high pressure mercury lamp focused through a liquid waveguide into the stage of the confocal microscope. The microscope stage helped to further focus the light through the photomask (USAF resolution mask) onto the surface of the resist. Once exposed, the resist was developed and the same microscope was used to record the DIC and fluorescent images. In the DIC images of the structure resulting from the contact photomask experiments (Figure III-2 A-C) clear, undistorted structures were obtained with up to ~3.5 μm size features.

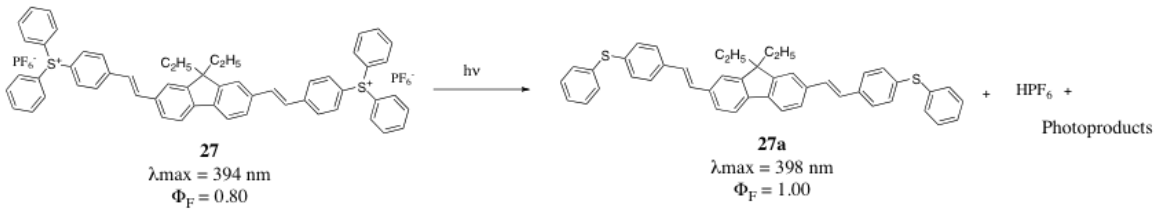

Figure III-1. Photodecomposition of PAG **27**.

The photodecomposition of triarylsulfonium salts has been known to generate Brønsted acids. Typically the counter ion of these salts is a heavy atom halide salt (commonly AsF_6^-, SbF_6^-, PF_6^-, BF_4^-). In these cases, the acid generated from this photolysis is a superacid. The superacid anions are very bulky and quite poor nucleophiles, which is why they are such efficient photoinitiators for acid-catalyzed ring opening polymerizations of epoxy-resins. Among the many products of decomposition of the aryl sulfonium salts, the most abundant are diaryl sulfides (Figure III-1). Because **27** and **(7)** have two sulfonium functionalities, they will probably have the symmetric and unsymmetrical aryl sulfide photoproducts. The symmetrical diaryl sulfide **27a** is the synthetic precursor of **27**, and was necessarily characterized during the synthesis of the sulfonium salt.[41] Sulfide **27** and **5** were found to possess fluorescence quantum yields of 1.00. When polymerization is carried out, this diarylsulfide is entrapped in the polymer matrix remaining after development. The high fluorescence quantum yield of **27**, **27a**, and other similar photoproducts then allows one to observe highly fluorescent structures after development (Figure III-2). Such a property could prove to be useful to monitor defects in structures that would otherwise be difficult to detect by other means.

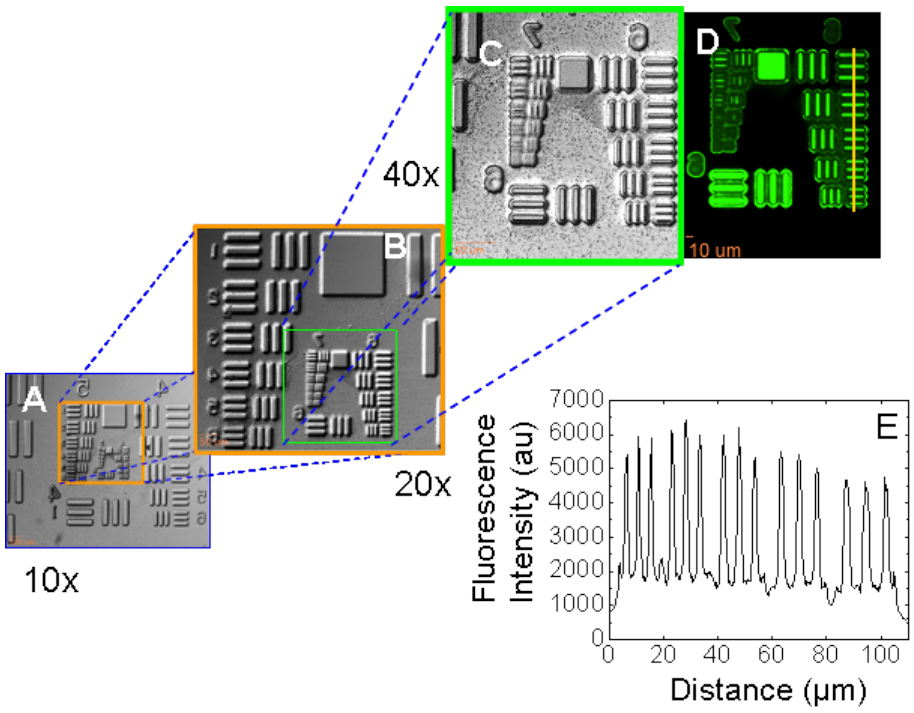

Figure III-2. DIC images of microstructure generated by one-photon contact lithography using USAF target resolution masks. Polymerization exposure time:300 s. A) Objective 10x (NA=.30); 62 ms. Scale bar 100 μm; B) Objective 20x (NA=0.45); 250 ms. Scale bar 50 μm. C) DIC (40x objective; NA=0.60; 62 ms) and D) fluorescence (40x objective; NA=0.60; 165 ms). E) fluorescence intensity along the line traced in D). Scale bar 10 μm.

III.3.2 2PA Microfabrication.

In order to evaluate if these PAGs would induce 2PA cationic ring opening polymerization (CROP) of epoxy resins, and making them suitable for two microfabrication, a mixture of SU-8:**11** or SU-8:**7** (5% W/W of the PAG) in cyclohexanone was spin coated on a glass cover slip. The stage was programmed to describe a pattern conformed by six 20 μm x 20 μm squares. This pattern was repeated at regular 6 μm depths within the epoxy resin by moving the microscope objective, by means of the stepper motor as described above, to make open boxes or cubes. After

inscribing the latent pattern into the resist, the sample was post exposure baked, and developed. The result was a free standing set of cubes (Figure III-3). The 3D structure of these cubes was "reconstructed" by recording the 1PA fluorescent image at different focal points within the structure (as described above for the 1PA readout experiments in the ODS section) and overlaying them sequentially. The result of this superimposition is shown in Figure III-3 C.

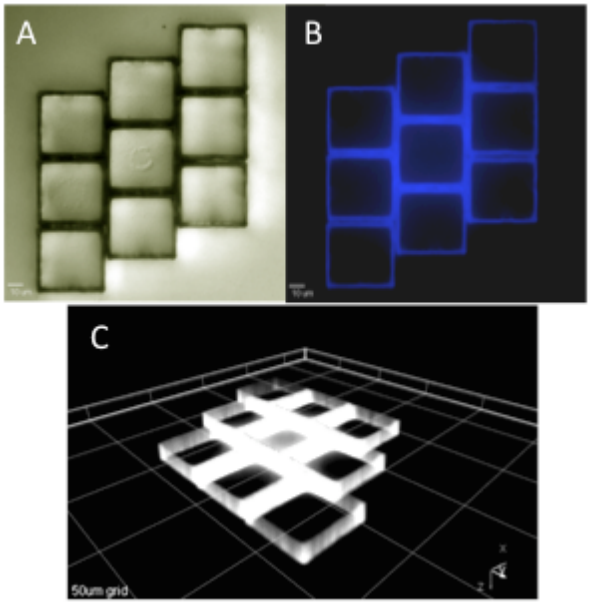

Figure III-3. SU-8:(5) (5% W/W). Freestanding structure resulting from scanning of 730nm pulsed (210 fs, 76MHz, 5mW) Ti:Sapphire laser. Two-photon microfabrication with a 60x, 1.4 N.A. oil immersion objective. One-photon readout was performed, layer by layer (~0.4mm), with a modified TRITC filter cube (Ex:525/40; DM: 555; Em:624/40), using a 40x, N.A.=0.45 objective. (A) DIC, Scale bar: 10 µm. (B) Confocal fluorescence image (one layer) Scale bar: 10 µm. (C) 3-D image reconstruction was done by overlaying all readout layers using SlideBook 4.1 (surface mode). Scale: 50 mm grid.

III.4 Experimental

III.4.1 Glass Functionalization.

No. 1 glass microscope cover slips or 2.5 x 2.5 cm microscope glass slides were treated with a piranha solution (7:3; sulfuric acid:30% hydrogen peroxide) for 10 min at 60 ºC and dried under a stream a nitrogen. The etched slides were placed in a 30% solution of 3-aminotrimetoxy silane in ethanol and dried again with nitrogen.

III.4.2 Spin Coating

Epon SU-8 and Sartomer K-126 (in an 8:2 ratio) were mixed with 1% weight of **(6)** and a minimal amount of propylene carbonate. The homogeneous mixture was dissolved (30%) in toluene. The resulting mixture was filtered through a 0.45 μm glass filter. Once filtered the resin was spin coated on the substrates (1. 500 rpm, 10 sec and 2. 1000 rpm, 30s). The samples were dried in a vacuum oven over night at 80 ºC.

III.4.3 Exposure and Developing.

The resin was exposed to the broadband UV radiation through (one-photon) and 760 nm (two-photon) for a number of different exposure times. Post-exposure baking was carried out on a hotplate at 90 ºC (10 min). The resist was developed by carefully washing away the unexposed resist with acetone, followed by isopropanol. The slide was then dried under nitrogen.

III.4.4 1PA and 2PA Polymerization.

1PA and 2PA Polymerizations were performed on the same respective systems described for ODS (Chapter II).

III.5 Conclusions

PAGs **7** and **11** are a promising addition to the very few 2PA PAGs that have been reported in the literature. The intrinsic fluorescence of these PAGs is helpful tool during the experimental intricacies of the two-photon polymerization, and the high fluorescence quantum yield of their main sulfide photoproducts enables the fabrication of fluorescent microstructures through one- and two-photon induced photolithography. This important feature affords the fluorescent images of the generated microstructures higher resolution, enabling the detection of smaller defects by means of florescence imaging. Furthermore, studying defects and periodicity in microstructures that contain substructures within them will be useful in areas such as microfluidics and photonic crystal structures. Significantly, these PAGs are successful photoinitiators in systems where two-photon induced CROP of epoxides and epoxy resins is needed.

CHAPTER IV: ONE- AND TWO-PHOTON STIMULATED EMISSION DEPLETION OF A SULFONYL-CONTAINING FLUORENE DERIVATIVE

Reproduced with permission from: Belfield, K. D.; Bondar, M. V.; Yanez, C. O.; Hernandez, F. E.; Przhonska, O. V. *Journal of Physical Chemistry B* **2009**, *113*, 7101-7106.

IV.1 Abstract

One- and two-photon stimulated emission transitions were investigated by the fluorescence quenching of a sulfonyl-containing fluorene compound, 2,7-bis(4-(phenylsulfonyl)styryl)-9,9-didecyl-9H-fluorene (**39**), in solution at room temperate using a picosecond pump-probe technique. The nature of stimulated transitions under various fluorescence excitation and quenching conditions were analyzed theoretically, and good agreement with experimental data was demonstrated. Two-photon stimulated transitions $S_1 \rightarrow S_0$ were shown for **39** at λ_q = 1064 nm. The two-photon stimulated emission cross section of fluorene **39** was estimated as $\delta_{2PE}(\lambda_q) \approx 240$ - 280 GM, making this compound a good candidate for use in two-photon stimulated emission depletion (STED) microscopy.

IV.2 Introduction

The nature of one- and two-photon stimulated transition processes in organic molecules is a subject of both scientific and technological interest due to a number of

nonlinear optical properties, such as two-photon induced fluorescence (2PF),[51,52] nonlinear transmittance,[53,54] two-photon absorption (2PA) processes,[55-57] light amplification of stimulated emission (lasing),[58,59] etc. A number of different types of stimulated transitions play an important role in the mechanisms of electric field-molecular structure interactions, and should be considered in a broad variety of nonlinear optical measurements. For example, possible effects of saturation[60] and stimulated emission[61] should be accounted for in the determination of 2PA by the 2PF method when sufficiently large pulse energies are used and the excitation wavelength overlaps with the fluorescence spectrum of the fluorophore. In the case of 2PA cross section measurements by the open aperture Z-scan method,[62] possible excited state absorption (ESA) and stimulated one-photon emission also need to be analyzed, as they may contribute to the observed data.[63]

Excited state dynamics and stimulated transitions that occur in organic molecules can be studied by fluorescence quenching methodology described previously by Lakowicz.[29,64,65] This methodology allows modification of the molecular orientational distribution in the excited states and creates anisotropic molecular ensembles with specific fluorescence properties.[64] As an example, fluorescence anisotropy properties of 4-dimethylamino-4'-cyanostilbene and tetraphenylbutadiene in the presence of stimulated light quenching have been described.[66] In some cases, a noticeable deviation from the quadratic dependence of fluorescence emission on excitation power was observed.[60] Quite significantly, the use of stimulated emission transitions has provided a means to overcome the diffraction limit in fluorescence microscopy,[67,68] resulting in the

development of high resolution (~60 nm) stimulated emission depletion (STED) microscopy.[69]

Herein, the nature of one- and two-photon stimulated emission transitions for a new sulfonyl-containing fluorene **39** (Figure IV-1a) are investigated in toluene and THF at room temperature via fluorescence quenching methodology based on different fluorescence excitation conditions. One-photon fluorescence excitation followed by one- or two-photon quenching was performed using a picosecond pump-probe technique and two laser beams at different wavelengths. Two-photon induced fluorescence along with concurrent one-photon quenching was detected using a single picosecond laser beam. Fluorene **39** is a particularly attractive as it is a highly fluorescent, photochemically stable compound that exhibits efficient one- and two-photon stimulated transitions.

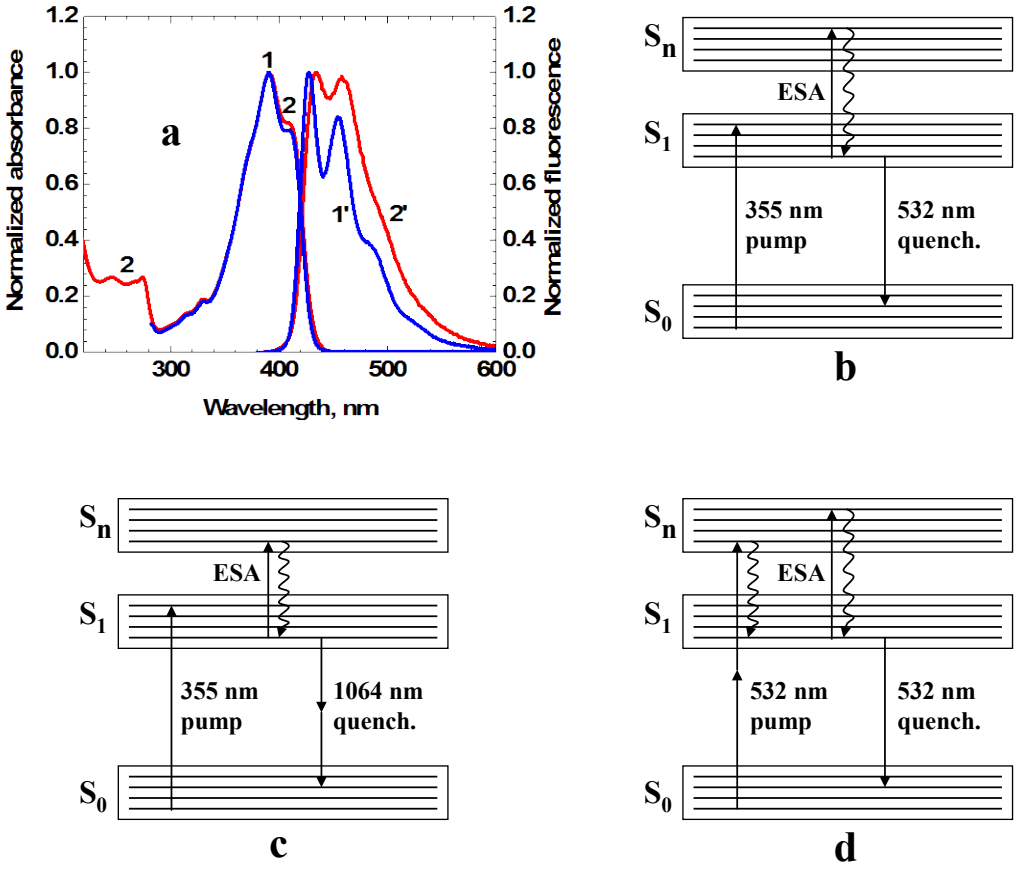

Figure IV-1. Chemical structure of fluorene **39** (top); (a) normalized absorption (1, 2) and emission (1', 2') spectra of **1** in toluene (1, 1') and THF (2, 2'); (b-d): electronic molecular model of **39** and corresponding stimulated transitions: (b) one-photon excitation (pump) laser beam at 355 nm and following delayed one-photon quenching (quench.) laser beam at 532 nm; (c) one-photon excitation (355 nm;) and delayed two-photon quenching (1064 nm); (d) two-photon excitation and simultaneous one-photon quenching by a single laser beam at 532 nm. ESA - possible excited state absorption processes.

IV.3 Theoretical description

The integral of the fluorescence emission, I_{FL} , excited and quenched in solution by laser pulses, reflects the type and efficiency of different stimulated optical transitions that may occur in a medium. The dependences of I_{FL} on excitation power provides insight into the nature of stimulated optical processes[60] while affording important information on

certain aspects of potential applications (such as the amplification parameters for stimulated emission[70] and potential spatial resolution in fluorescence microscopy[68]). In this paper, the simplest 3-level molecular model of **39** (Figures IV-1b-d) was utilized for an analytical description of the observed fluorescence emission under different fluorescence excitation and quenching conditions. For simplicity, only singlet electronic states, S_0, S_1, and S_n (the ground, first, and higher excited states, respectively) were taken into account. Laser pulses were assumed to be Gaussian in space (transverse beam radius, r_0 (HW1/e^{2}M)) and time (pulse duration, τ (HW1/eM)) with peak irradiance (in [cm^{-2}·s^{-1}]), $I_0 = \frac{\lambda_P . 2E_P}{\pi^{3/2} . h . c . r_0^2 . \tau}$, where λ_P , E_P, h, and c are the excitation wavelength, pulse energy, Planck's constant, and velocity of light in vacuum, respectively.[63] Two different sets of fluorescence excitation and quenching conditions were analyzed. In the first case, two beams were employed (pump-probe technique) with different excitation and quenching wavelengths: one-photon fluorescence excitation and, after some delay, one- or two-photon fluorescence quenching (Figure IV-1b, c). The second case corresponds to a single laser beam for two-photon fluorescence excitation and simultaneous (during the same laser pulse) one-photon fluorescence quenching (Figure IV-1d). It was assumed: (i) that the laser beams excited a nearly cylindrical volume inside of the cuvette containing an isotropic molecular solution; (ii) linear and nonlinear transmittance of the solution was ~100%, i.e., the beam irradiance was constant in the longitudinal direction; (iii) the population of the first excited state $N_1 >> N_n$ and $N_1 << N_0 \approx N$, where N_0, N_n, and N are the populations of S_0 and S_n per unit volume and total concentration, respectively; (iv)

the molecular fluorescence lifetime $\tau_F >> \tau$ (the pulse duration); (v) the fluorescence quantum yield η is constant within the entire absorption range, i.e., possible ESA processes do not lead to losses in I_{FL} due to radiationless transitions $S_n \rightarrow S_0$; and (vi) the laser repetition rate $f << 1/\tau_F$ and no accumulative effects occur in the medium, all reasonable assumptions given the carefully controlled sets of experimental conditions employed.

IV.3.1 One-photon excitation and one-photon fluorescence quenching

In the case of one-photon excitation and the assumptions above, each laser pulse creates the population $N_1(r,t)$, which can be obtained from the following equations:

$$\frac{dN_1(r,t)}{dt} = N_0(r,t)\sigma_{01}(\lambda_P)^P I(r,t) - N_1(r,t)\frac{1}{\tau_F}$$

$$N_0(r,t) + N_1(r,t) = N, \quad (1)$$

where r , t , and λ_P are the transverse coordinate, time, and excitation wavelength, respectively; $\sigma_{01}(\lambda_P)$ is the one-photon absorption cross section at λ_P; ${}^P I_0 \exp(-t^2/\tau^2 - 2r^2/{}^P r_0^2)$ is the pulse irradiance, while the subscript "*p*" corresponds to the pump beam. According to the assumptions (iii), (iv), and the dominant role of the stimulated transition $\sigma_{01}(\lambda_P)^P I(r,t) >> 1/\tau_F$, the population $N_1(r,t)$ reaches its largest value $N_1^P(r)$ towards the end of the excitation pulse and can be expressed as:

$$N_1^P(r) \approx N\sigma_{01}(\lambda_P) 2 \int_0^\infty {}^P I(r,t)dt . \quad (2)$$

The value of $N_1^P(r)$ determines the total number of induced fluorescence photons per excitation pulse, I_{F_0}, which can be registered by the detection system as:

$$I_{F_0} = \phi\eta L \int_0^{\infty} \int_0^{2\pi} N_1^P(r) r dr d\varphi, \quad (3)$$

where ϕ, η, and L are the collection efficiency of the registration system, fluorescence quantum yield of the molecule, and length of the cuvette, respectively. The second one-photon quenching laser pulse at wavelength λ_q decreases the value of $N_1^P(r)$ after time delay, τ_d ($2\tau < \tau_d << \tau_d$). The quenching laser pulse overlaps in space with the pumping volume and propagates in the same direction. The decrease in $N_1^P(r)$ is determined by the stimulated one-photon transitions $S_1 \rightarrow S_0$ with corresponding cross section $\sigma_{10}(\lambda_q)$ (Figure IV-1b). This leads to a decrease in I_{F_0}, which is recorded perpendicular to the pumping and quenching beams. Thus, the value of $N_1^P(r)$ after one pulse (quenching) can be obtained as:

$$N_1^q(r) \approx N_1^P(r)[1 - 2\sigma_{10}(\lambda_q) \int_0^{\infty} {}^q I(r,t) dt], \quad (4)$$

where subscript "q" corresponds to quenching. In this case, the total number of experimentally registered fluorescence photons is:

$$I_F = \phi\eta L \int_0^{\infty} \int_0^{2\pi} N_1^q(r) r dr d\varphi. \quad (5)$$

The degree of fluorescence quenching can be obtained from Eqs. (3) and (5):

$$1 - I_F \Big/ I_{F_0} = \frac{2\lambda_q \sigma_{10}(\lambda_q)}{\pi h c ({}^p r_0^2 + {}^q r_0^2)} {}^q E_P, \quad (6)$$

where ${}^{P}r_0$, ${}^{q}r_0$, and ${}^{q}E_P$ are the pump and quenching beam radius (HW1/e^{2}M) and pulse energy of the quenching beam, respectively. According to Eq. (6), the value of $1-I_F/I_{F_0}$ is directly proportional to the quenching pulse energy in the case of one-photon quenching.

IV.3.2 One-photon excitation and two-photon fluorescence quenching

For one-photon excitation and two-photon fluorescence quenching the same population $N_1^P(r)$, created by one-photon excitation (Eq. (4)), can be quenched by an IR pulse at the wavelength $2\lambda_q$ with the same duration τ , and propagating in the same direction with time delay τ_d (Figure IV-1c). Any ESA processes at $2\lambda_q$ don't affect the integrated fluorescence intensity (assumption (v)), two-photon stimulated transitions $S_1 \rightarrow S_0$ (with corresponding two-photon emission cross section $\delta_{2PE}(2\lambda_q)$) should be the only reason for a decrease in I_{F_0}. It is interesting to note that this fluorescence quenching methodology allows one to elucidate two-photon stimulated emission transitions, distinguishing this from possible one-photon ESA effects. In this case, the value of S_1 population after the quenching pulse, N_1^{2Pq}, can be expressed as:

$$N_1^{2Pq}(r) \approx N_1^P(r)[1-\delta_{2PE}(2\lambda_q)\int_0^{\infty} {}^{q}I^2(r,t)dt], \quad (7)$$

and the total number of registered fluorescence photons as:

$$I_F = \phi\eta L\int_0^{\infty}\int_0^{2\pi} N_1^{2Pq}(r)rdrd\varphi, \quad (8)$$

Taking into account Eqs. (3) and (8), the degree of fluorescence quenching can be represented as:

$$1 - I_F / I_{F_0} = (2/\pi^5)^{1/2} \frac{(2\lambda_q)^2 \delta_{2PE}(2\lambda_q)}{h^2 c^2 \tau^q r_0^2 (2^p r_0^2 + {}^q r_0^2)} {}^q E_P^2. \quad (9)$$

From Eq. (9), for the case of two-photon quenching, the value of $1 - I_F / I_{F_0}$ is directly proportional to the square of quenching pulse energy, and the slope of the dependence $1 - I_F / I_{F_0} = f({}^q E_P^2)$ allows one to determine the two-photon emission cross section $\delta_{2PE}(2\lambda_q)$.

IV.3.3 Two-photon excitation and one-photon fluorescence quenching with a single laser beam

A single laser beam can be used for two-photon excitation and simultaneous one-photon quenching of the induced fluorescence emission (Figure IV-1d). In this case Eq. (1) should be changed to:

$$dN_1(r,t)/dt = N_0(r,t) \frac{\delta_{2PA}(\lambda_P)}{2} {}^P I^2(r,t) - N_1(r,t)[\sigma_{10}(\lambda_P) {}^P I^2(r,t) + 1/\tau_F]$$

$$N_0(r,t) + N_1(r,t) = N, \quad (10)$$

where $\sigma_{10}(\lambda_P)$ is the one-photon stimulated emission cross section of the transition $S_1 \rightarrow S_0$. For sufficiently low pulse irradiance: ${}^P I(r,t) << (1/[\tau_F \sigma_{10}(\lambda_P)],\ 1/[\tau_F \delta_{2PA}(\lambda_P)^{1/2}])$, solving Eq. (10) gives the value of $N_1^q(r)$, and the corresponding registered integrated fluorescence emission can be obtained as:

$$I_{FL} \approx \phi \eta L N \frac{\lambda_P^2 \delta_{2PE}(\lambda_P)}{\pi^{3/2} h^2 c^2 \tau^p r_0^2} E_P^2, \quad (11)$$

From Eq. (11), the value of $I_{FL} \sim E_P^2$, in the range of relatively low excitation irradiance. In general, the numerical solution of Eq. (10) affords a nearly linear

dependence: $I_{FL} \sim E_P$; for intermediate excitation irradiance: $1/[\tau_F \sigma_{10}(\lambda_P)] << {}^P I(r,t) << \sigma_{10}(\lambda_P)/\delta_{2PA}(\lambda_P)$; and I_{FL} is a nearly constant for ${}^P I(r,t) >> (\sigma_{10}(\lambda_P)/\delta_{2PA}(\lambda_P), 1/[\tau_F \sigma_{10}(\lambda_P)])$.

IV.4 Experimental

IV.4.1 Synthesis and Characterization

The synthesis of sulfonyl-containing fluorene derivative **39**, is shown in Scheme IV-1. Synthesis precursors **1**, **2**, **3**, and **4** was done according to the literature.[41] Compound **40** was obtained from the oxidation of **2**, which was done from a modified literature procedure.[71] The Horner-Emmons-Wadsworth coupling was performed as described below yielding compound **39** in 38%. All glassware was flamed dried and cooled in a desiccator over calcium chloride. All reactions were carried out under N_2 atmosphere. All solvents and commercially available reagents were used without further purification unless otherwise indicated.

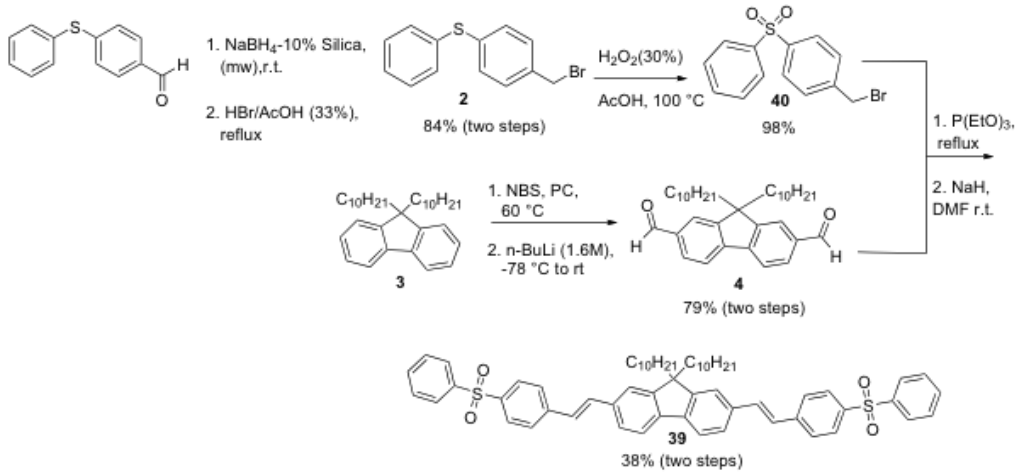

Scheme IV-1. Synthesis of sulfonyl containing fluorene derivative **39.**

Preparation of (4-(bromomethyl)phenyl)(phenyl)sulfone, 40. The synthesis of (4-(bromomethyl) phenyl)(phenyl)sulfone was performed based on a modified procedure from Hsiao *et al*.[27] Hydrogen peroxide (30%, 0.100 g, 0.80 mmol) was added to a solution of (4-(bromomethyl)phenyl) (phenyl) sulfide, **2** (0.141 g, 0.51 mmol) in commercial glacial acetic acid (0.200 g). The mixture was mildly heated until the exothermic reaction was initiated and additional 0.100 g of 30% hydrogen peroxide was added. The mixture was then taken to 100 °C and followed by TLC every 15 min. Upon completion (2 h), cooled to room temperature and the acetic acid evaporated in vacuo. The crude was dissolved in ethyl ether, washed with a saturated sodium bicarbonate solution (2x), brine (2x), dried (anhydrous $MgSO_4$), and filtered. After concentration of the filtrate, in vacuo, the crude was purified by column recrystalization (acetone:water 1:1) to obtain 0.155 g (98%) of a colorless solid. ^{1}H NMR (300 MHz, $CDCl_3$) 7.94 (m, 4H, Ar-H), 7.92 (m, 5H, Ar-H); 4.45 (s, 2H, -CH_2-). ^{13}C NMR (75 MHz, $CDCl_3$) 143.3 (C), 141.6 (C), 141.4 (C), 133.6 (CH), 130.1 (CH), 129.6 (CH), 128.4 (CH), 127.9 (CH), 31.8 (CH_2). mp 135-136 ºC (lit. 132 ºC).[28]

Preparation of (4,4'-(1E,1'E)-2,2'-(9,9-didecyl-9H-fluorene-2,7-diyl)bis(ethene-2,1-diyl)bis(4,1-phenylene))bis(phenylsulfone), **39**. In a two-neck, 250 mL round bottom flask, 0.245 g (0.79 mmol of (4-(bromomethyl)phenyl)(phenyl)sulfone, 6, were dissolved in 6 mL of dry, freshly distilled triethylphosphite. The mixture was taken to reflux and monitored by TLC until complete conversion of the starting material was observed (5 h). The unreacted triethylphosphite was evaporated by vacuum distillation, affording a viscous, pale yellow oil, which was used for the Horner-Emmons-Wadsworth reaction

without further purification. The phosphonate, was dissolved in 10 mL of dry DMF and 0.228 g of NaH was added portion-wise to the solution. The mixture was stirred at room temperature for 1 h. A solution of 2,7-diformylflourene, 6, (0.198 g, 0.39 mmol, in 5 mL of dry DMF) was added drop wise to the solution, which was then monitored by TLC until no 2,7-diformylflourene was observed (24 h). Once the reaction was complete, the solution was added (2x) and washed (3x) with water, and dried with magnesium sulfate. The crude was purified by column chromatography on silica gel using an ethyl acetate:hexane mixture of 1:1 and run under N_2. A yellow solid was obtained 0.142 g (38% in two steps). mp 150.9-151.5 ºC; ^{1}H NMR (300 MHz, $CDCl_3$) 7.96 (m, 8H), 7.63 (m, 16H), 7.28 (d, 2H); 7.12 (d, 16.5 Hz, 2H), 1.99 (m, 4H), 1.10 (m, 28H), 0.77 (t, .6.3 Hz, 6H), 0.63 (m, .4H); ^{13}C NMR (75 MHz, $CDCl_3$) 151.5 (C), 142.3 (C), 141.5 (C), 139.4 (C), 135.3 (C), 132.9 (C), 132.8 (CH), 131.2 (CH), 129.1 (CH), 128.0 (CH), 127.3 (CH), 126.7 (C), 126.7 (CH), 121.0 (C), 120.2 (C). 108.1 (C), 55.0 (C), 31.8 (C), 29.9 (C), 29.5 (C), 29.2 (C), 23.7 (C), 22.6 (C), 14.0 (C). HRMS. for ($C_{61}H_{70}O_4S_2$): Theoretical $[M+H]^+$: 931.4788, $[M+NH_4^+]^+$: 948.5054, $[M+Na]^+$: 953.4608. Found: $[M+H]^+$: 931.4769, $[M+NH_4^+]^+$: 948.5057, $[M+Na]^+$: 953.4604.

IV.4.2 Optical measurements

All measurements were performed in spectroscopic grade toluene and THF at room temperature. The absorption spectra were obtained with an Agilent 8453 UV–visible spectrophotometer in 10 mm path length quartz cuvettes for concentrations $C \approx (1\text{-}2)\cdot10^{-5}$ M. The steady-state fluorescence spectra were recorded with a PTI Quanta Master spectrofluorometer in 10 mm spectrofluorometric quartz cuvettes for dilute solutions (C ~

10^{-6} M). All spectra were corrected for the spectral responsivity of PTI detection system. The fluorescence quantum yields of **39** were determined relative to 9,10-diphenylanthracene in cyclohexane (η = 0.95).[29] Fluorescence lifetimes were measured with a time-correlated single photon counting system PicoHarp300 and 76 MHz femtosecond excitation (MIRA 900, Coherent).

Optical stimulated transitions in **1** were investigated using a picosecond Nd:YAG laser (PL 2143 B Ekspla) operating with exit wavelengths 1064 nm (base), 532 nm (second harmonic), and 355 nm (third harmonic), pulse duration $\tau \approx 21$ ps (HW1/eM), nearly Gaussian time and space pulse intensity distributions, and a 10 Hz repetition rate. The experimental setup is illustrated in Figure 2. Two separate laser beams were used (pump-probe method[70]) for one-photon excitation and one- or two-photon induced quenching. Excitation laser pulses at λ_P = 355 nm with $E_P \leq 12$ μJ were focused into a 1 mm quartz cuvette (concentration C ≈ $5 \cdot 10^{-5}$ M) with a waist of radius ${}^{P}r_0 \approx 0.15$ mm. Fluorescence emission was observed perpendicular to the excitation beam. This fluorescence was partially quenched by another laser pulse at λ_q = 532 nm (one-photon quenching, ${}^{q}E_P \leq 50$ μJ), propagating in the same direction, fully overlapped in space with the excitation volume and delayed for $\tau_d \approx 80$ ps relative to the excitation pulse. The amount of spontaneously emitted fluorescence photons during delay time τ_d was negligible due to $\tau_d << \tau_F$. After the quenching pulse, the energy of the rest of the collected fluorescence photons was measured with a silicon photodetector. For two-photon induced quenching, the laser beam at λ_q = 1064 nm (${}^{q}E_P \leq 200$ μJ) was used at

the same excitation conditions as for one-photon quenching: λ_q = 355 nm, $E_P \leq$ 12 μJ, ${}^{P}r_0 \approx$ 0.15 mm, $\tau_d \approx$ 80 ps and full spatial overlap.

A single laser beam at λ_q = 532 nm was used in the case of two-photon excitation and simultaneous one-photon induced quenching of the fluorescence emission of **39**. According to Figure IV-1a, the wavelength λ_q = 532 nm is within the fluorescence emission spectral range of **39** and the losses of pulse energy E_P, determined by the ground state one-photon absorption, are negligible. In this case, the laser beam with $E_P \leq$ 200 μJ was focused in a 10 mm quartz cuvette (concentration C ≈ $3 \cdot 10^{-4}$ M) to a waist of radius ${}^{P}r_0 \approx$ 0.3 mm. It should be mentioned, that in all measurements, the polarization of the laser beams was vertical and the quality of the filtered scattered excitation and quenching light was controlled by a fiber optic spectrometer USB2000 (Ocean Optics Inc.). No photochemical and other accumulative effects were observed.

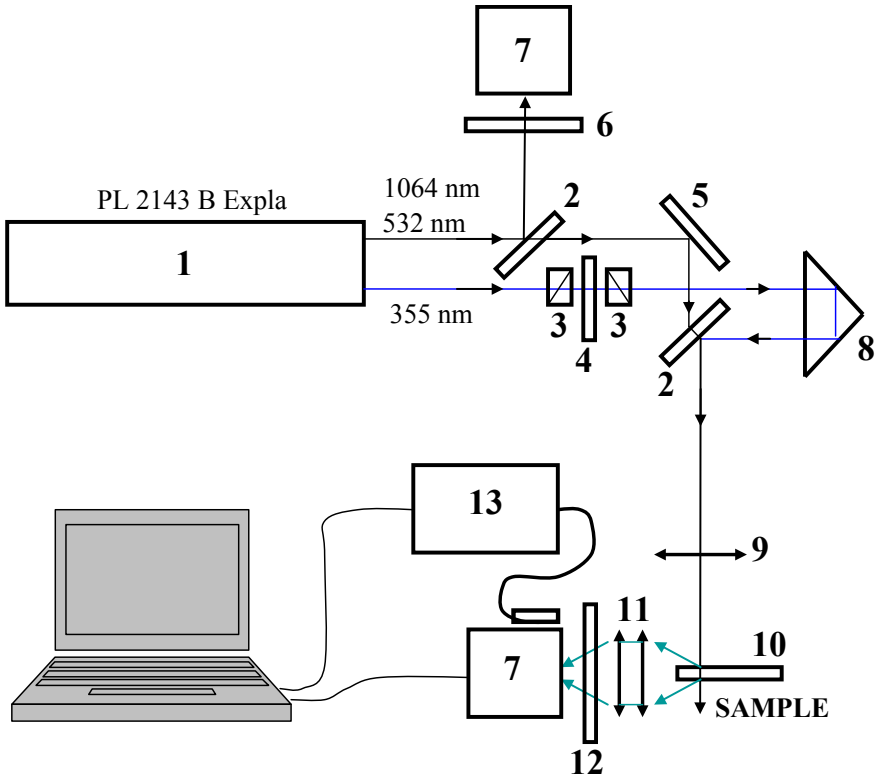

Figure IV-2. Experimental setup: 1 - picosecond laser; 2 - beam splitters; 3 - polarizer; 4 - wave plate $\lambda/2$; 5 - 100% reflection mirror; 6 - neutral density filters; 7 - calibrated silicon photodetectors; 8 - time delay line; 9 - focusing lens (25 cm); 10 - 1 mm or 10 mm quartz cuvettes with investigated solutions; 11 - optical collection system; 12 - set of neutral and interferometric filters; 13 - fiber optic spectrometer. Optical elements (3, 4) were used for ease of changing the pulse energies for the wavelengths used.

IV.5 Results and Discussion

The linear absorption and steady-state fluorescence spectra of **39** in toluene and THF at room temperature are presented in Figure IV-1a. The absorption spectra were nearly independent of solvent properties while the fluorescence spectra exhibited some solvatochromic dependence. Fluorene **39** possesses nearly identical extinction coefficients (molar absorptivity) in toluene and THF, $\varepsilon_{abs}^{max} \approx (92 - 95)\cdot 10^{-3}$ $M^{-1}\cdot cm^{-1}$ and a single exponential fluorescence decay with lifetimes: $\tau_F \approx 0.85$ (toluene) and 0.74 ns

(THF). The fluorescence quantum yields of **39** were $\eta \approx 1$ and independent of the excitation wavelength in all solvents, as shown in Figure IV-3a. This suggests no participation of direct radiationless transitions $S_n \rightarrow S_0$. Therefore, the fluorescence intensity of **39** is not quenched by an ESA mechanism. A comprehensive analysis of the linear spectral properties of **39**, including excitation anisotropy spectra, was reported in one of our previous papers.[72]

One-photon induced fluorescence of **39**, and its delayed one- and two-photon quenching, can be analyzed from the data presented in Figure IV-3b-f. The dependences of the integrated fluorescence emission I_{FL} on the excitation pulse energy E_P at $\lambda_P = 355$ nm (Figure IV-3b) revealed a linear one-photon population of the fluorescent level S_1 over the energy range used. A linear dependence $I_{FL} = f(E_P)$ confirmed the validity of assumptions (ii), (iii), and (v). The one-photon quenching wavelength $\lambda_q = 532$ nm was chosen to be within the fluorescence emission spectral range of **1**, and the quenching pulse was delayed to $\tau_d \approx 80$ ps $> 2\,\tau$ to avoid overlap with the excitation pulse.

The dependences of $1 - I_F / I_{F_0}$ on the quenching pulse energy ${}^{q}E_P$ for one-photon excitation at 355 nm and one-photon quenching at 532 nm are presented in Figure IV-3c, d. Deduced from this data, the values of $1 - I_F / I_{F_0}$ were found to exhibit a linear dependence on ${}^{q}E_P$ in both solvents, in agreement with Eq. (6). The values of the one-photon stimulated transition cross sections, $\sigma_{10}(\lambda_q)$,was estimated from the slope of these dependences. For example: $\sigma_{10}(532nm) \approx 2.5 \cdot 10^{-17}$ cm^2 in toluene, which is close

to the corresponding value $\sigma_{10}(532nm) \approx 3 \cdot 10^{-17}$ cm^2 calculated from the known steady-state absorption $\varepsilon_{abs}(\lambda)$ and fluorescence $I_{FL}(\lambda)$ spectra.

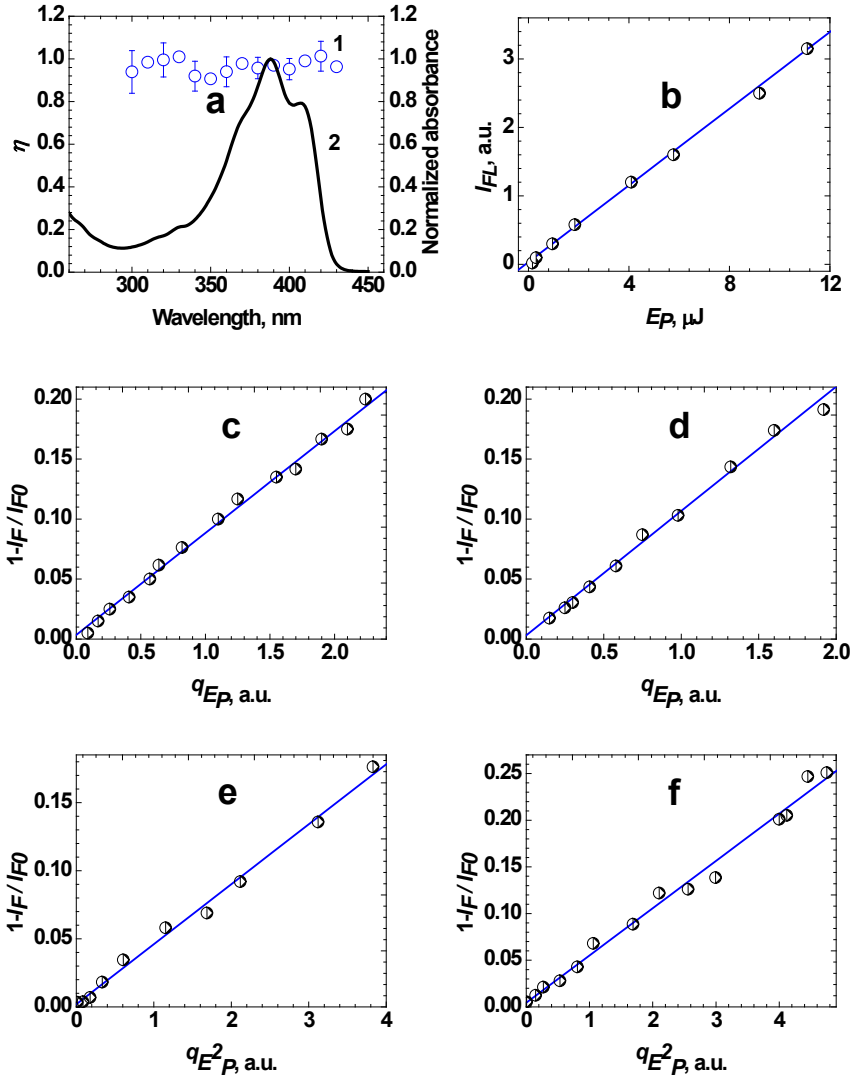

Figure IV-3. Spectral dependence of the fluorescence quantum yield η (1) and normalized absorption spectrum of **39** in toluene (a); dependence of integral fluorescence emission in toluene (b); dependences $1 - I_F / I_{F_0} = f({}^qE_P)$ for one-photon fluorescence quenching at λ_q = 532 nm in

toluene (c) and THF (d), and two-photon fluorescence quenching at λ_q = 1064 nm in toluene (e) and THF (f).

The values of $1-I_F/I_{F_0}$ exhibited a quadratic dependence on quenching pulse energy ${}^qE_P$ (see Figure IV-3e, f) in the case of two-photon fluorescence quenching at λ_q = 1064 nm, which was in good agreement with Eq. (9). It should be mentioned that λ_q= 1064 nm is out of the fluorescence emission spectral range of **1**, and, thus, one-photon stimulated transitions at this wavelength are negligible. Possible ESA processes at λ_q = 1064 nm from the S_1 electronic state cannot affect the fluorescence intensity, as discussed previously. As a result, the quadratic dependences $1-I_F/I_{F_0}=f({}^qE_P)$ reveal a pure two-photon stimulated quenching of the fluorescence. The values of the corresponding cross sections were estimated from the slope of the dependences in Figure IV-3e, f : $\delta_{2PE}(1064nm)\approx$ 240 GM and ≈ 280 GM for **39** in toluene and THF, respectively.

The nature of the stimulated transitions under two-photon fluorescence excitation and simultaneous one-photon fluorescence quenching at 532 nm was analyzed from the dependences presented in Figure IV-4. The quenching wavelength is located sufficiently far from the linear absorption bands and can be absorbed only through the 2PA mechanism. The dependences of the integrated fluorescence emission I_{FL} of **39** with excitation pulse energy E_P exhibited nearly quadratic character at low excitation irradiance ($E_P\leq$ 15 μJ), as shown in the insets of Figure IV-4. These results are in good agreement with Eq. (11), describing a pure 2PA mechanism when the stimulated transitions $S_1 \rightarrow S_0$ are neglected. Apparent in Figure IV-4, the dependence $I_{FL}=f(E_P)$

becomes close to linear in the intermediate range of excitation irradiance (E_P > 15 μJ), providing evidence for the contribution of one-photon quenching at 532 nm. Further increase in the pulse energy E_P > 200 μJ, along with an expected saturation effect, was not realized due to laser damage of the cuvette. For comparison, the same dependence $I_{FL} = f(E_P)$ was obtained for p-terphenyl in toluene, see Figure IV-5. The fluorescence spectrum of this compound (curve 2 in Figure IV-5a) did not overlap with λ_P = 532 nm. Thus, one-photon stimulated quenching is negligible. As can be seen in Figure IV-4b, the dependence $I_{FL} = f(E_P)$ was close to quadratic over the entire energy range. These results for p-terphenyl in toluene at λ_P= 532 nm was anticipated, reflecting two-photon excitation origin of the induced fluorescence.

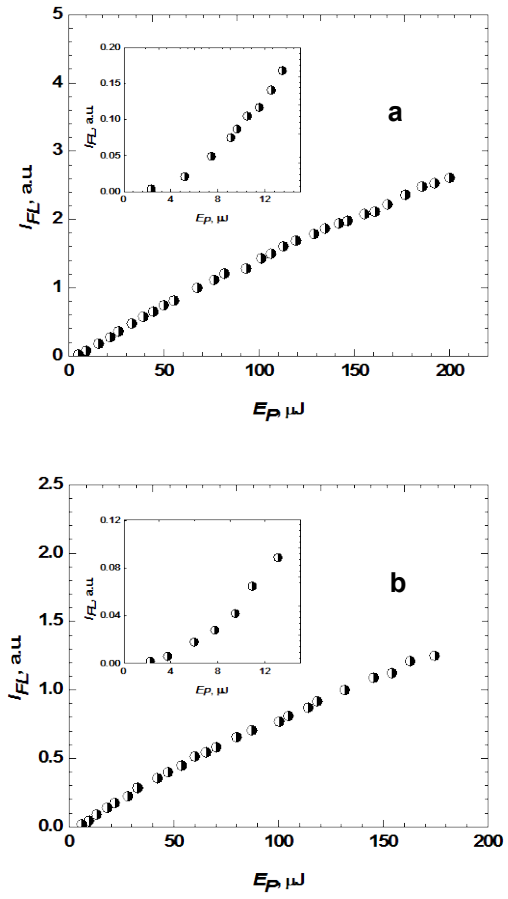

Figure IV-4. Dependences of the integrated fluorescence intensity of **39** in toluene (a) and THF (b) on excitation pulse energy E_P at $\lambda_P = 532$ nm. Insets reveal the initial parts of the corresponding dependences.

IV.6 Conclusion

A comprehensive investigation of stimulated transitions in sulfonyl-containing fluorene **39** in toluene and THF was accomplished with a picosecond fluorescence quenching method at room temperature. The fluorescence quenching processes exhibited good agreement with theoretical predictions, and can be used to study the nature of stimulated transitions and for the determination of the corresponding one- and two-

photon quenching cross sections. Pure two-photon stimulated transitions $S_1 \rightarrow S_0$ with $\delta_{2PE}(\lambda_q) \approx$ 240 - 280 GM were shown for **39** at λ_q = 1064 nm. A complex, nonquadratic dependence of two-photon induced fluorescence intensity on excitation pulse energy was obtained at λ_P = 532 nm, providing compelling evidence of the contribution of one-photon induced quenching upon two-photon excitation. The determination of the spectral dependence and absolute values of one- and two-photon stimulated emission cross sections is important for both fundamental scientific research and to develop the tenets for a number of nonlinear optical applications that may exploit STED. In particular, the two-photon stimulated emission processes can be harnessed to further increase the spatial resolution of fluorescence microscopy imaging. Based on the results of this study, sulfonyl-containing fluorene derivative **39**, exhibiting high fluorescence quantum yield and photochemical stability, is a promising fluorescence probe for one- and two-photon STED microscopy, a subject of further investigation in our laboratory.

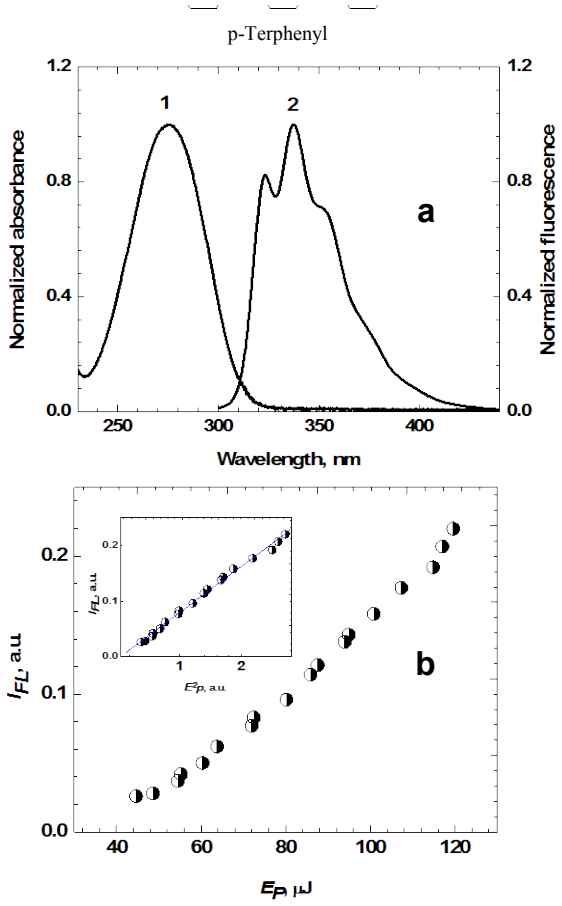

Figure IV-5. Normalized absorption (1) and fluorescence (2) spectra of p-terphenyl in toluene (a); dependence $I_{FL} = f(E_P)$ at λ_P = 532 nm for p-terphenyl in toluene (b). Inset represents the quadratic dependence.

CHAPTER V: FUTURE WORK

Further development of new 3D ODS systems may be based on the utilization of different types of optical stimulated transitions induced in organic molecules by laser radiation. The nature of one- and two-photon stimulated transition processes has attracted the scientific community for decades in areas such as two-photon induced fluorescence (2PF),[51,52] nonlinear transmittance,[53,54] two-photon absorption (2PA) processes,[55-57] and light amplification of stimulated emission (lasing).[58,59] Excited state dynamics and stimulated transitions of organic molecules can be studied by fluorescence quenching methodology reported by Lakowicz.[64,73,74] This methodology allows modification of the molecular orientational distribution in the excited states and creates anisotropic molecular ensembles with specific fluorescence properties.[64] Special excitation and quenching conditions, which can be induced in the storage medium, noticeably enhance the potential of materials in nonlinear optical applications. One innovative example is the use of one-photon stimulated emission transitions as a means to overcome the diffraction limit in fluorescence microscopy.[67,68] This resulted in the development of high resolution (~60 nm, see Figure V-1) stimulated emission depletion (STED) fluorescence microscopy, an illustrative example is shown in Figure V-1.[69,75] The spatial resolution that can be achieved by one- or two-photon optical excitation is also a primary parameter for 3D ODS techniques that can be further improved under specific excitation and quenching conditions. We propose that the advantages of two-photon excitation in combination with nonlinear two-photon STED quenching will

provide a breakthough in increasing the current capacity of two-photon 3D ODS systems (10^{12} bits/cm^3)[5] even further.

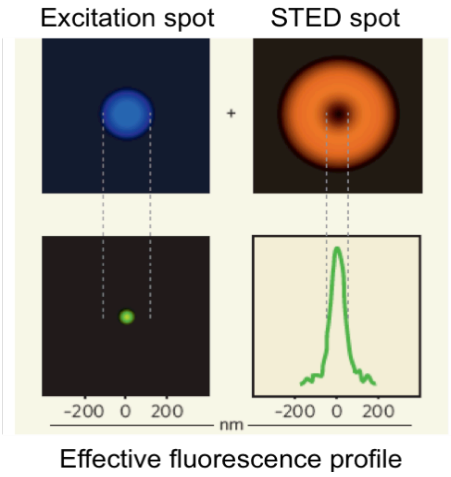

Figure V-1. STED microscopy. The blue excitation beam excites the fluorophore and is focused down to a diffraction-limited spot. The orange STED beam depletes the molecules in the excited states, by pumping them down out of the excited state before they fluoresce. Superimposition of the STED beam on the excitation beam, results in a reduction of the fluorescence area to about 50 nm by the STED beam (sub diffraction limit).[76]

In summary, further increase of the data storage capacity of a WORM system similar to the one described above (Chapter II) could be achieved by applying stimulated emission depletion (STED) both for data encoding and data readout, providing unprecedented storage capacity in a two-photon 3D WORM ODS PAG-based system. These systems will take advantage of the tremendous increase in resolution provided by double STED process. The first step, the writing process where the generation of the photoacid will be highly localized in the storage media by light stimulated depletion. Successive fluorescence readout will also take advantage of the nonlinearity of the 2PA dye to induce the STED readout. The library of 2PA compounds we have made will enable us to evaluate the response of these compounds to STED. Furthermore, the

experience that we possess in nonlinear ODS systems will allow us to compare the increase in storage capacity between nonlinear ODS systems that are STED based to those that do not utilize the STED advantage. Thus, a future aim is to investigate double or tandem STED-based 2PA processes in a PAG-fluorophore system for high density, nanoscopic WORM 3D optical data storage. For such a project, two final goals can be identified: (1) understand the application and limitations of two-photon STED for 3D spatially-localized photoacid production and sub-100 nm voxel formation, (2) understand the application and limitations of two-photon STED for sub-100 nm voxel 3D readout. These efforts should lead to a breakthough in 3D optical data storage, providing the tenets for future photonic materials and systems design.

V.1 Proposed Reasearch Plan

V.1.1 STED Solution Studies of System Components.

Developing a STED-based 3D WORM ODS system can be seen as the next logical step once its nonlinear WORM precursors has been developed and optimized. The design and optimization of a nonlinear WORM ODS system has been described above (Chapter II) based on efficient 2PA PAGs and fluorine-based fluorescent dyes. Therefore, the first step in developing a STED-based system is to evaluate the stimulated emission depletion response of its components, i.e. the PAGs (for data encoding) and the unprotonated and protonated 2PA dyes (for data readout). Initially this response will be evaluated in solution. Standard procedure calls for the linear photophysical characterization of all PAGs and dyes. We have most of the dyes and PAGs on hand in the lab. The ones that are not in large enough quantity will be scaled up. Slight

modifications will be made to the PAG and dye structures, in an iterative manner, to influence the wavelengths of their 2PA for STED and 3D ODS. Properties to be evaluated are UV-vis absorption, fluorescence emission, fluorescence anisotropy (important in discerning positions/energies of the various electron transitions), fluorescence quantum yields (Φ_F), photoacid quantum yields (Φ_{H+} for PAGs only), linear absorption cross sections (σ_{01}) and emission cross sections (σ_{10}). Nonlinear characterization will consist of the measurement of the 2PA cross sections (δ_{PA}). The cross section of the 2PA fluorescent dyes can be determined by either the fluorescence[77] or the Z-scan method.[62] However, determination of the PAG cross sections will be conducted by the Z-scan method because of the low fluorescence quantum yields of these molecules. Furthermore, these experiments should be carried out in flow cells to account for the decomposition of the photoacids upon excitation (acid generation). The equipment to conduct these studies is already in place.

The first PAG to be analyzed is **7**, the high fluorescence quantum yield (Table II-2), though not ideal for a conventional PAG, makes it an attractive candidate for emission depletion. First the PAG solution will be excited by one-photon fluorescence excitation and its emission quenched by either one- or two-photon irradiation using a femtosecond pump-probe technique and the two laser beams at different wavelengths, as described above for **39** (Chapter IV). This experiment will be followed by the induction of two-photon fluorescence and its concurrent one-photon depletion using a single femtosecond laser beam as described above (Chapter IV). This series of experiments will be performed for each of the PAG and dye components of the system. For the PAGs, these

experiments will be carried out in a flow cell to compensate for photodecomposition of the analyte.

V.1.2 STED Data Storage Capacity in Polymer Films.

To evaluate the increase in data storage capacity of the STED-based WORM ODS systems, a solution of the PAG–dye could be made in polymer **31** at the concentrations discussed above. The solutions can be spin-coated or drop casted onto a 22x 22 mm glass cover slip. Once the film has dried the slides can be mounted on the stage of an inverted Olympus IX-80. This microscope is equipped with a Fluoview 300 laser scanning head through which two laser wavelengths will be fed for the writing and readout. Two-photon STED recording will be performed by exciting the photoacid by two-photons, by pumping at one wavelength, and depleting the excited state by pumping at another wavelength with an appropriate delay. Two different STED writing experiments can be done, the first willbe one-photon depletion (one-photon-STED) and the second will be two-photon depletion (two-photon-STED).

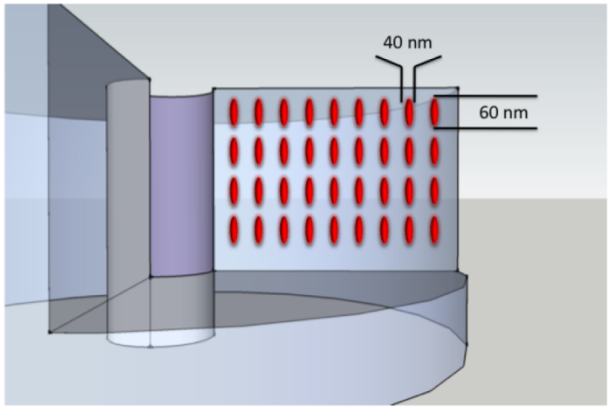

Figure V-2. Representation of 3D STED ODS. Voxels could reach 40 nm and 60 nm in radial and axial lengths respectively reaching storage densities of up to $\approx 10^{15}$ bytes/cm^3 (or Terabyte in a 1 mm cube).

Technically, the STED data storage experiments in polymer films can be done as described below. During the STED writing the galvanometers in the microscope scan head will remain in a fixed position. The exposure times will be controlled by an external electronic shutter, and the positions will be dictated by the piezo positioner that serves as a stage for the microscope. After recording (60x, 1.4 N.A., oil immersion objective) an x-y layer of voxels, the stage will moved in z- axis at fixed intervals to focus deeper into the polymer matrix generating successive sets of voxels. The two sets of voxels (those recorded by 1PA-STED and those 2PA-STED) will then be readout by one and two-photon STED, respectively, generating 2 assemblies of voxels to compare for resolution enhancement, i.e. one-photon-STED writing/one-photon-STED readout and two-photon-STED writing/two-photon-STED readout. Readout will be performed by scanning consecutive 0.06 μm layers of the polymer, pumping at different wavelengths and delays in order to obtain the one-photon-STED and two-photon-STED images of the protonated 2PA dyes. These results will ultimately be compared to those discussed above (Chapter II, Figures II-9 to II-12). According to our approximations voxels can reach 40 nm and 60 nm in radial and axial lengths, respectively, giving this system a storage density capacity of up to $\approx 10^{15}$ Bytes/cm^3, suggesting that a Terabyte of information in this system can be stored in a 1 mm cube (Figure IV-2).

APENDIX A: ^{1}H AND ^{13}C, AND DEPT NMR SPECTRA OF NEW MOLECULES IN CHAPTER I

^{1}H NMR Spectrum of (4-(phenylthio)phenyl)methanol.

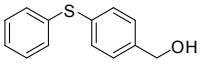

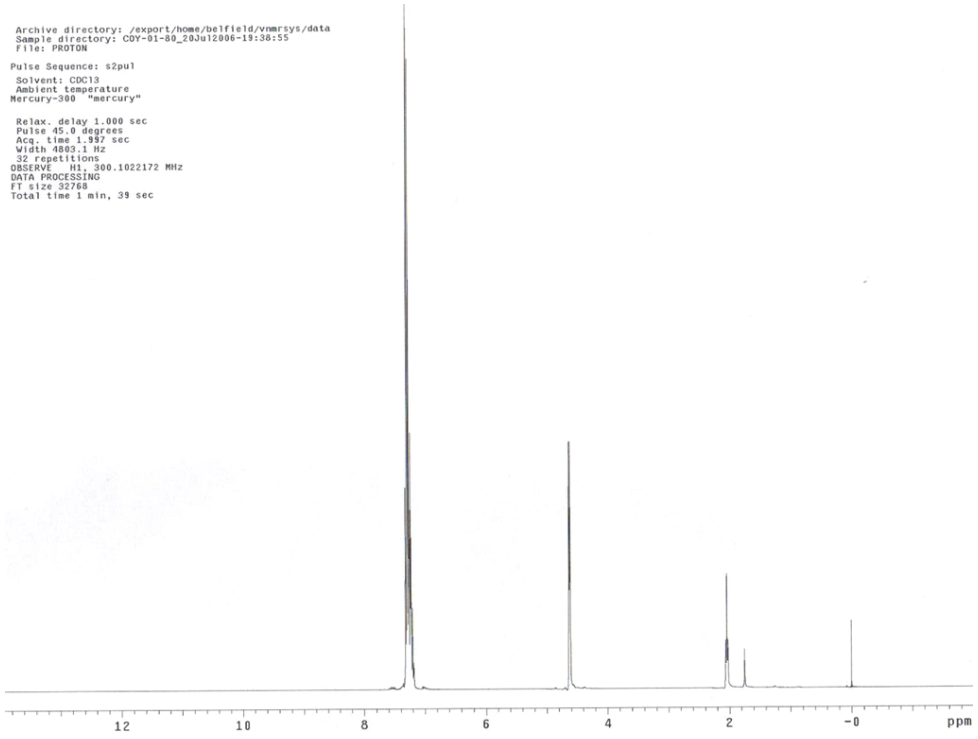

^{13}C NMR Spectrum of (4-(phenylthio)phenyl)methanol.

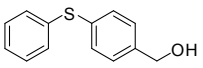

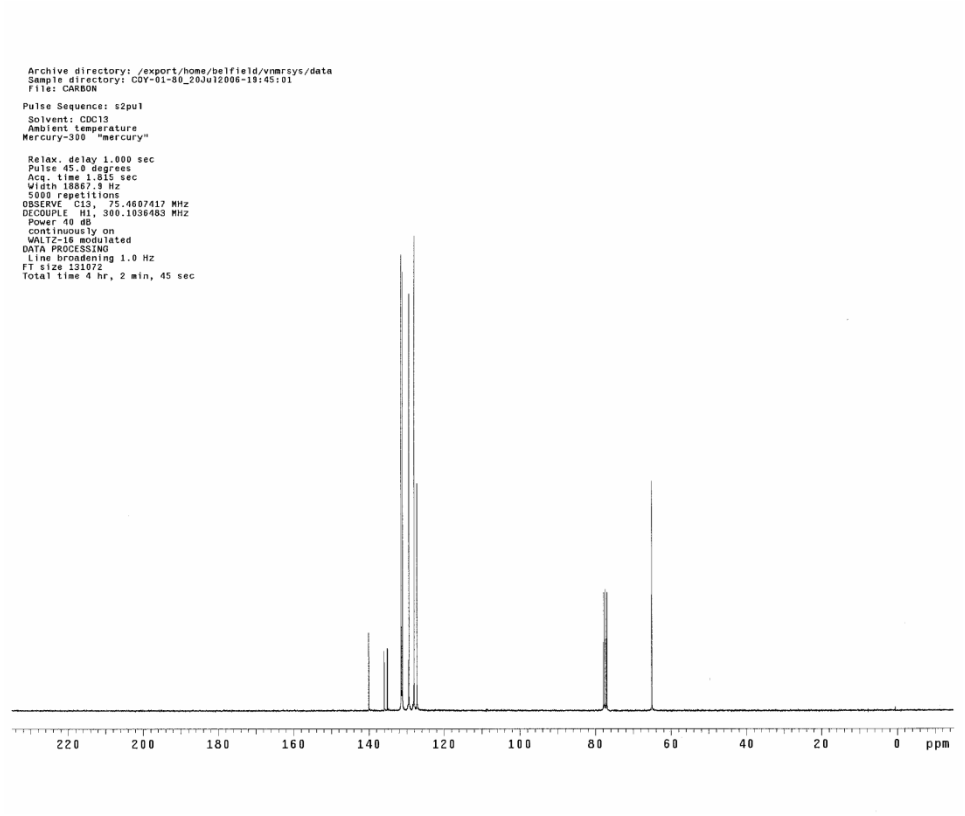

DEPT 135 Spectrum of (4-(phenylthio)phenyl)methanol.

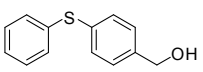

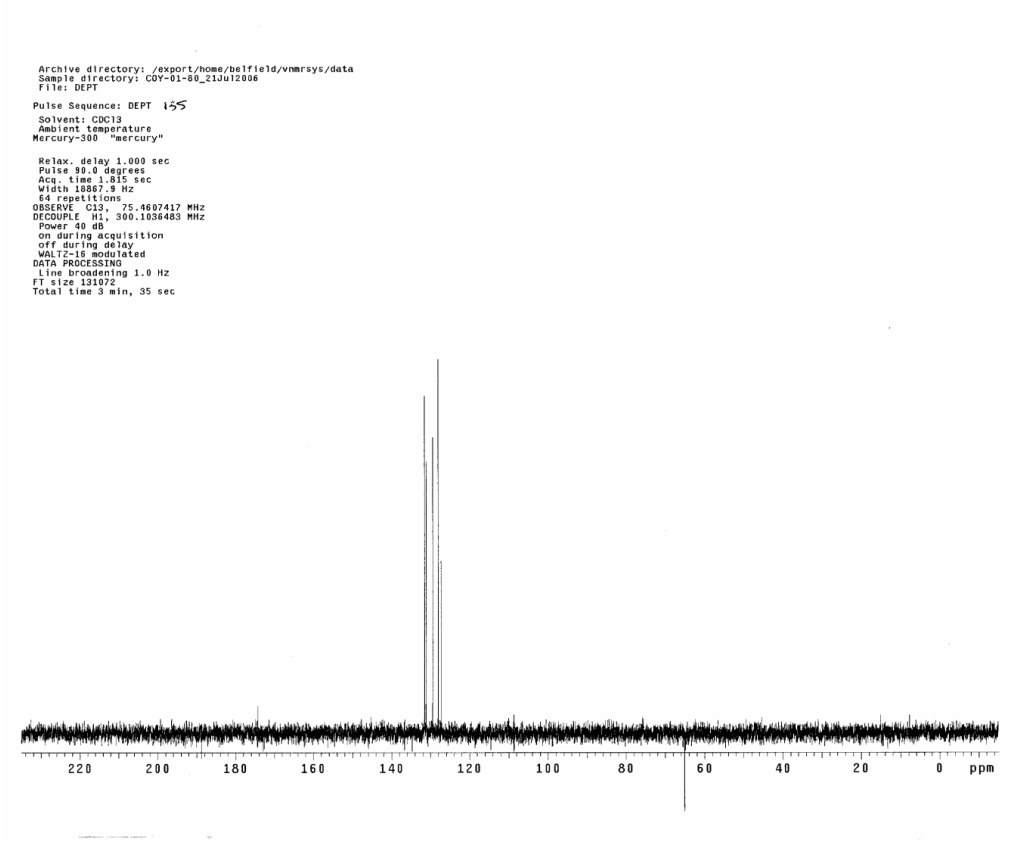

^{1}H NMR Spectrum of **2.**

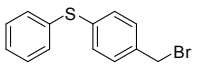

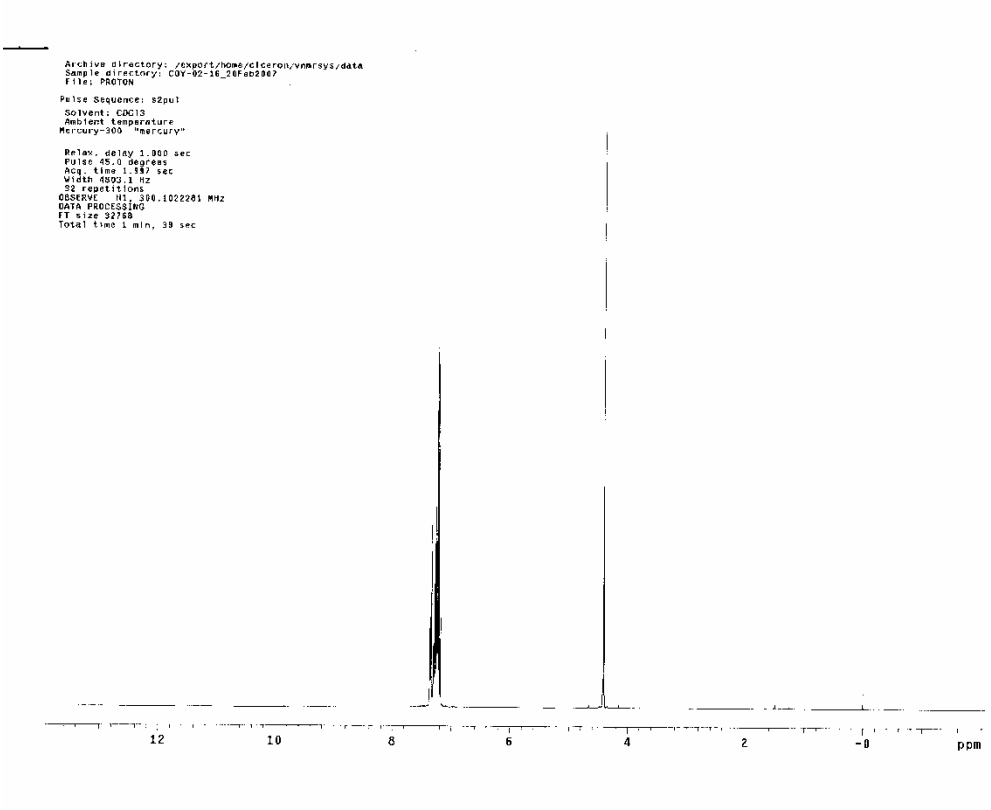

^{13}C NMR Spectrum of **2.**

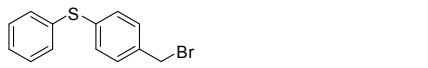

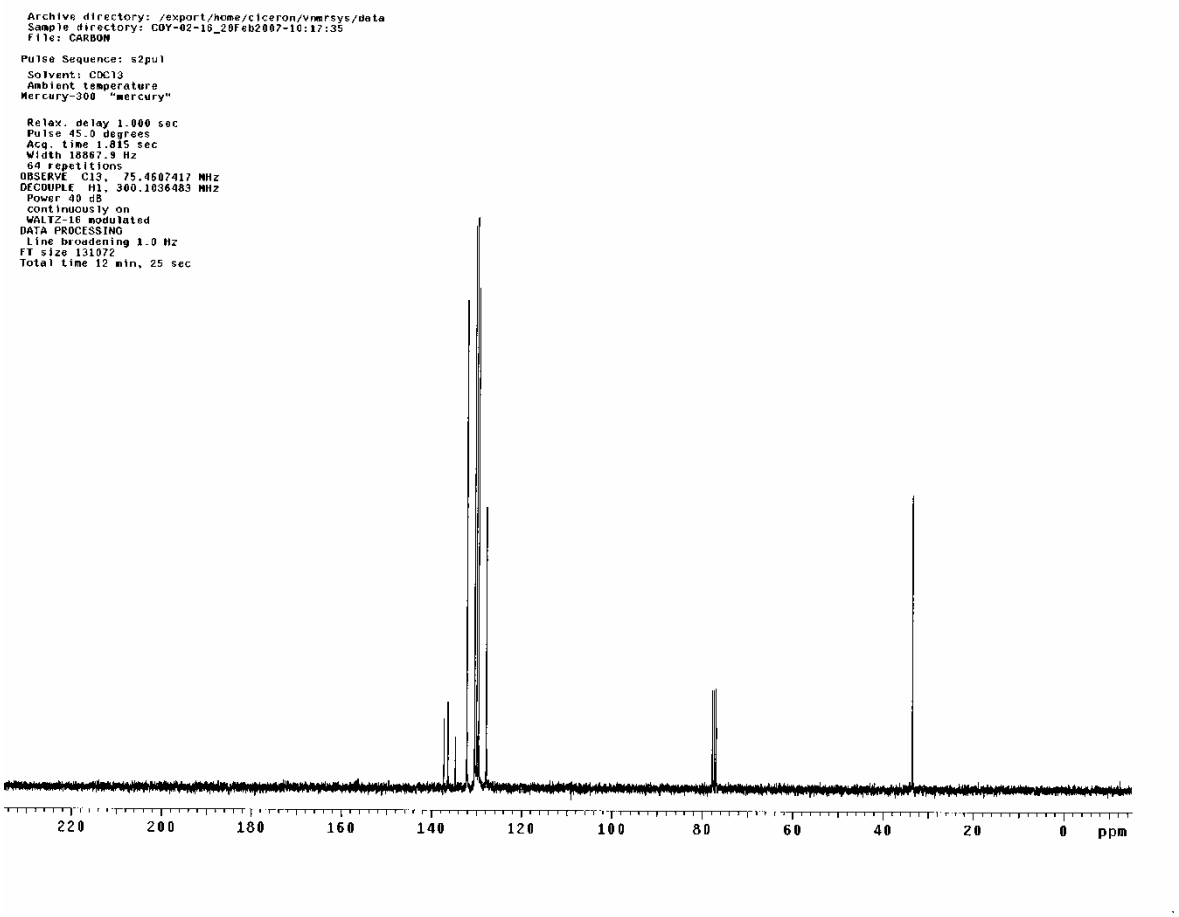

DEPT 135 NMR Spectrum of **2.**

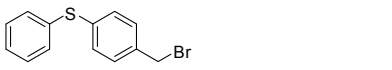

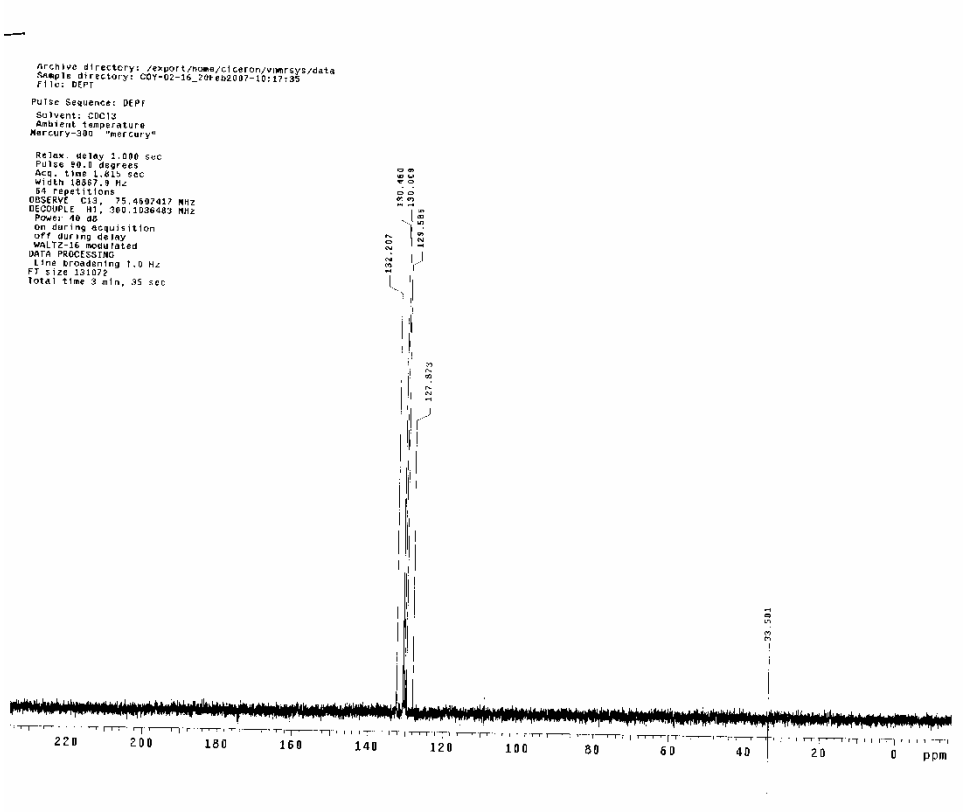

^{1}H NMR Spectrum of **5.**

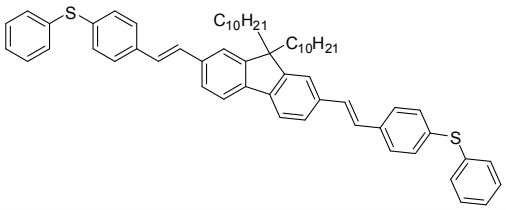

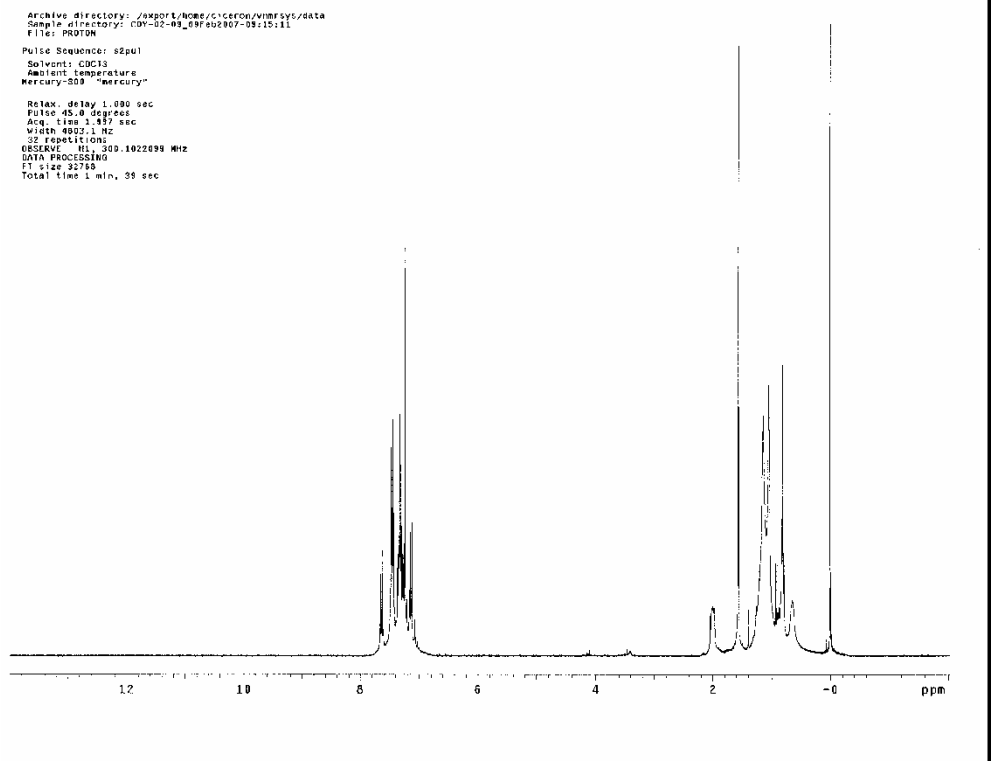

^{13}C NMR Spectrum of **5.**

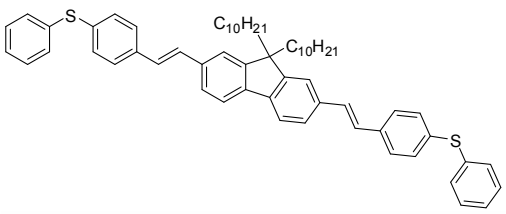

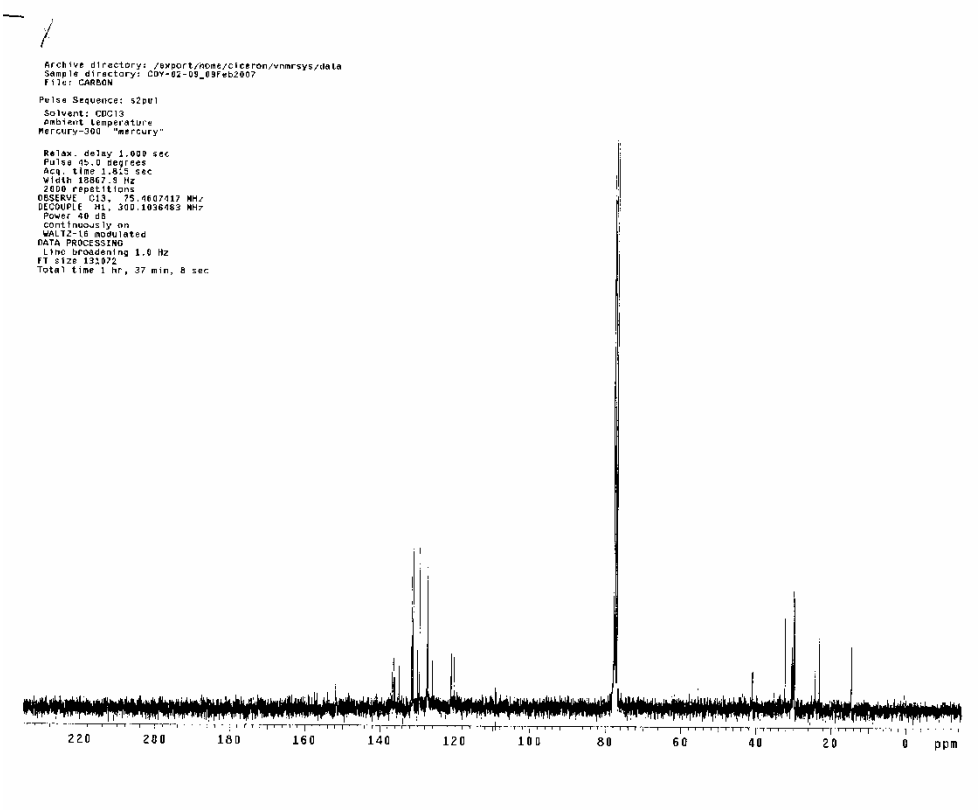

^{1}H NMR Spectrum of **7.**

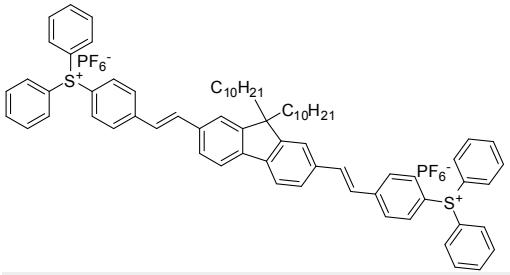

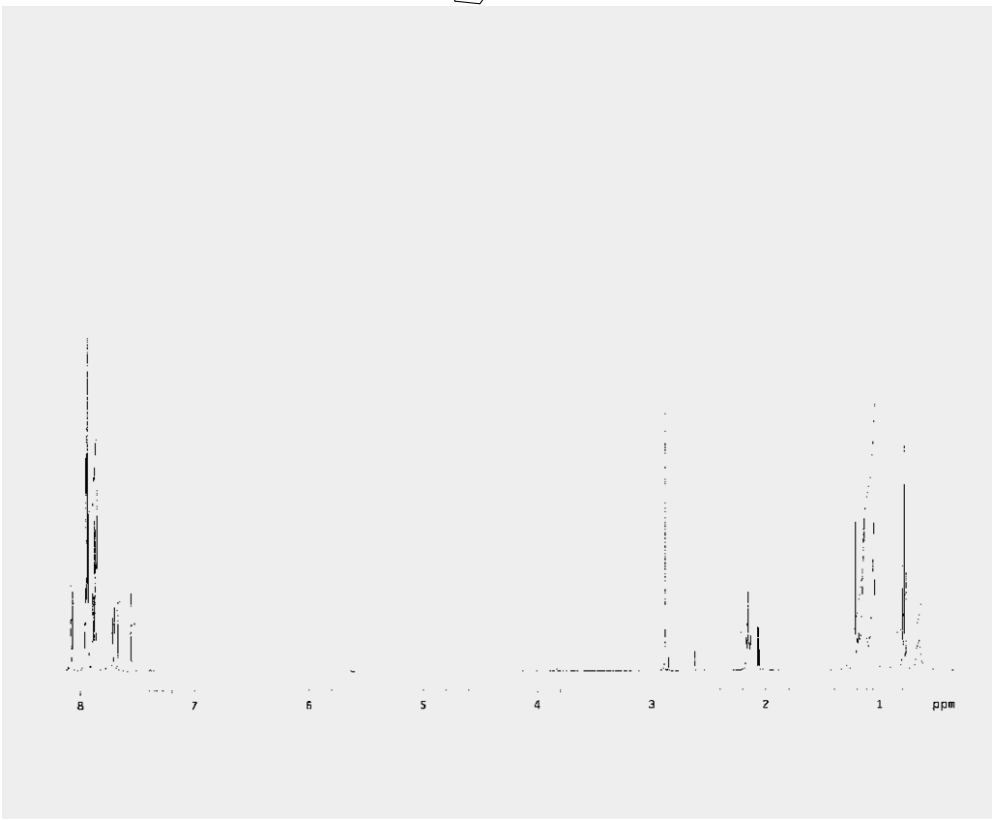

^{13}C NMR Spectrum of **7.**

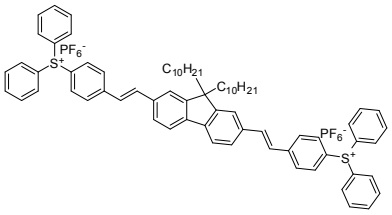

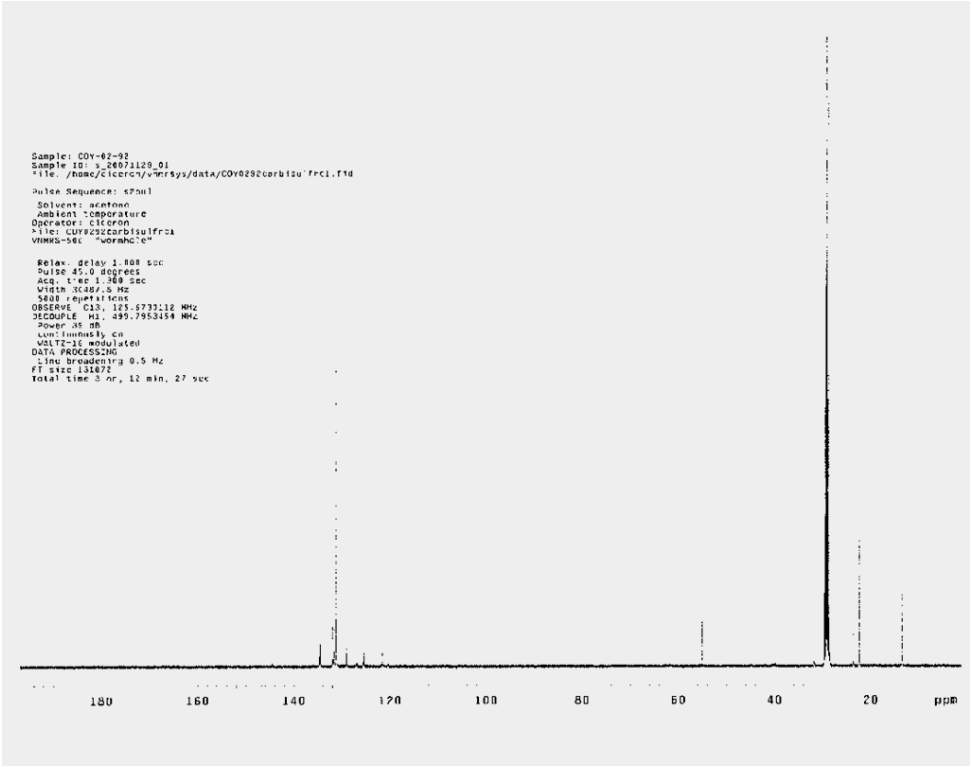

^{1}H NMR Spectrum of **8.**

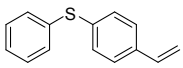

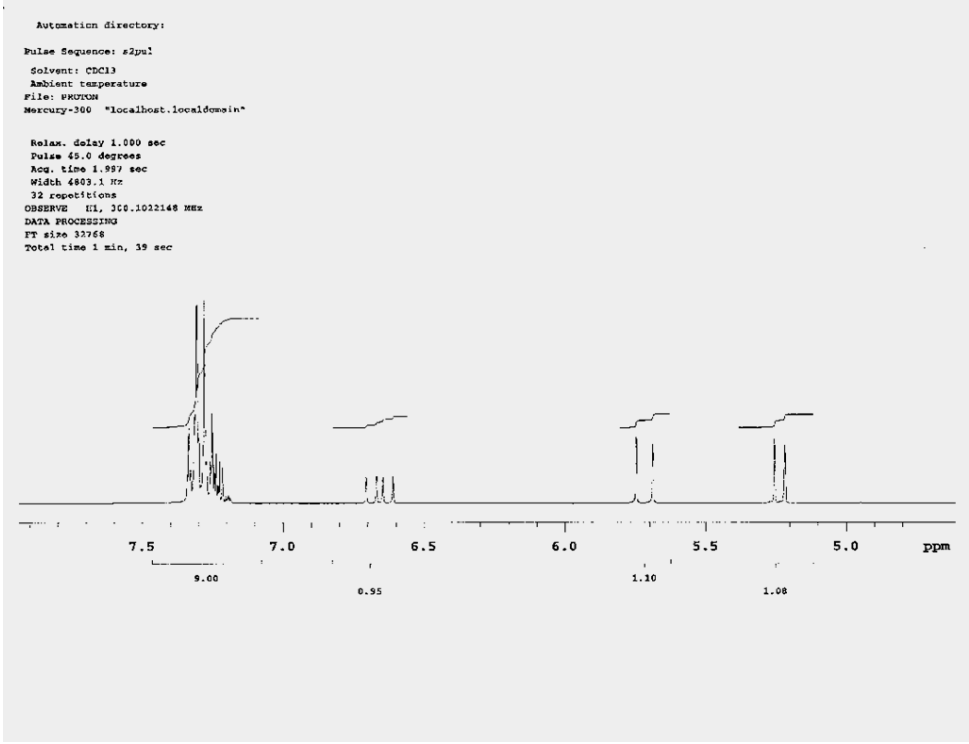

^{1}H NMR Spectrum of **10.**

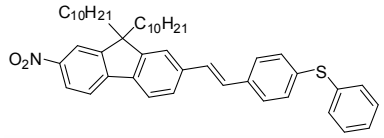

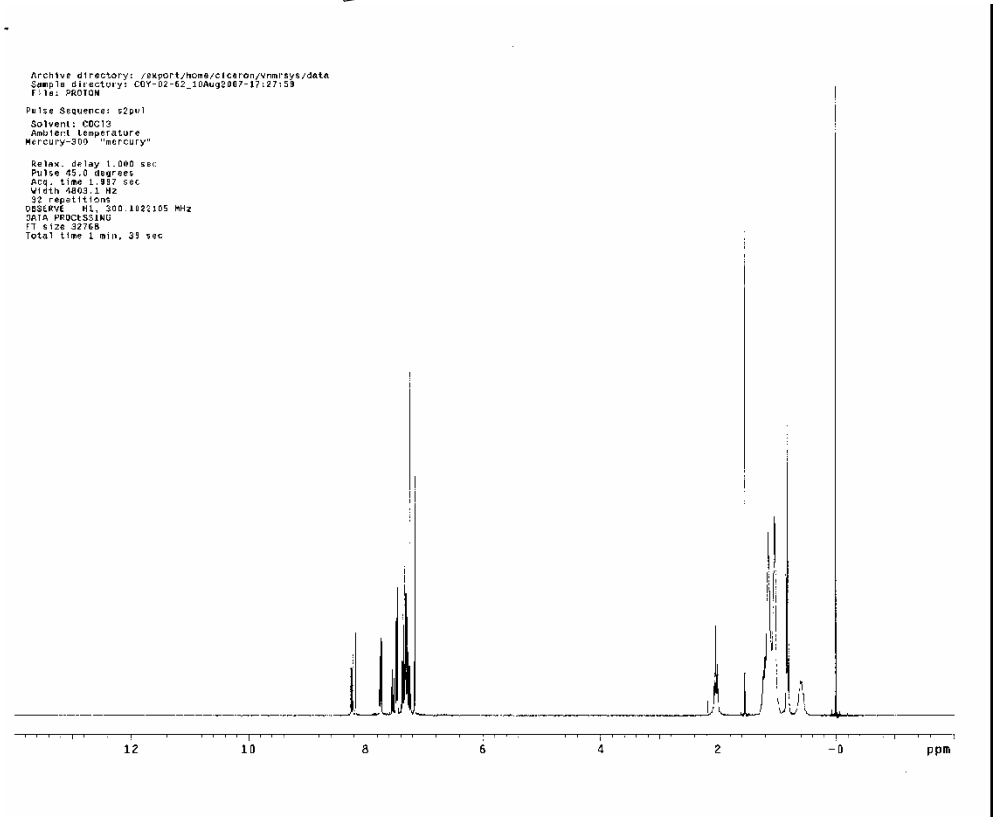

^{13}C NMR Spectrum of **10.**

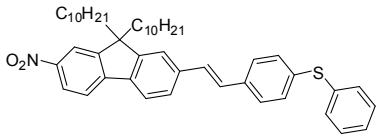

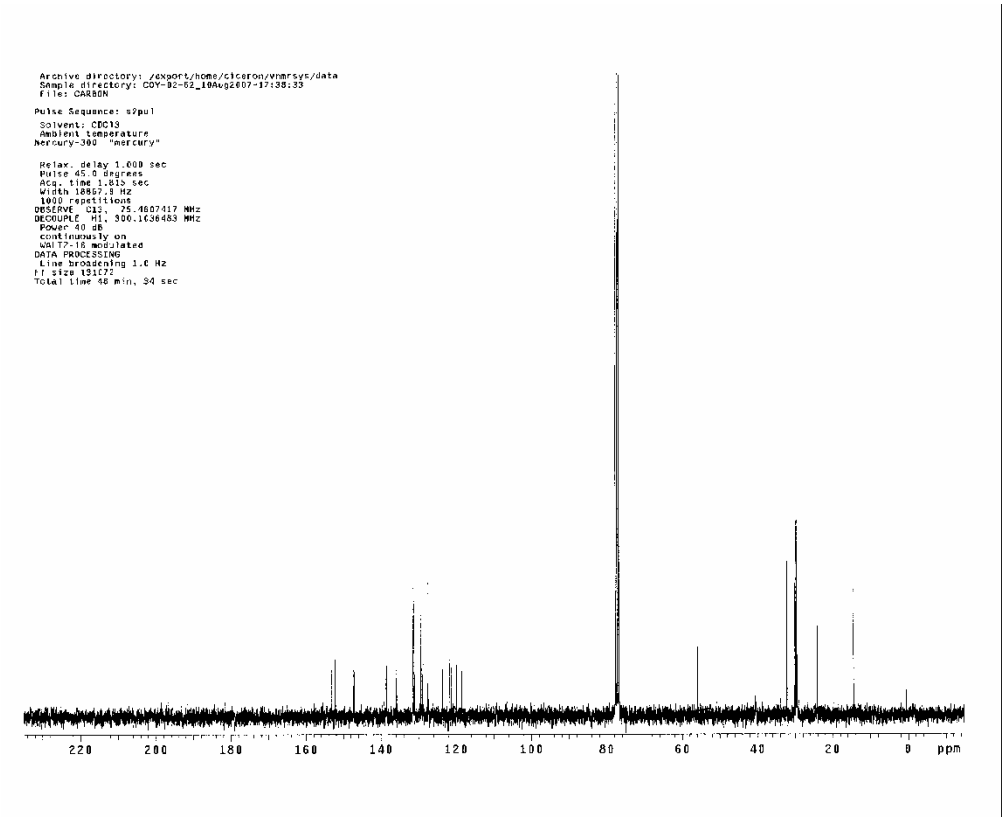

^{1}H NMR Spectrum of **11.**

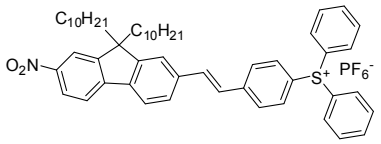

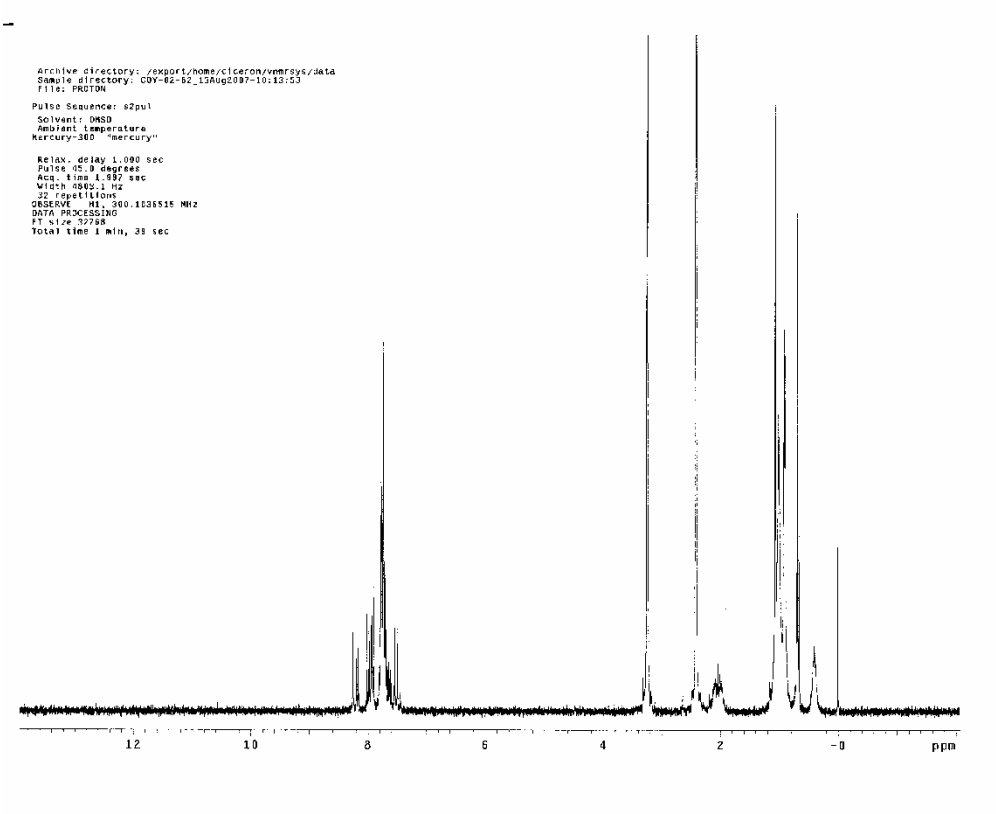

^{13}C NMR Spectrum of **11.**

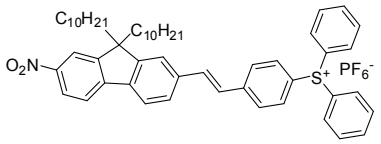

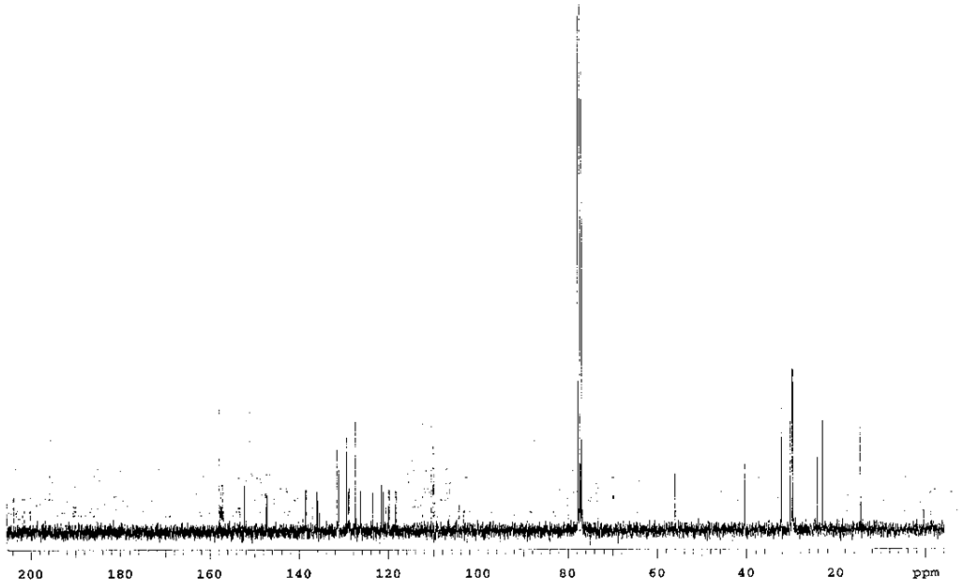

^{1}H NMR Spectrum of **12.**

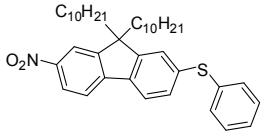

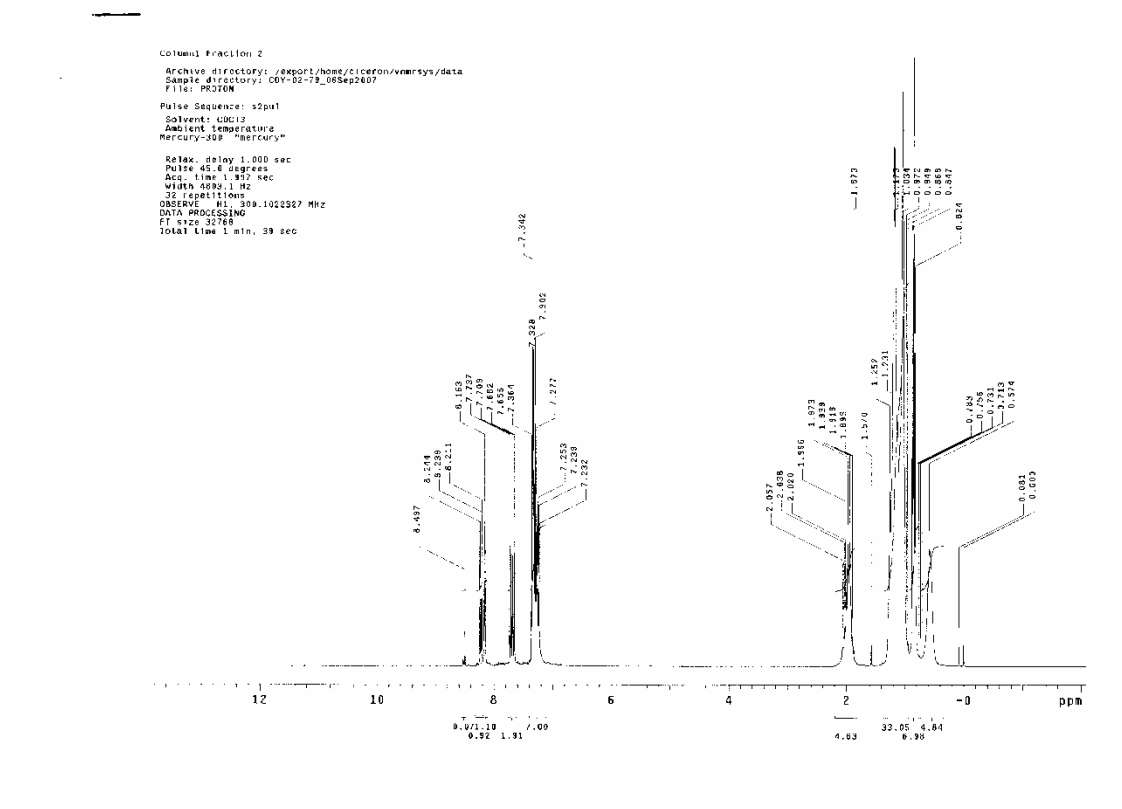

^{13}C NMR Spectrum of **12.**

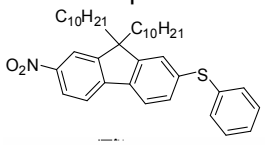

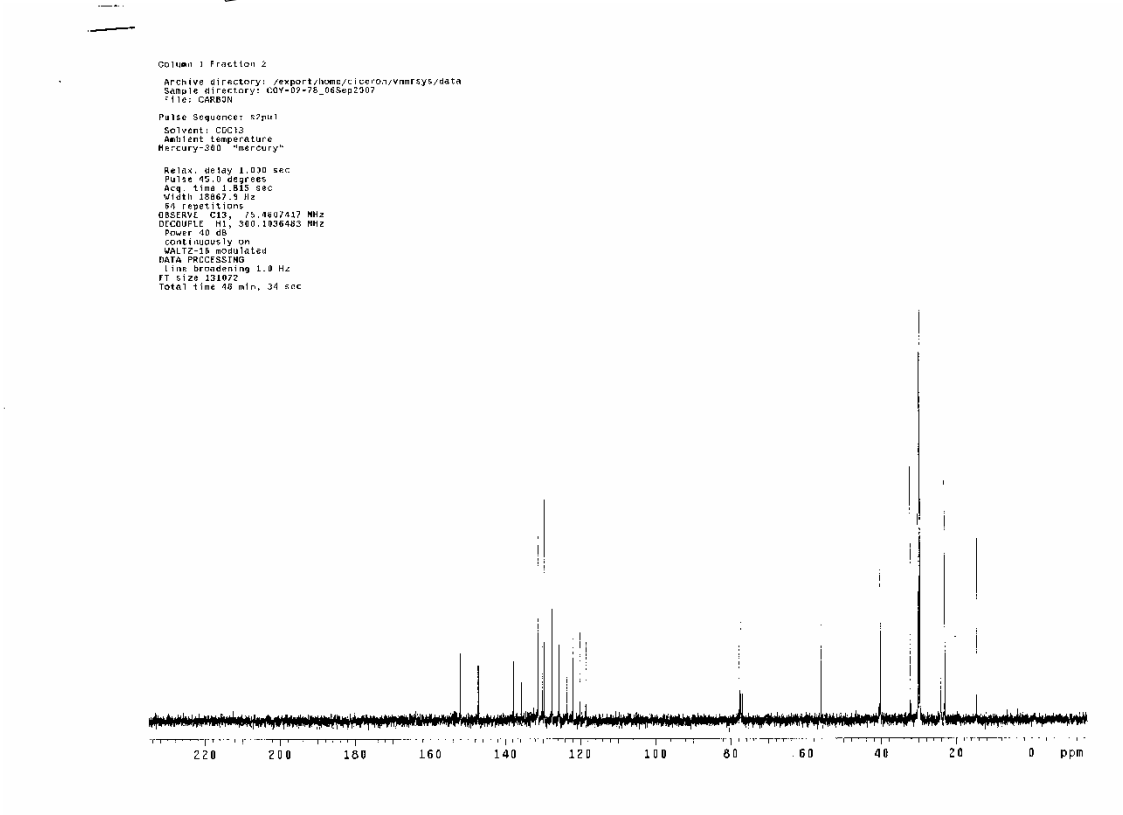

^{1}H NMR Spectrum of **13.**

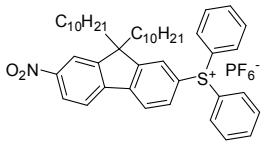

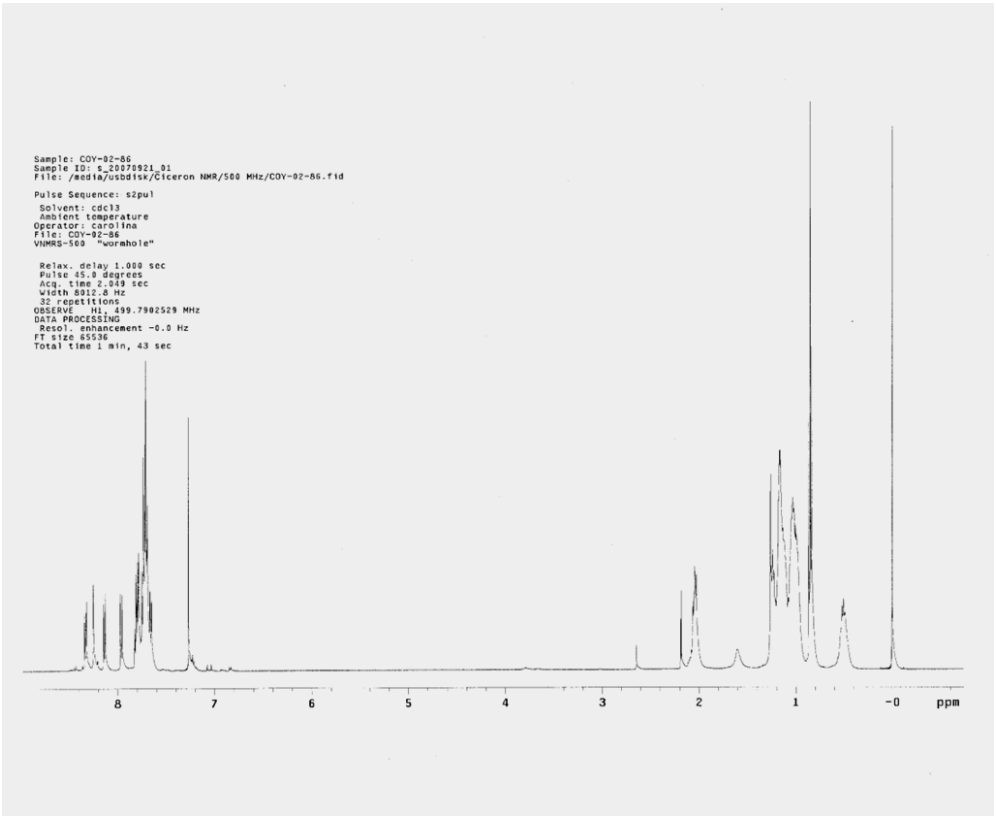

^{1}H NMR Spectrum of **15.**

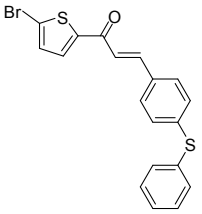

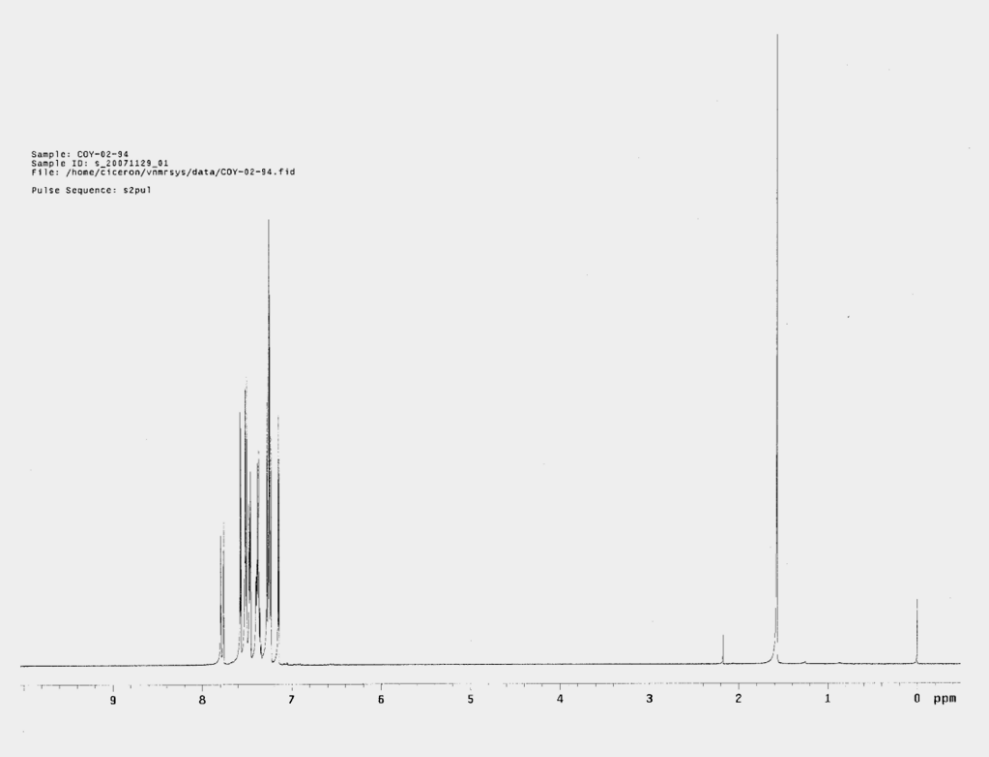

^{13}C NMR Spectrum of **15.**

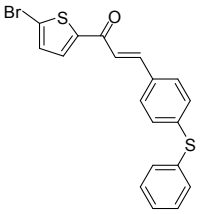

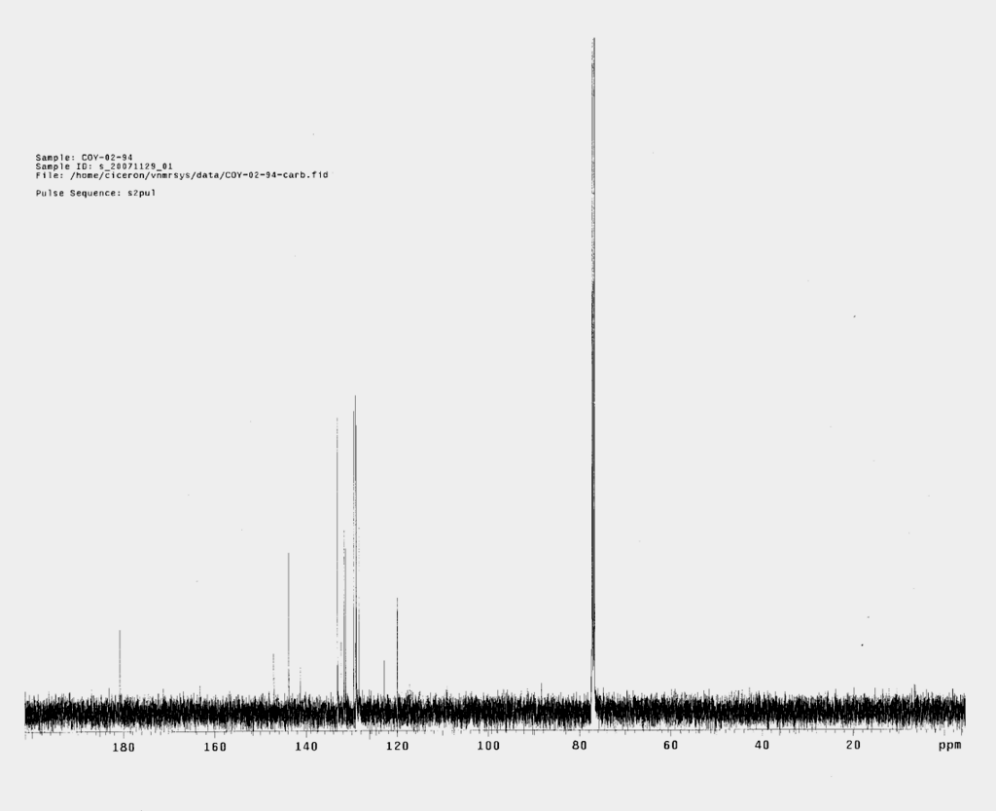

^{1}H NMR Spectrum of **16**.

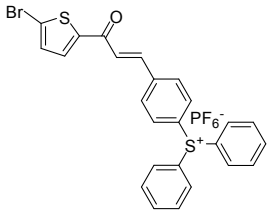

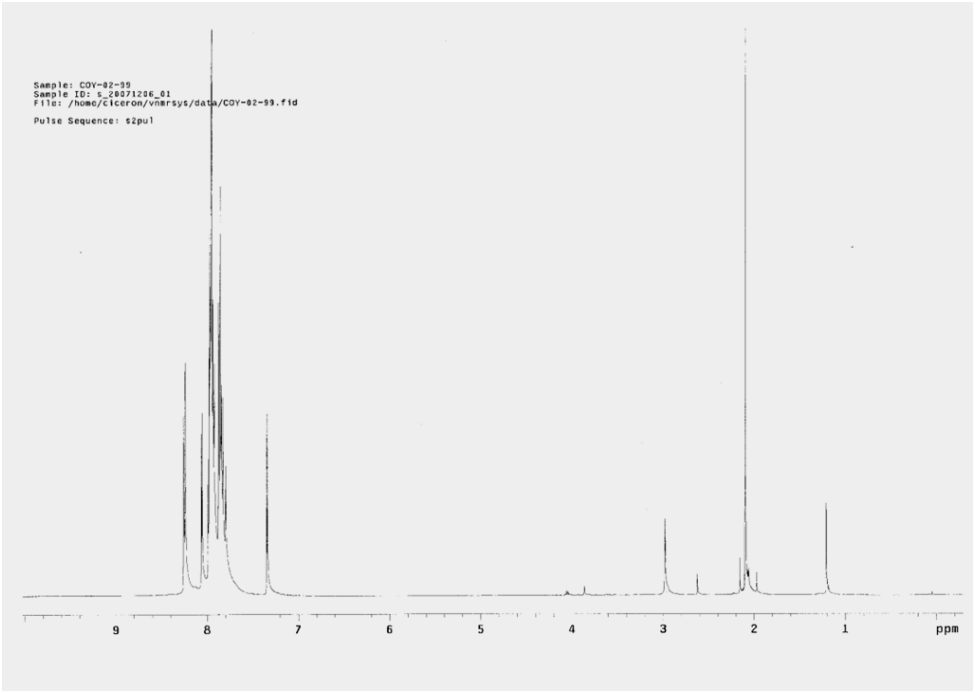

^{13}C NMR Spectrum of **16.**

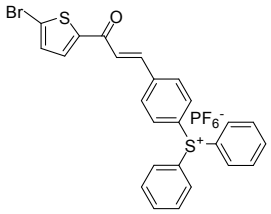

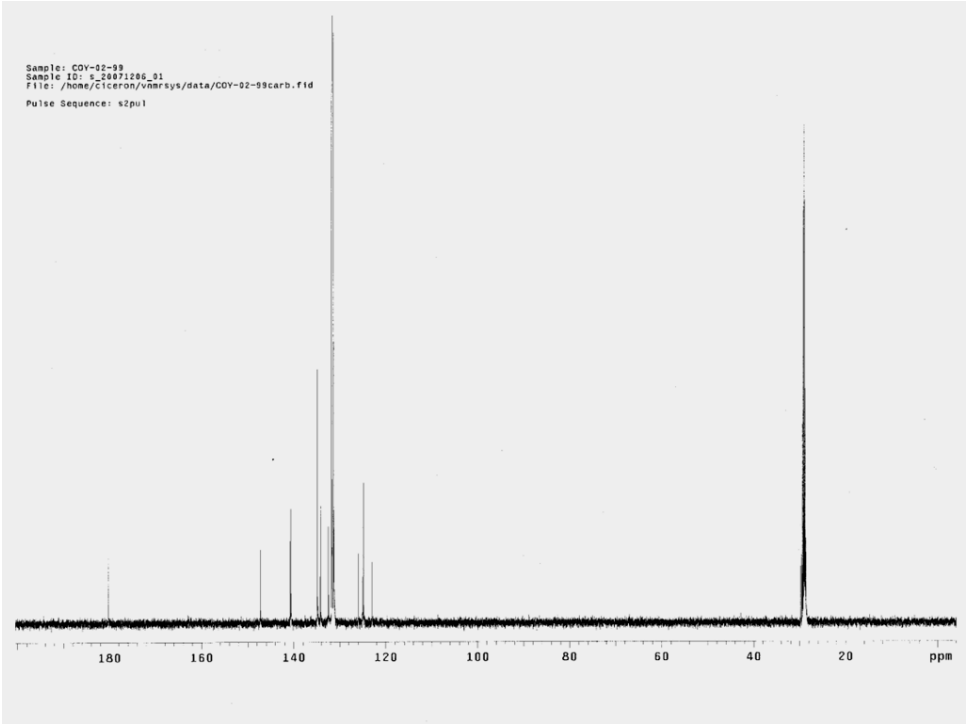

^{1}H NMR Spectrum of **22.**

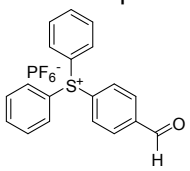

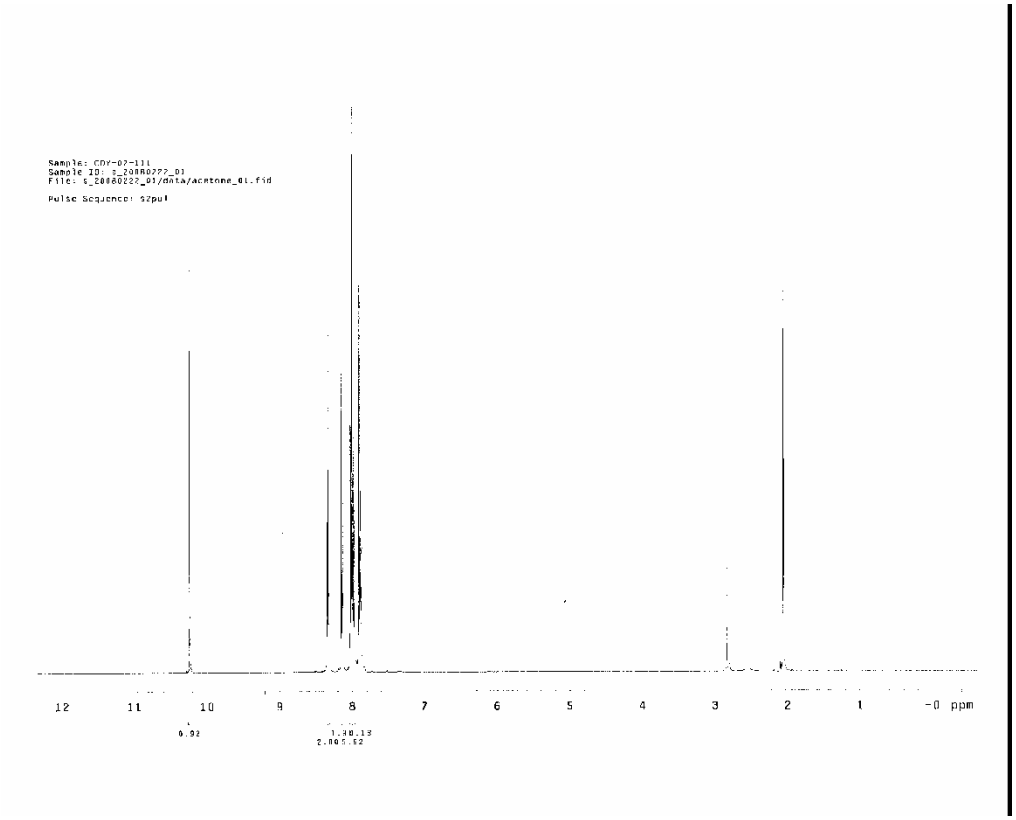

^{13}C NMR Spectrum of **22.**

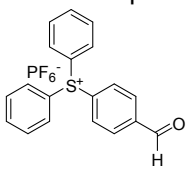

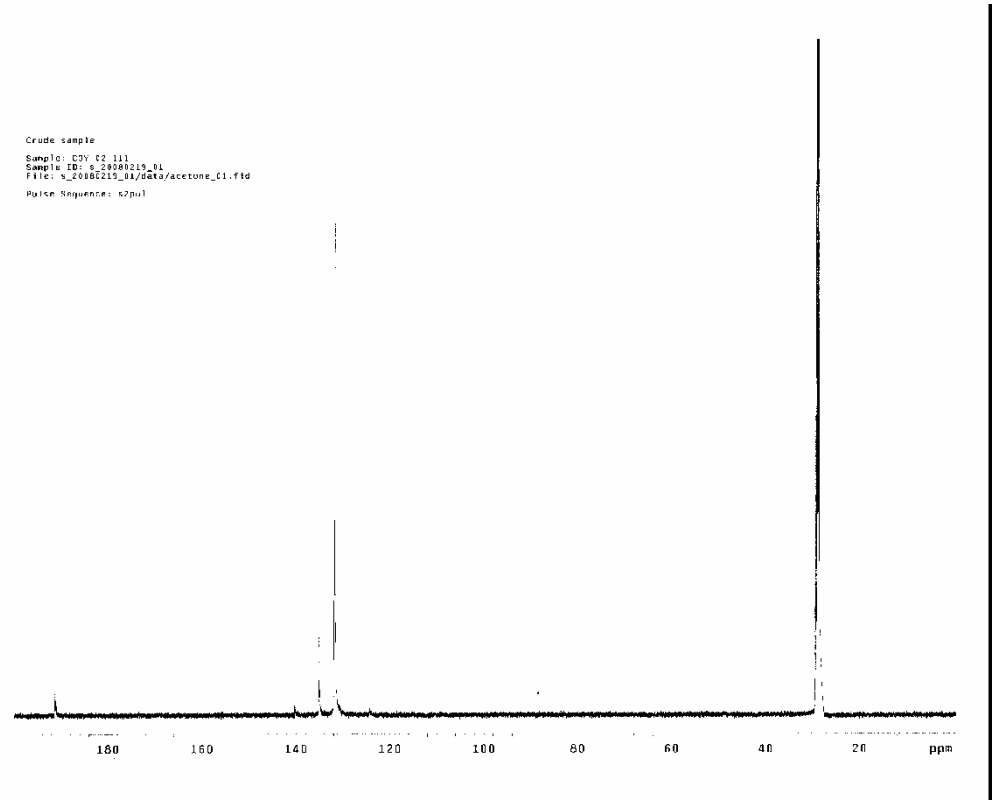

APENDIX B: ^{1}H AND ^{13}C, AND DEPT NMR SPECTRA OF NEW MOLECULES IN CHAPTER II

^{1}H NMR for **25.**

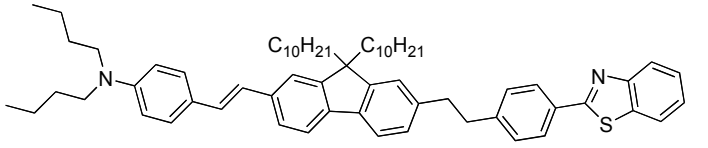

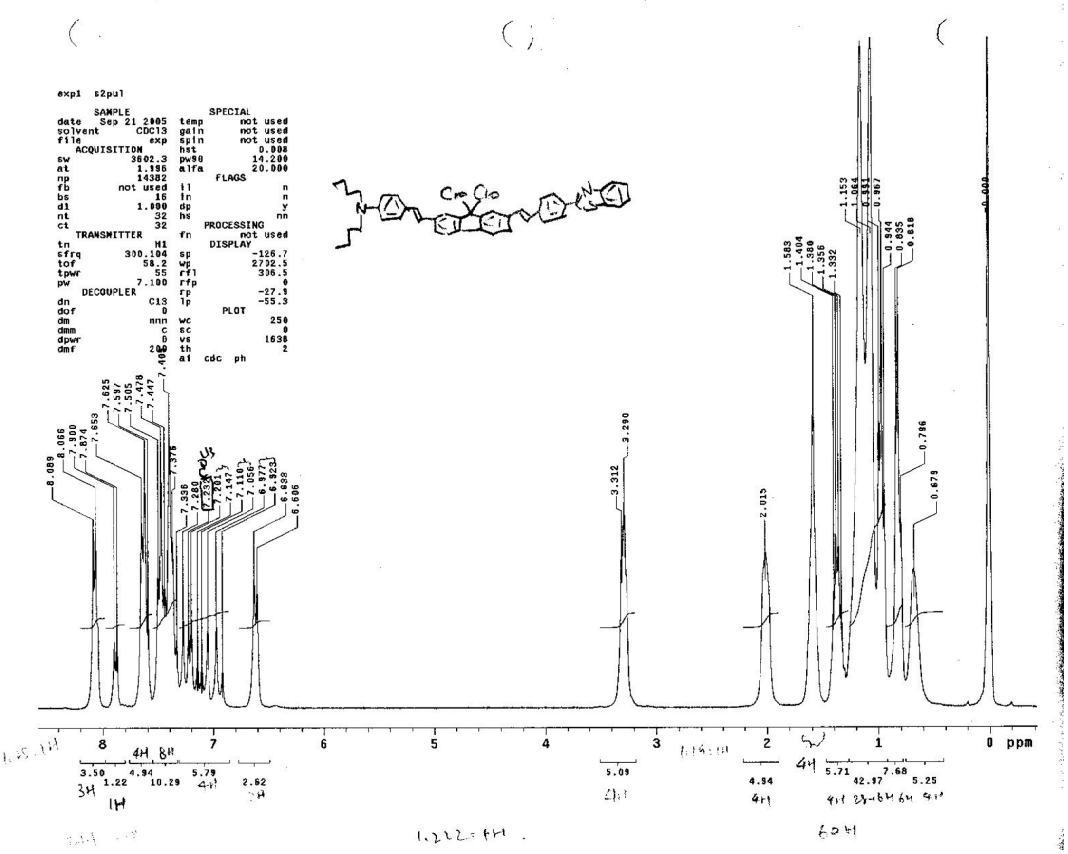

^{13}C NMR for **25.**

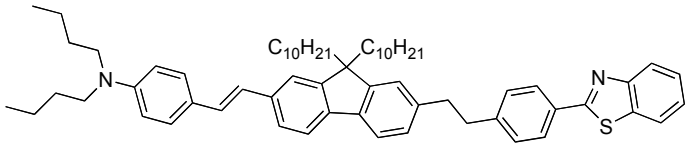

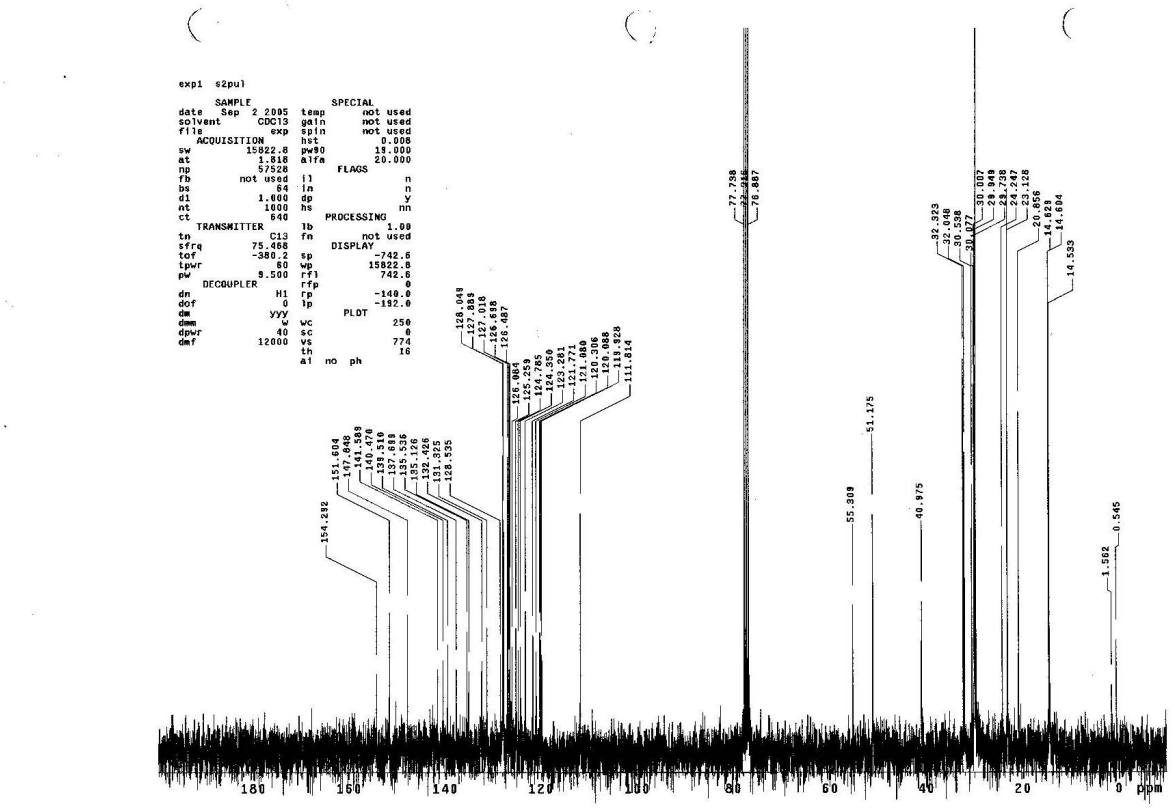

^{1}H NMR for **35.**

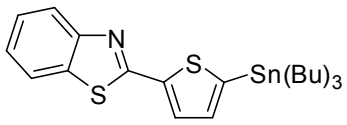

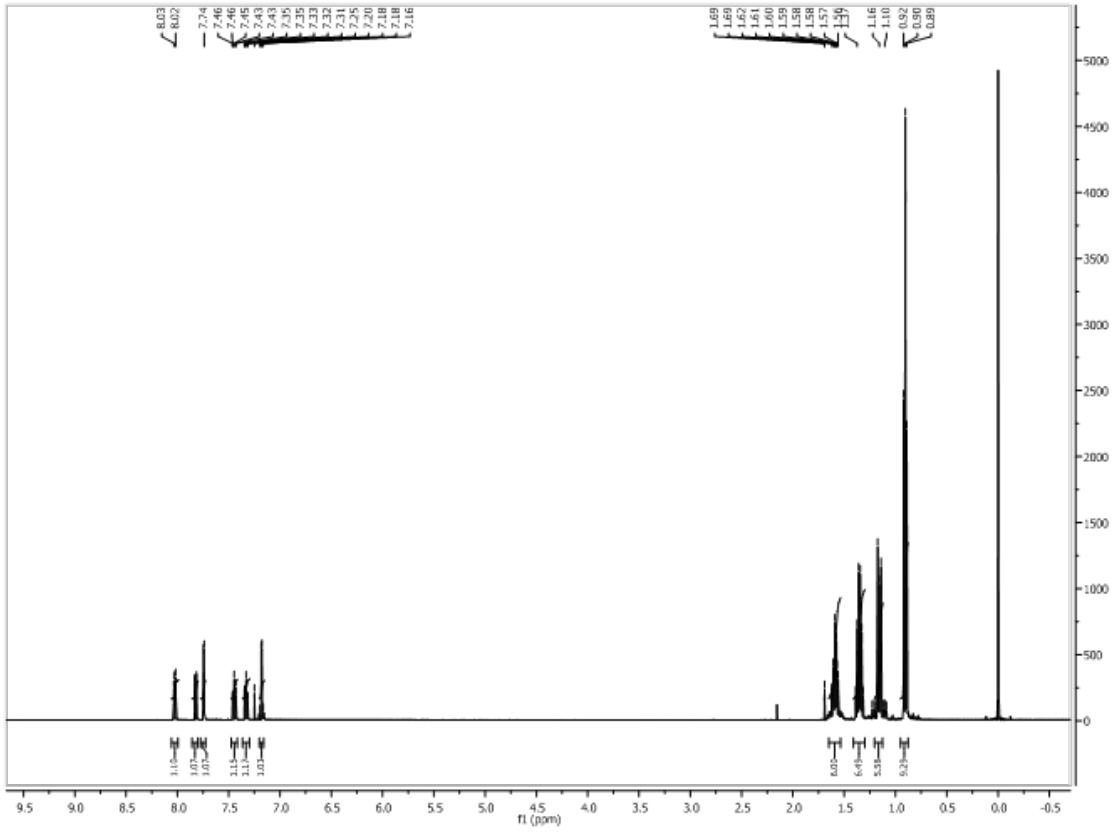

^{13}C NMR for **35.**

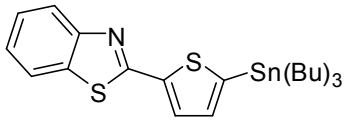

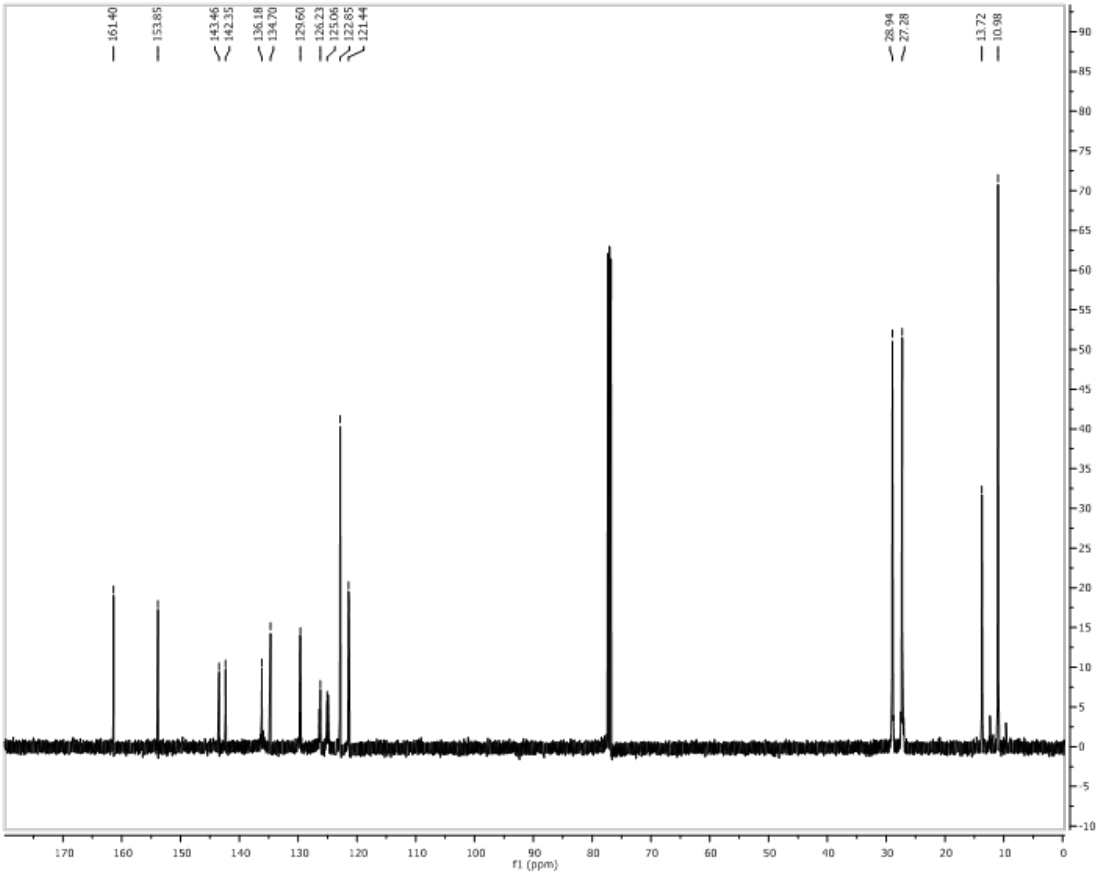

^{1}H NMR for **37.**

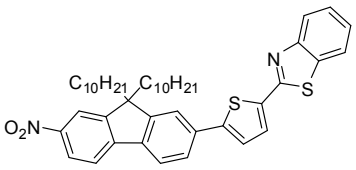

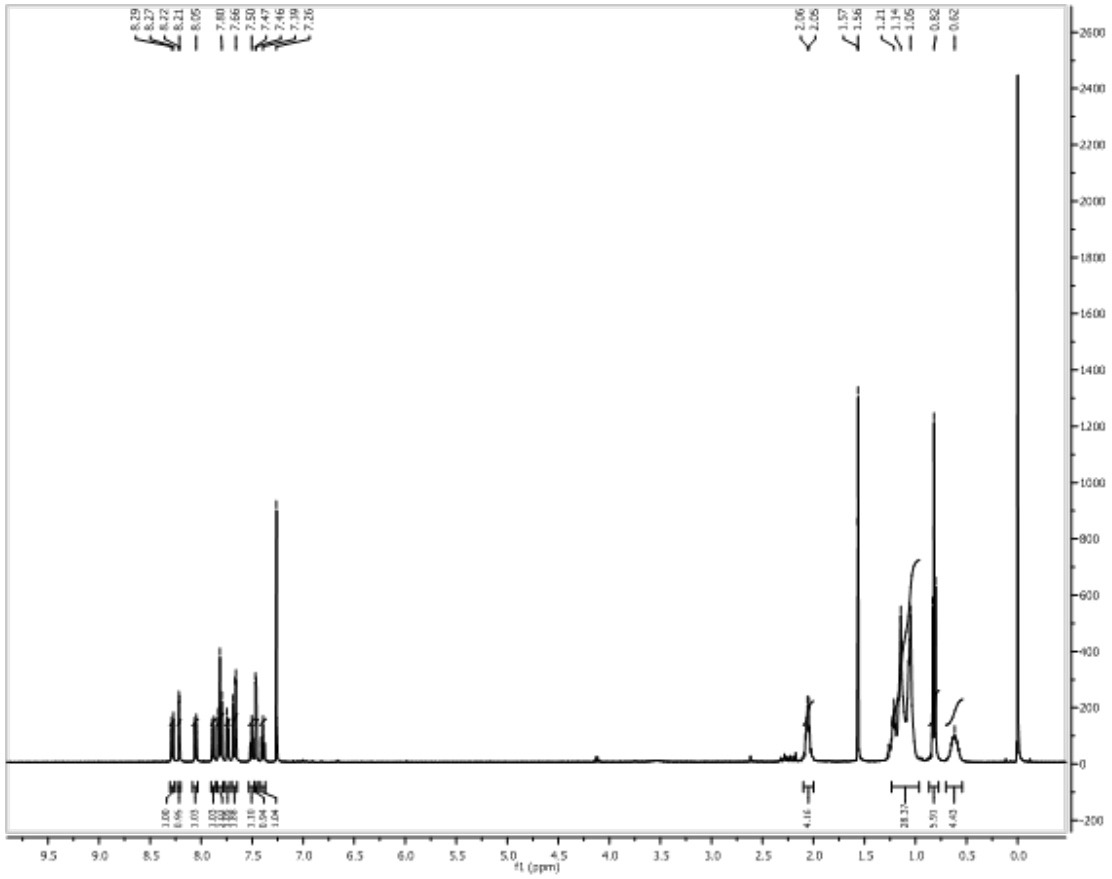

^{13}C NMR for **37.**

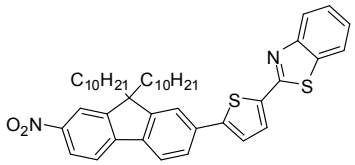

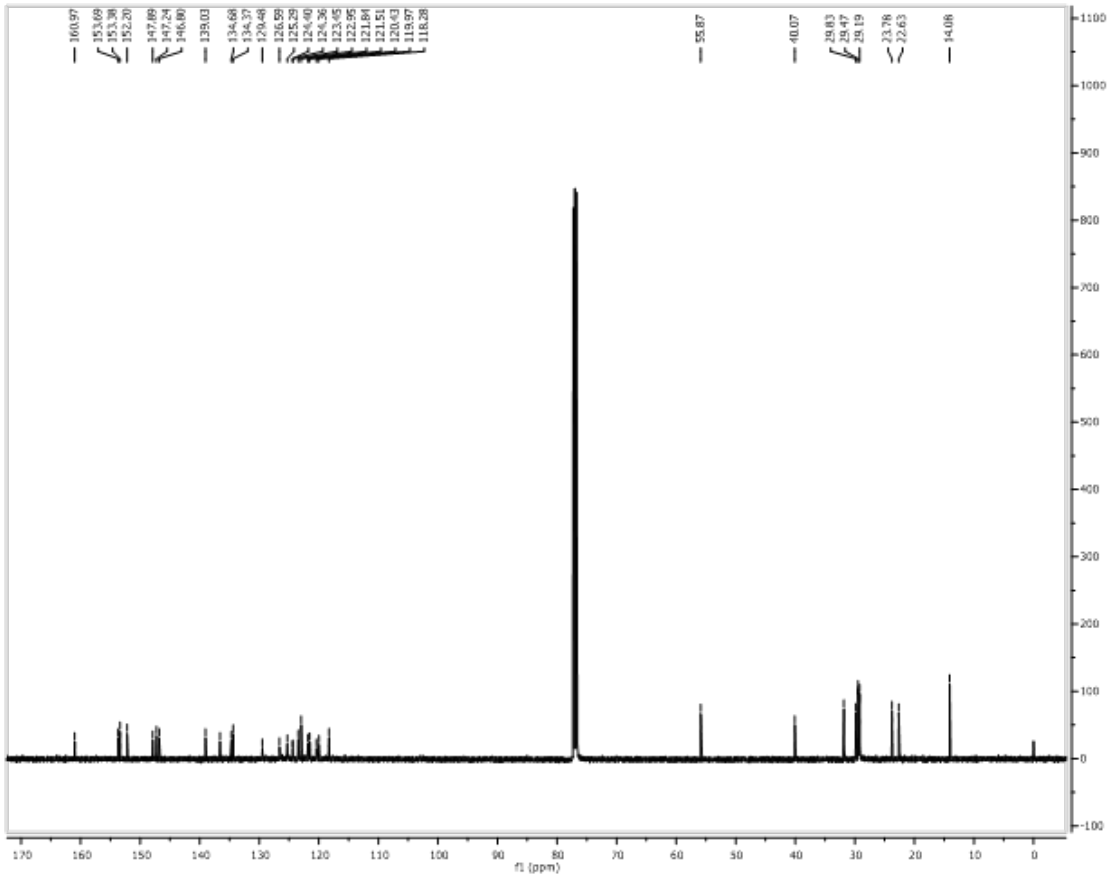

^{13}C NMR for **37**. (expansion)

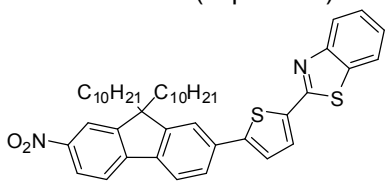

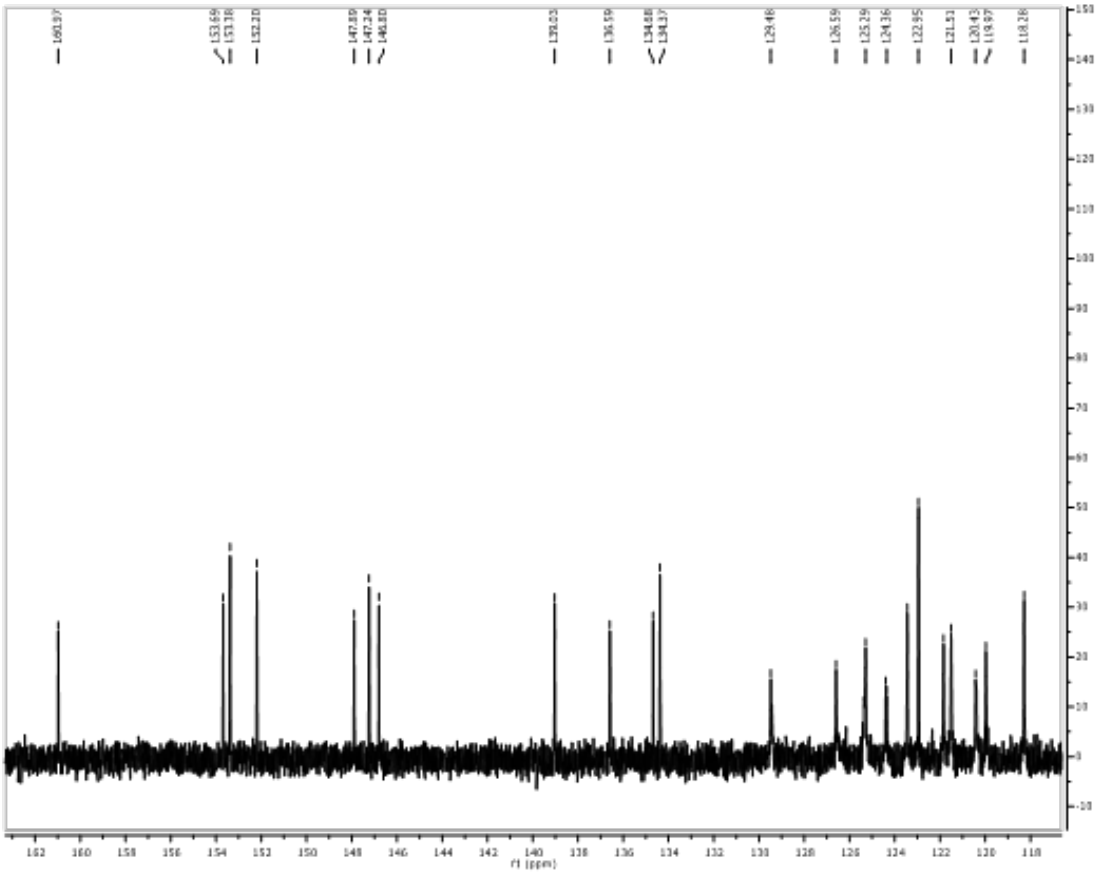

^{1}H NMR for **38.**

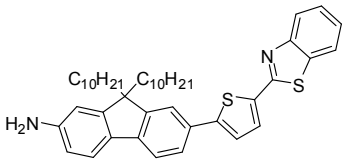

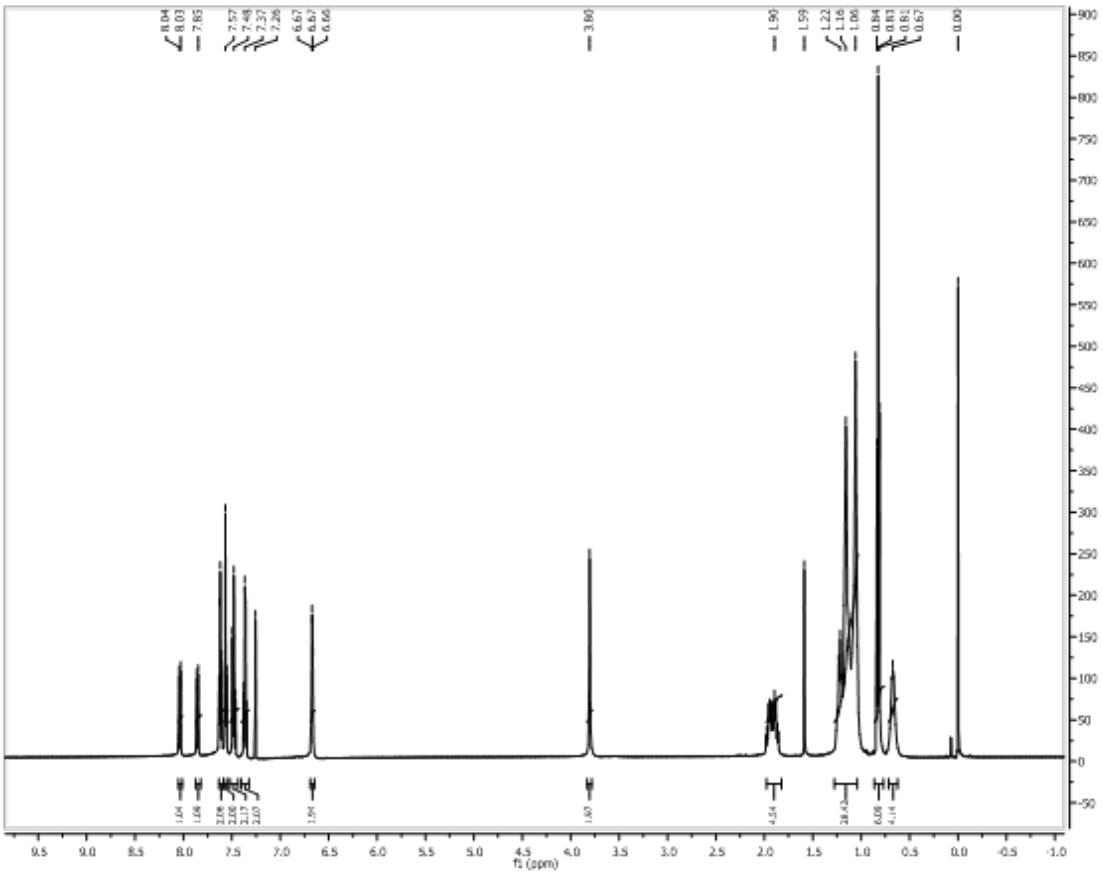

^{13}C NMR for **38.**

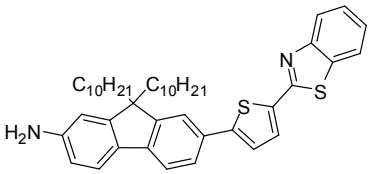

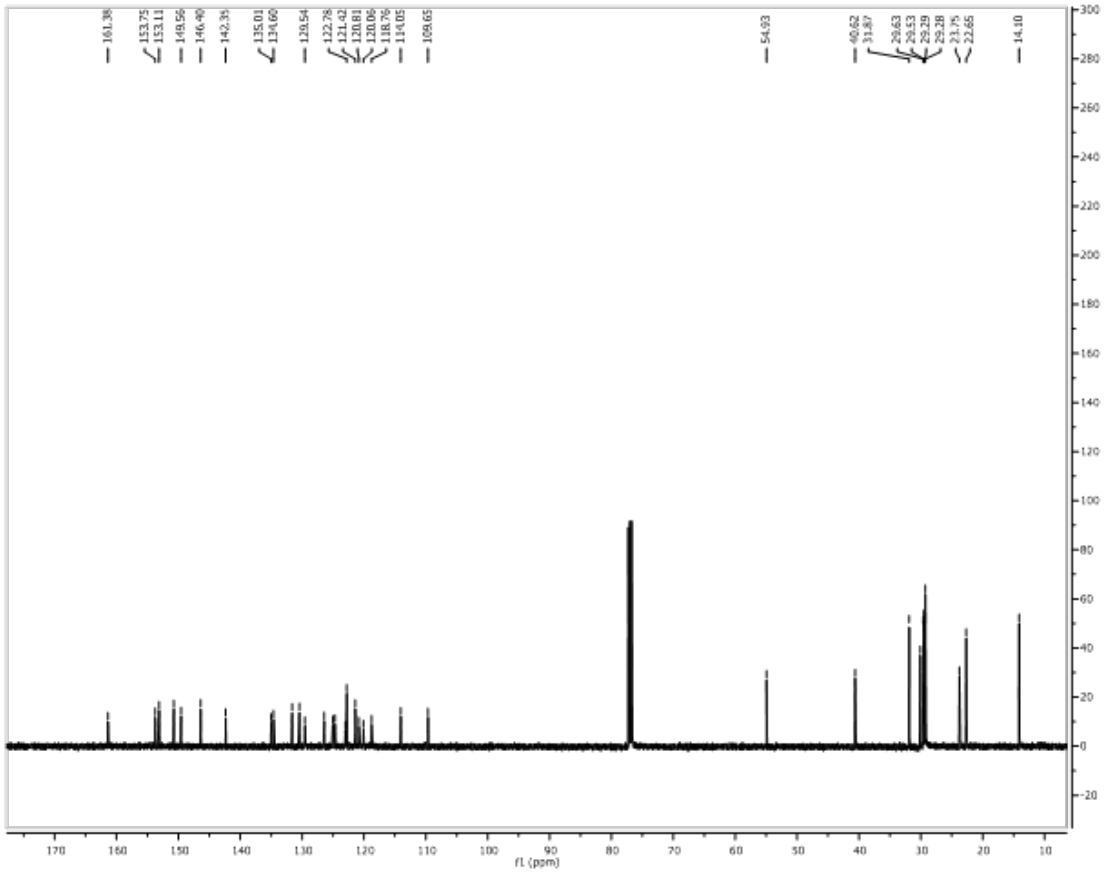

^{13}C NMR for **38**. (expansion)

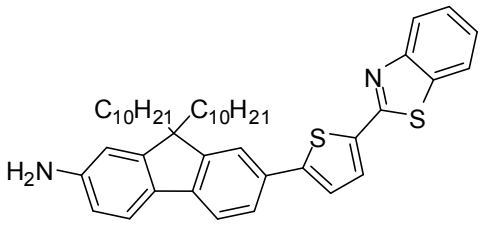

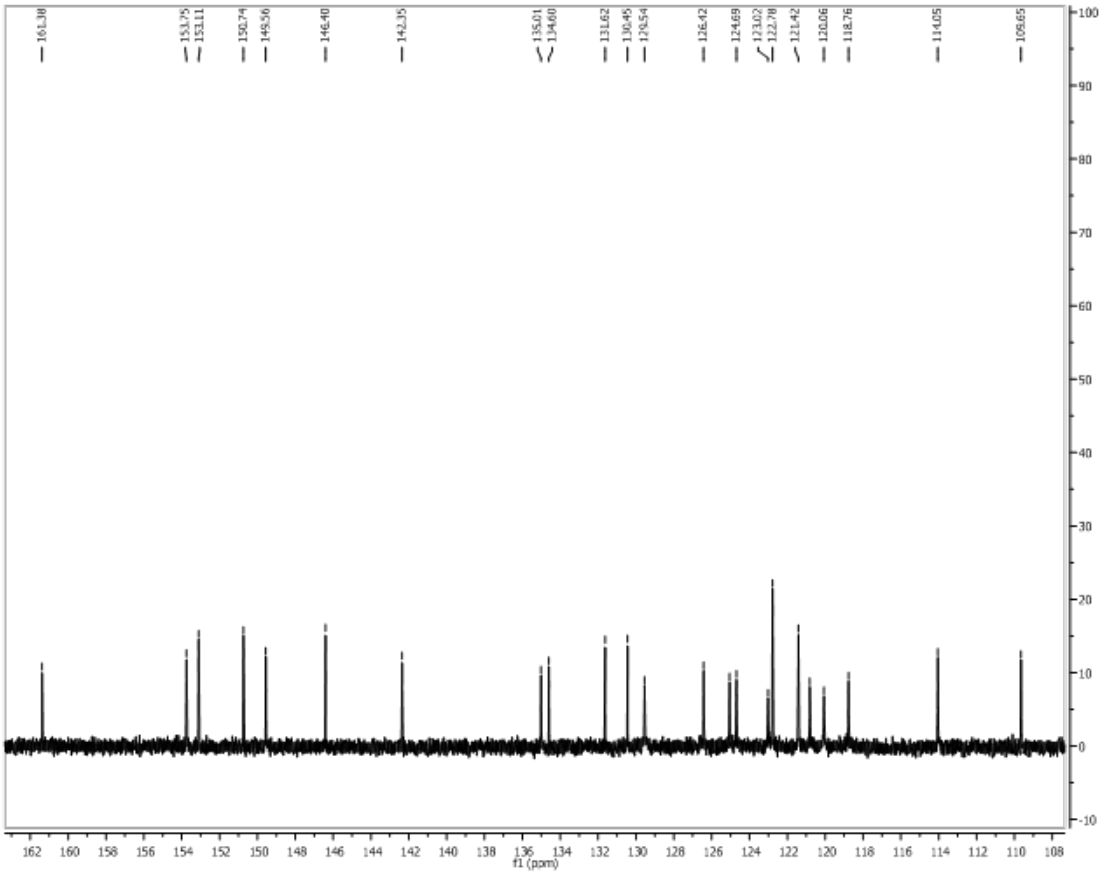

^{1}H NMR for **24.**

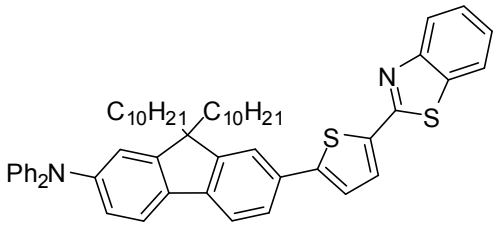

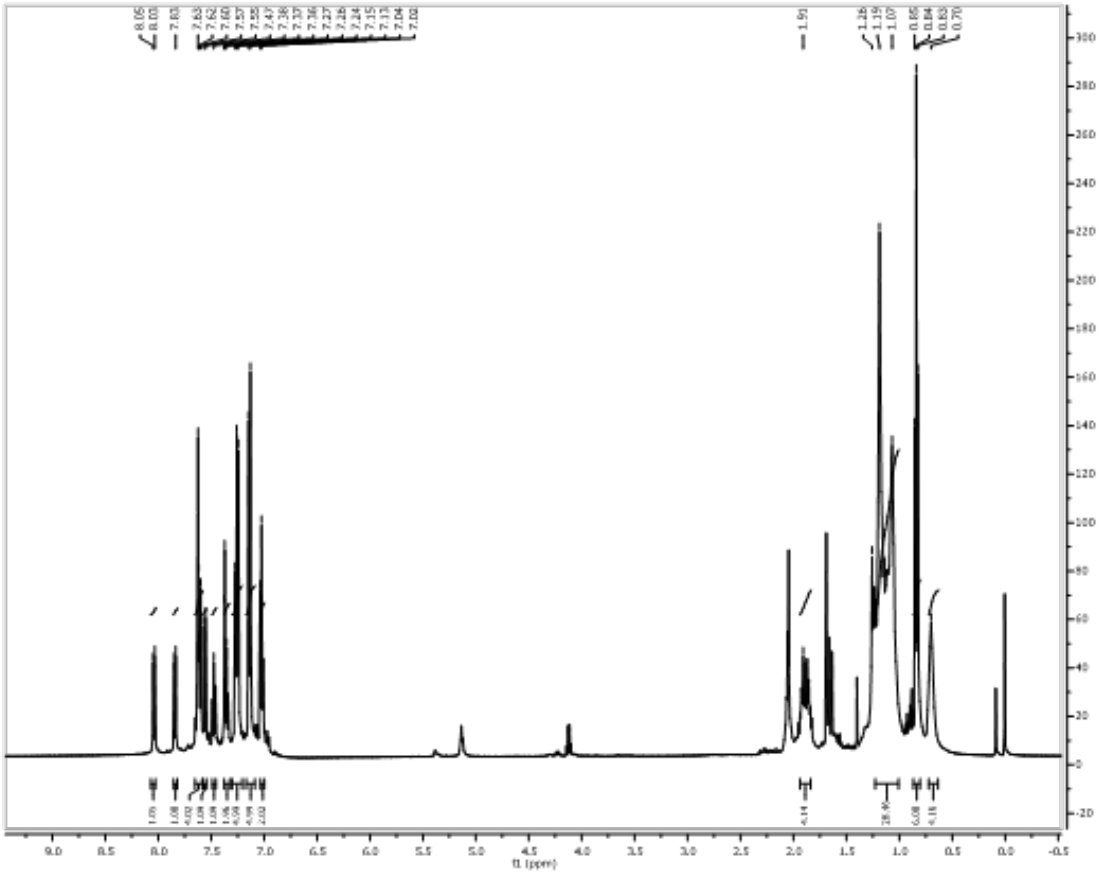

^{13}C NMR for **24.**

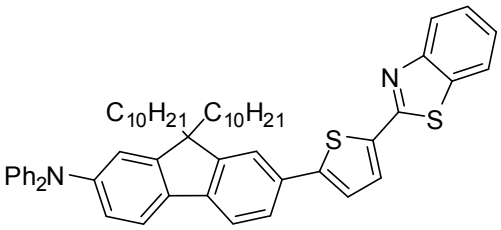

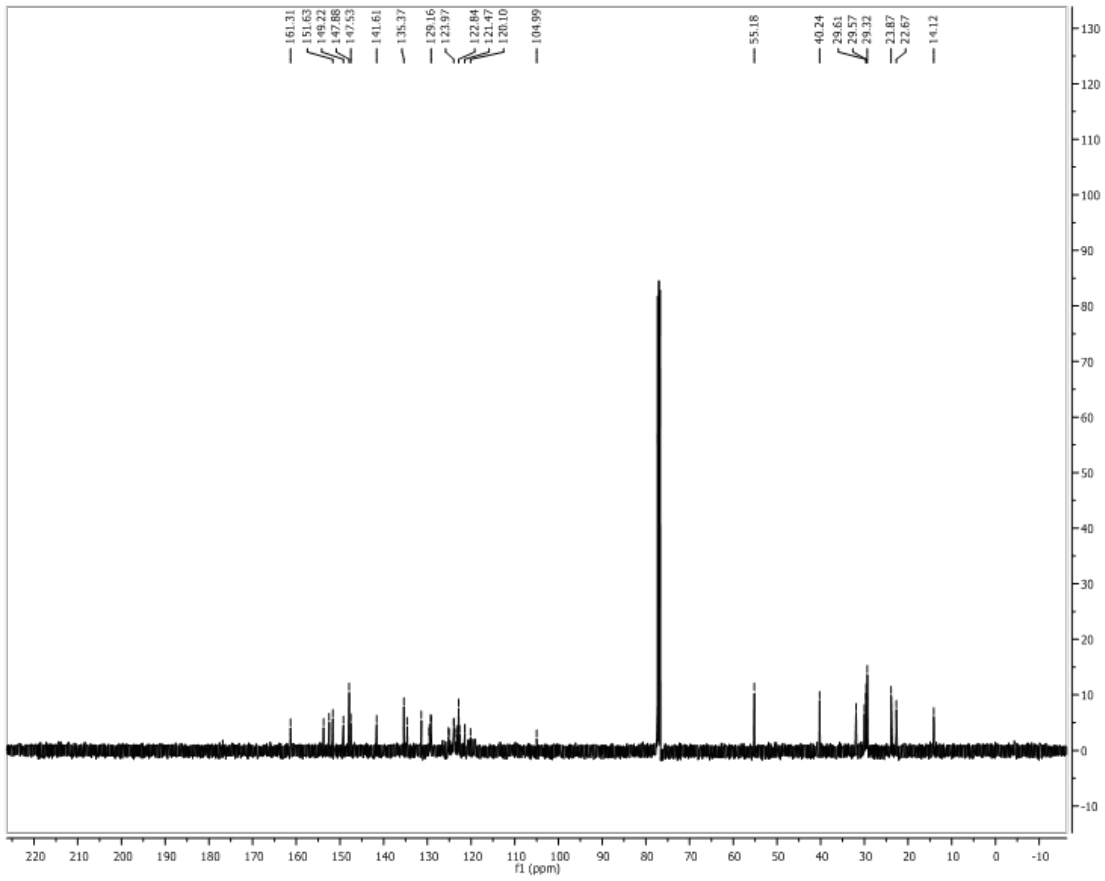

^{13}C NMR for **24.** (expansion)

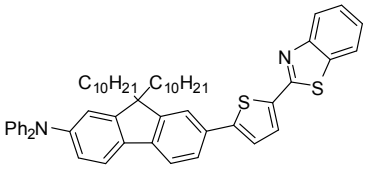

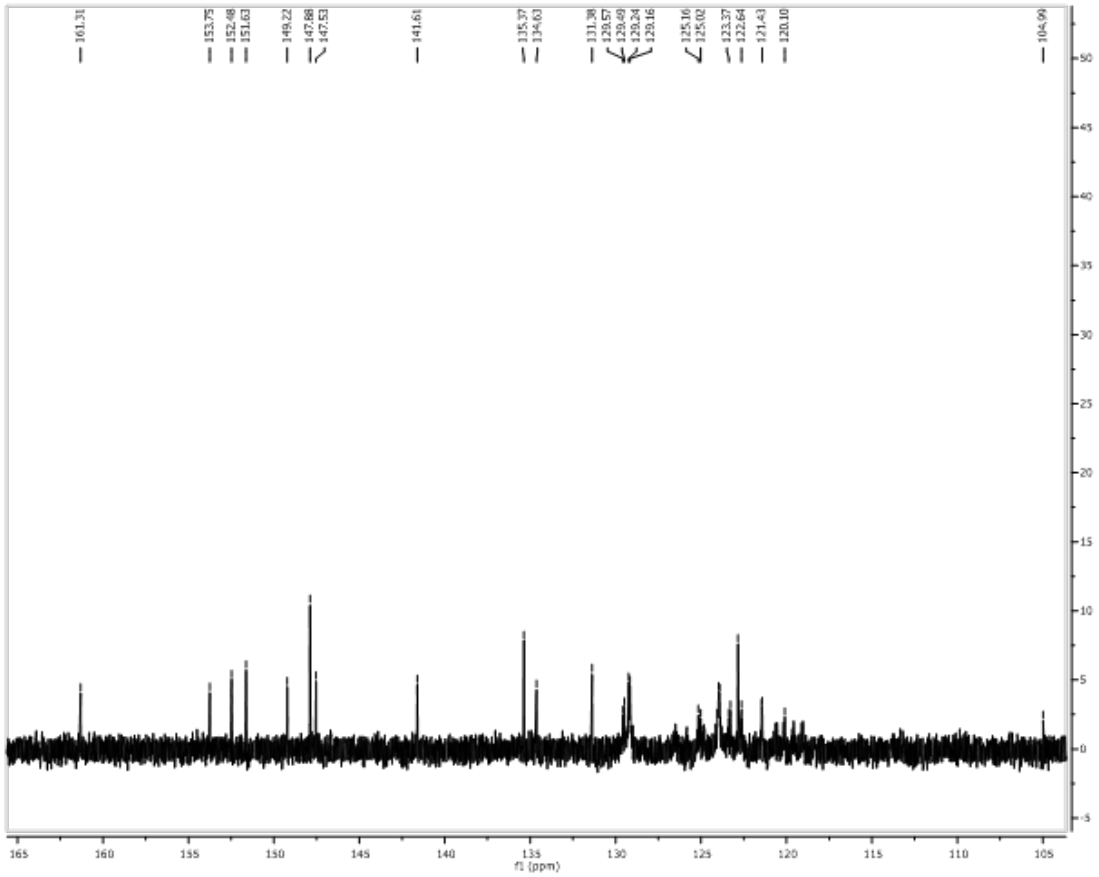

^{13}C NMR for **24.** (expansion)

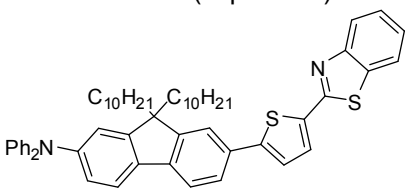

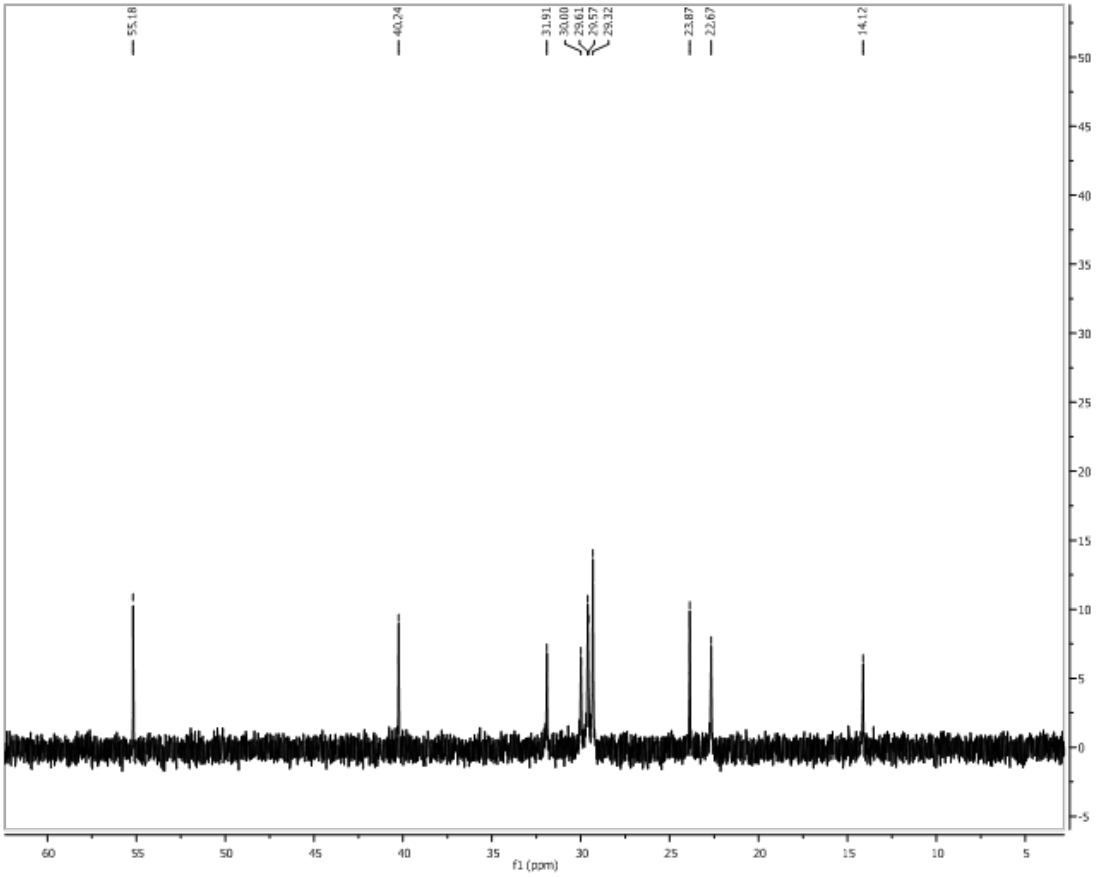

APENDIX C: ADDITIONAL GRAPHS AND FIGURES

Temperature vs. Time profile of the synthesis of sulfonium salt 11. (Chapter I)

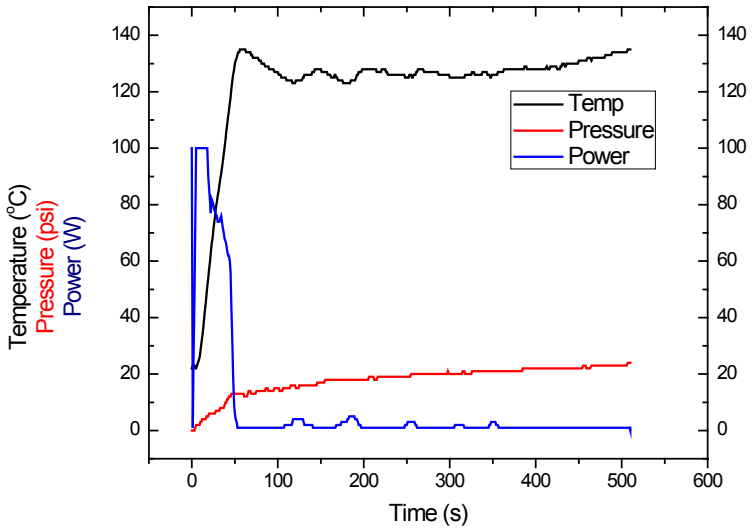

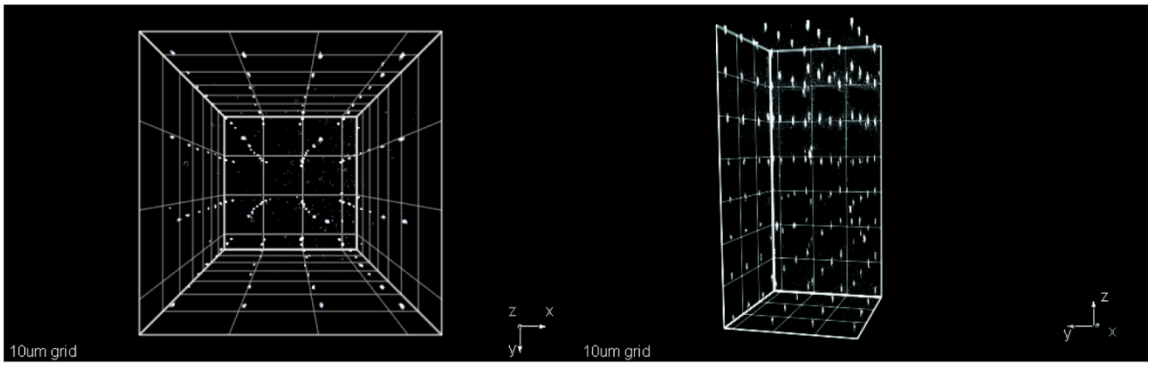

Figure C.1. Photosensitive polymeric system used for 3D, two-photon optical data storage of eight layers. Composition 11 5%; 24 1%; 31 94%. Two-photon writing was performed at 710 nm (1.6 mW), 200 fs, 60 ms exposure/voxel with a 60x, 1.4 N.A. oil immersion objective. Two-photon readout was performed, layer-by-layer (~0.4 mm/scaning), at 860 nm (9 mW), 200 fs, with same objective used for writing. This 3D image reconstruction was done by overlaying all readout layers using SlideBook 4.1.

LIST OF REFERENCES

(1) Crivello, J. V. *Journal of Polymer Science Part a-Polymer Chemistry* **1999**, *37*, 4241-4254.

(2) Jeon, S.; Malyarchuk, V.; Rogers, J. A.; Wiederrecht, G. P. *Optics Express* **2006**, *14*, 2300-2308.

(3) Kim, E. K.; Ekerdt, J. G.; Willson, C. G. *Journal of Vacuum Science & Technology B* **2005**, *23*, 1515-1520.

(4) Goeppert-Mayer, M. *Ann. Phys. (Paris)* **1931**, *9*, 273.

(5) Parthenopoulos, D. A.; Rentzepis, P. M. *Science* **1989**, *245*, 843-845.

(6) Belfield, K. D.; Schafer, K. J. *Chemistry of Materials* **2002**, *14*, 3656-3662.

(7) Corredor, C. C.; Huang, Z. L.; Belfield, K. D. *Advanced Materials* **2006**, *18*, 2910-+.

(8) Denk, W.; Strickler, J. H.; Webb, W. W. *Science* **1990**, *248*, 73-76.

(9) Schafer-Hales, K. J.; Belfield, K. D.; Yao, S.; Frederiksen, P. K.; Hales, J. M.; Kolattukudy, P. E. *Journal of Biomedical Optics* **2005**, *10*.

(10) Maruo, S.; Nakamura, O.; Kawata, S. *Optics Letters* **1997**, *22*, 132-134.

(11) Belfield, K. D.; Schafer, K. J.; Liu, Y. U.; Liu, J.; Ren, X. B.; Van Stryland, E. W. *Journal of Physical Organic Chemistry* **2000**, *13*, 837-849.

(12) Belfield, K. D.; Ren, X. B.; Van Stryland, E. W.; Hagan, D. J.; Dubikovsky, V.; Miesak, E. J. *Journal of the American Chemical Society* **2000**, *122*, 1217-1218.

(13) Schafer, K. J.; Hales, J. M.; Balu, M.; Belfield, K. D.; Van Stryland, E. W.; Hagan, D. J. *Journal of Photochemistry and Photobiology a-Chemistry* **2004**, *162*, 497-502.

(14) Yu, T. Y.; Ober, C. K.; Kuebler, S. M.; Zhou, W. H.; Marder, S. R.; Perry, J. W. *Advanced Materials* **2003**, *15*, 517-521.

(15) Lidstrom, P.; Tierney, J.; Wathey, B.; Westman, J. *Tetrahedron* **2001**, *57*, 9225-9283.

(16) Nilsson, P.; Ofsson, K.; Larhed, M. In *Microwave Methods in Organic Synthesis* 2006; Vol. 266, p 103-144.

(17) Seipel, K. R.; Platt, Z. H.; Nguyen, M.; Holland, A. W. *J. Org. Chem.* **2008**, *73*, 4291-4294.

(18) Crivello, J. V.; Lam, J. H. W. *Journal of Organic Chemistry* **1978**, *43*, 3055-3058.

(19) Crivello, J. V.; Lam, J. H. W. *Abstr Pap Am Chem S* **1978**, *176*, 8-8.

(20) Belfield, K. D.; Bondar, M. V.; Przhonska, O. V.; Schafer, K. J. *Photochemical & Photobiological Sciences* **2004**, *3*, 138-141.

(21) Dektar, J. L.; Hacker, N. P. *Journal of the American Chemical Society* **1990**, *112*, 6004-6015.

(22) Dektar, J. L.; Hacker, N. P. *Journal of Organic Chemistry* **1990**, *55*, 639-647.

(23) Pohlers, G.; Scaiano, J. C.; Sinta, R.; Brainard, R.; Pai, D. *Chemistry of Materials* **1997**, *9*, 1353-1361.

(24) Varma, R. S.; Saini, R. K. *Tetrahedron Letters* **1997**, *38*, 4337-4338.

(25) Belfield, K. D.; Schafer, K. J.; Mourad, W.; Reinhardt, B. A. *Journal of Organic Chemistry* **2000**, *65*, 4475-4481.

(26) Beak, P.; Sullivan, T. A. *Journal of the American Chemical Society* **1982**, *104*, 4450-4457.

(27) Sivasubramanian, S.; Ravichandran, K. *Indian Journal of Chemistry Section B-Organic Chemistry Including Medicinal Chemistry* **1991**, *30*, 1148-1149.

(28) Belfield, K. D.; Yao, S.; Morales, A. R.; Hales, J. M.; Hagan, D. J.; Van Stryland, E. W.; Chapela, V. M.; Percino, J. *Polymers for Advanced Technologies* **2005**, *16*, 150-155.

(29) Lakowicz, J. R. *Principles of Fluorescence Spectroscopy*; Kluwer Academic Publishers: New York, 1999.

(30) Otsubo, T.; Gray, R.; Boekelheide, V. *Journal of the American Chemical Society* **1978**, *100*, 2449-2456.

(31) van de Nes, A. S. B., J. M. ; Pereira, S. F. *REPORTS ON PROGRESS IN PHYSICS* **2006**, 2323-2363.

(32) Strickler, J. H.; Webb, W. W. *Optics Letters* **1991**, *16*, 1780-1782.

(33) Dvornikov, A. S.; Rentzepis, P. M. *Opt Commun* **1997**, *136*, 1-6.

(34) Dey, J. K.; Dogra, S. K. *Bulletin of the Chemical Society of Japan* **1991**, *64*, 3142-3152.

(35) Arnett, E. M.; Quirk, R. P.; Burke, J. J. *Journal of the American Chemical Society* **1970**, *92*, 1260-1266.

(36) Belfield, K. D.; Bondar, M. V.; Przhonska, O. V.; Schafer, K. J.; Mourad, W. *Journal of Luminescence* **2002**, *97*, 141-146.

(37) Belfield, K. D. C., James C. *Photoinitiated Polymerization*; Oxford University Press: Washington D. C., 2003.

(38) Belfield, K. D.; Wang, J. X. *Journal of Polymer Science Part a-Polymer Chemistry* **1995**, *33*, 1235-1242.

(39) Ehrlich, J. E.; Wu, X. L.; Lee, I. Y. S.; Hu, Z. Y.; Rockel, H.; Marder, S. R.; Perry, J. W. *Optics Letters* **1997**, *22*, 1843-1845.

(40) Belfield, K. D.; Morales, A. R.; Kang, B. S.; Hales, J. M.; Hagan, D. J.; Van Stryland, E. W.; Chapela, V. M.; Percino, J. *Chemistry of Materials* **2004**, *16*, 4634-4641.

(41) Yanez, C. O.; Andrade, C. D.; Belfield, K. D. *Chemical Communications* **2009**, 827-829.

(42) Bredereck, M.; G., S.; Griebenow, W. *Chem. Ber.* **1973**, *106* 3732.

(43) Yoshino, K.; Kohno, T.; Uno, T.; Morita, T.; Tsukamoto, G. *Journal of Medicinal Chemistry* **1986**, *29*, 820-825.

(44) Zeng, D. X.; Chen, Y. *Journal of Photochemistry and Photobiology a-Chemistry* **2007**, *186*, 121-124.

(45) Belfield, K. D.; Bondar, M. V.; Yanez, C. O.; Hernandez, F. E.; Przhonska, O. V. *Journal of Materials Chemistry* **2009**, -.

(46) Zhou, W. H.; Kuebler, S. M.; Braun, K. L.; Yu, T. Y.; Cammack, J. K.; Ober, C. K.; Perry, J. W.; Marder, S. R. *Science* **2002**, *296*, 1106-1109.

(47) Zhou, W. H.; Kuebler, S. M.; Carrig, D.; Perry, J. W.; Marder, S. R. *Journal of the American Chemical Society* **2002**, *124*, 1897-1901.

(48) Crivello, J. V.; Lam, J. H. W. *Macromolecules* **1977**, *10*, 1307-1315.

(49) Kaehr, B.; Shear, J. B. *Journal of the American Chemical Society* **2007**, *129*, 1904-+.

(50) Kuebler, S. M.; Braun, K. L.; Zhou, W. H.; Cammack, J. K.; Yu, T. Y.; Ober, C. K.; Marder, S. R.; Perry, J. W. *Journal of Photochemistry and Photobiology a-Chemistry* **2003**, *158*, 163-170.

(51) Bykova, E. E.; Zemlyanov, A. A.; Geints, Y. E.; Gennadii, G. M., Victor, A. B., Eds.; SPIE: 2006; Vol. 6522, p 65220Y.

(52) Shao, P.; Li, Z.; Qin, J. G.; Gong, H. M.; Ding, S.; Wang, Q. Q. *Australian Journal of Chemistry* **2006**, *59*, 49-52.

(53) Correa, D. S.; Goncalves, V. C.; Balogh, D. T.; Mendonca, C. R.; De Boni, L. *Polymer* **2006**, *47*, 7436-7440.

(54) De Boni, L.; Gaffo, L.; Misoguti, L.; Mendonca, C. R. *Chemical Physics Letters* **2006**, *419*, 417-420.

(55) Allain, C.; Schmidt, F.; Lartia, R.; Bordeau, G.; Fiorini-Debuisschert, C.; Charra, F.; Tauc, P.; Teulade-Fichou, M. P. *Chembiochem* **2007**, *8*, 424-433.

(56) Gu, B.; Ji, W.; Patil, P. S.; Dharmaprakash, S. M. *Journal of Applied Physics* **2008**, *103*.

(57) Webster, S.; Fu, J.; Padilha, L. A.; Przhonska, O. V.; Hagan, D. J.; Van Stryland, E. W.; Bondar, M. V.; Slominsky, Y. L.; Kachkovski, A. D. *Chemical Physics* **2008**, *348*, 143-151.

(58) Kobayashi, T.; Savatier, J.-B.; Jordan, G.; Blau, W. J.; Suzuki, Y.; Kaino, T.; James, G. G., Toshikuni, K., Eds.; SPIE: 2004; Vol. 5351, p 210-216.

(59) Lattante, S.; Barbarella, G.; Favaretto, L.; Gigli, G.; Cingolani, R.; Anni, M. *Applied Physics Letters* **2006**, *89*.

(60) Wang, C. H.; Tai, O. Y. H.; Wang, Y. X.; Tsai, T. H.; Chang, N. C. *Journal of Chemical Physics* **2005**, *122*.

(61) Galanin, M. D.; Kirsanov, B. P.; Chizhiko.Za; Lebedev, P. N. *Jetp Letters-Ussr* **1969**, *9*, 304-&.

(62) Sheikbahae, M.; Said, A. A.; Wei, T. H.; Hagan, D. J.; Vanstryland, E. W. *Ieee Journal of Quantum Electronics* **1990**, *26*, 760-769.

(63) Belfield, K. D.; Bondar, M. V.; Hernandezt, F. E.; Przhonska, O. V.; Yao, S. *Journal of Physical Chemistry B* **2007**, *111*, 12723-12729.

(64) Kusba, J.; Lakowicz, J. R. *Journal of Chemical Physics* **1999**, *111*, 89-99.

(65) Lakowicz, J. R.; Gryczynski, I. *Non-linear and Two-Photon-Induced Fluorescence*; Plenum Press: New York, 1997; Vol. 5.

(66) Gryczynski, I.; Kusba, J.; Gryczynski, Z.; Malak, H.; Lakowicz, J. R. *Journal of Fluorescence* **1998**, *8*, 253-261.

(67) Hell, S. W.; Wichmann, J. *Optics Letters* **1994**, *19*, 780-782.

(68) Klar, T. A.; Jakobs, S.; Dyba, M.; Egner, A.; Hell, S. W. *Proceedings of the National Academy of Sciences of the United States of America* **2000**, *97*, 8206-8210.

(69) Westphal, V.; Rizzoli, S. O.; Lauterbach, M. A.; Kamin, D.; Jahn, R.; Hell, S. W. *Science* **2008**, *320*, 246-249.

(70) Belfield, K. D.; Bondar, M. V.; Hernandez, F. E.; Morales, A. R.; Przhonska, O. V.; Schafer, K. J. *Applied Optics* **2004**, *43*, 6339-6343.

(71) Hsiao, C. N.; Shechter, H. *Tetrahedron Letters* **1982**, *23*, 1963-1966.

(72) Belfield, K. D.; Bondar, M. V.; Yanez, C. O.; Hernandez, F. E.; Przhonska, O. V. *Journal of Materials Chemistry* **2009**.

(73) Lakowicz, J. R.; Gryczynski, I. *Fluorescence quenching by stimulated emission, Nonlinear and Two-Photon-Induced Fluorescence*; Plenum Press: New York, 1997; Vol. Vol. 5.

(74) Lakowicz, J. R.; Gryczynski, I.; Kusba, J.; Bogdanov, V. *Photochemistry and Photobiology* **1994**, *60*, 546-562.

(75) Westphal, V.; Seeger, J.; Salditt, T.; Hell, S. W. *Journal of Physics B-Atomic Molecular and Optical Physics* **2005**, *38*, S695-S705.

(76) Simpson, G. J. *Nature* **2006**, *440*, 879-880.

(77) Makarov, N. S.; Drobizhev, M.; Rebane, A. *Optics Express* **2008**, *16*, 4029-4047.